3.2. SEAFRAME sea level record and trend

A fundamental goal of the Project is to establish the rate of sea level change. It has been recognised since the beginning that this would require several decades of continuous, high quality data. The preliminary findings are being provided, but caution should be exercised in interpreting this information. Figure 6 shows that confidence in trend estimates improve as more data becomes available.

As at December 2010, based on the short-term sea level rise analyses performed by the National Tidal Centre using the Port Vila SEAFRAME data, a rate of **+5.7 mm per year** has been observed. Accounting for the inverted barometric pressure effect and vertical movements in the observing platform, the net sea level trend is **+4.9 mm per year**. By comparison, the Intergovernmental Panel on Climate Change (IPCC) in its Fourth Assessment Report (IPCC AR4, 2007) estimates that global average long-term sea level rise over the last hundred years was of the order of 1 to 2 mm/yr.

Figure 4 shows how the trend estimate has varied over time. In the early years, the trend appeared to indicate an enormous rate of sea level rise. Later, due to the 1997/1998 El Niño when sea level fell about 12 cm below average, the trend dropped substantially. Given the sea level record is relatively short, it is still too early to deduce a long-term trend.

The sea level data recorded since installation is summarised in Figure 17. The middle curve (green) represents the monthly mean sea level. The upper and lower curves show the highest and lowest values recorded each month. Unlike many of the SEAFRAME sites, sea level at Port Vila did not experience a dramatic decrease in 1998 as a result of El Niño, although it did disrupt the normal seasonal cycle and produced a negative sea level anomaly. Port Vila is relatively far from the equator, where El Niño signals are most pronounced.

By inspection of the monthly maxima (red curve) it appears that Vanuatu, like Fiji, the Cook Islands, Tonga and Tuvalu, experiences highest sea levels near the start of the year. At mid-year, the highest sea levels are typically about 20 cm less than when at the maximum. However, this pattern does not occur every year. The mean sea level over the duration of the record is 0.887 metres, with a maximum of 1.785 metres on 28th of February 2010 (as a result of tsunami waves arriving following the Mw8.8 earthquake off Chile), and a minimum of -0.237 metres on 26th of November 1999 due to the arrival of a tsunami at low tide.

Figure 17

Monthly sea level at Port Vila, Vanuatu
SEAFRAME gauge

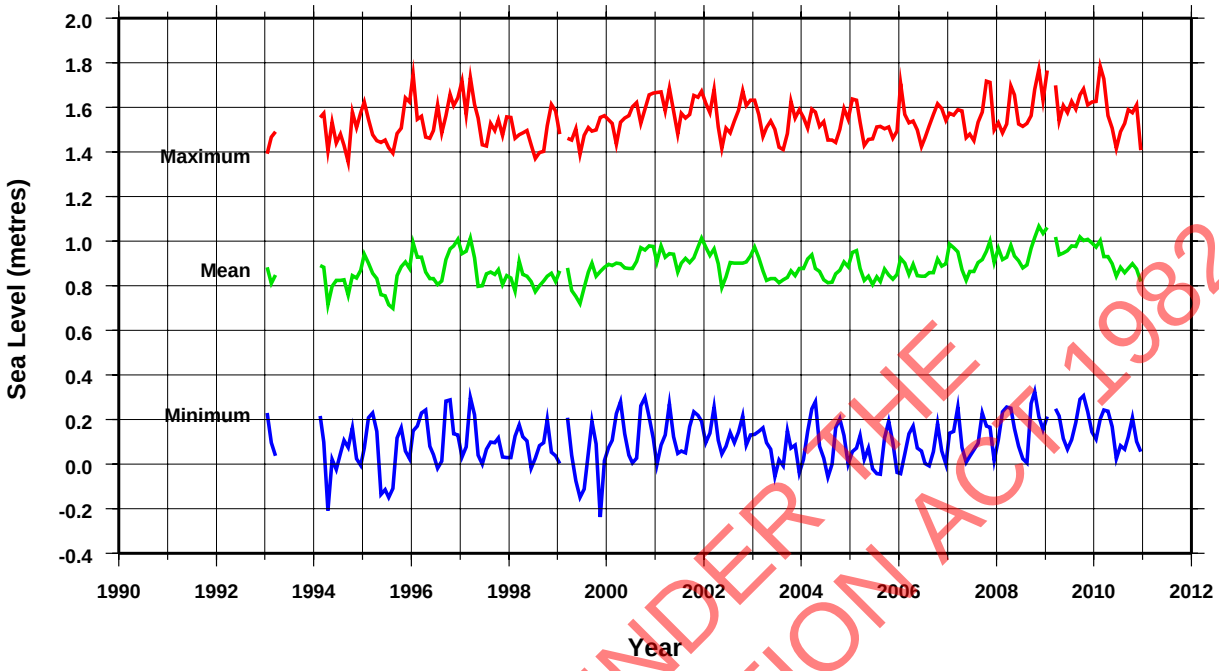

3.3. Additional sea level records and trend

An additional sea level record for Vanuatu is available from the Joint Archive for Sea Level for Port Vila, where a tide gauge operated from 1977 to 1982. The monthly sea level data from this station is shown in Figure 18, but the relative sea level trend of +13.5 mm/year is large since it is derived from a very short record. Older tide gauges such as these were primarily designed for monitoring tides and shorter-term oceanic fluctuations such as El Niño rather than long-term sea level monitoring which requires a high level of precision and datum control.

Figure 18

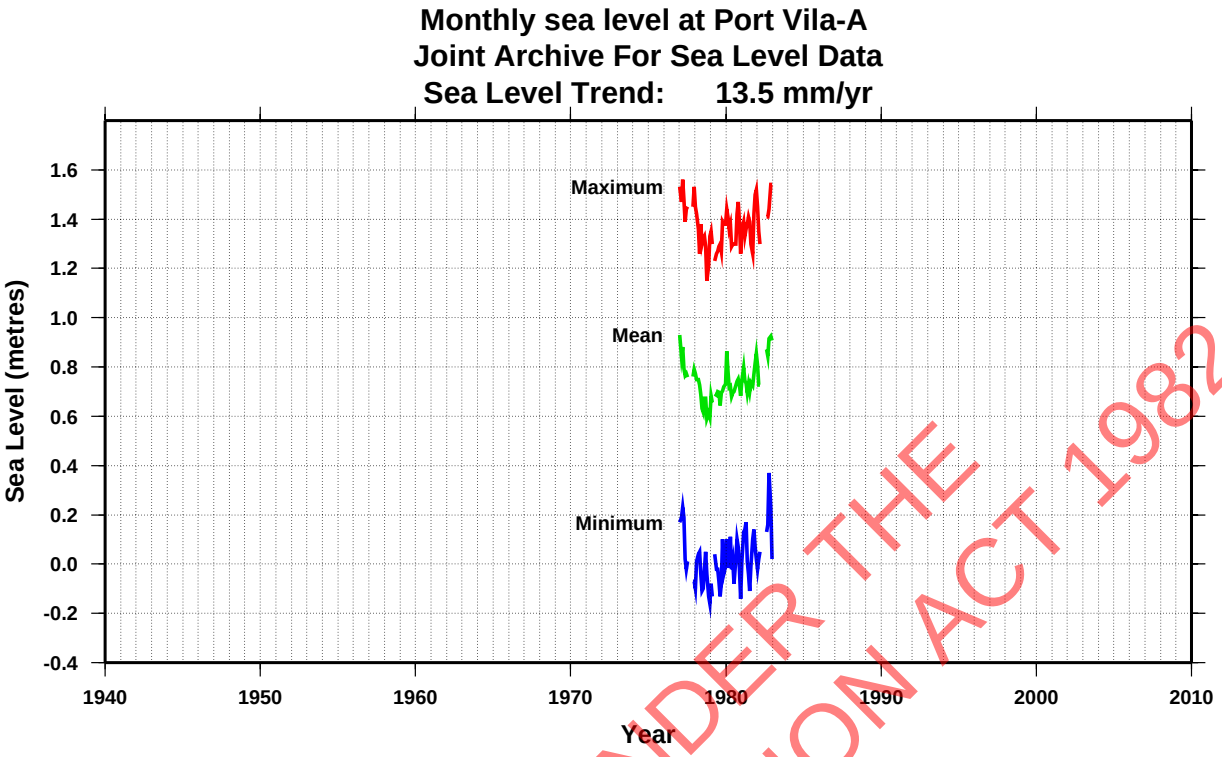

3.4. Predicted highest astronomical tide

The component of sea level that is predictable due to the influence of the Sun and the Moon and some seasonal effects allow us to calculate the highest predictable level each year. The highest astronomical tide is the highest sea level that can be predicted under any combination of astronomical conditions, including the proximity of the earth to the sun and the moon. Figure 19 shows that the highest predicted level (1.58 m) over the period 1990 to 2016 was at 17:28 Local Time on 24 November 2003.

Figure 19

Predicted highest tide each year for Port Villa

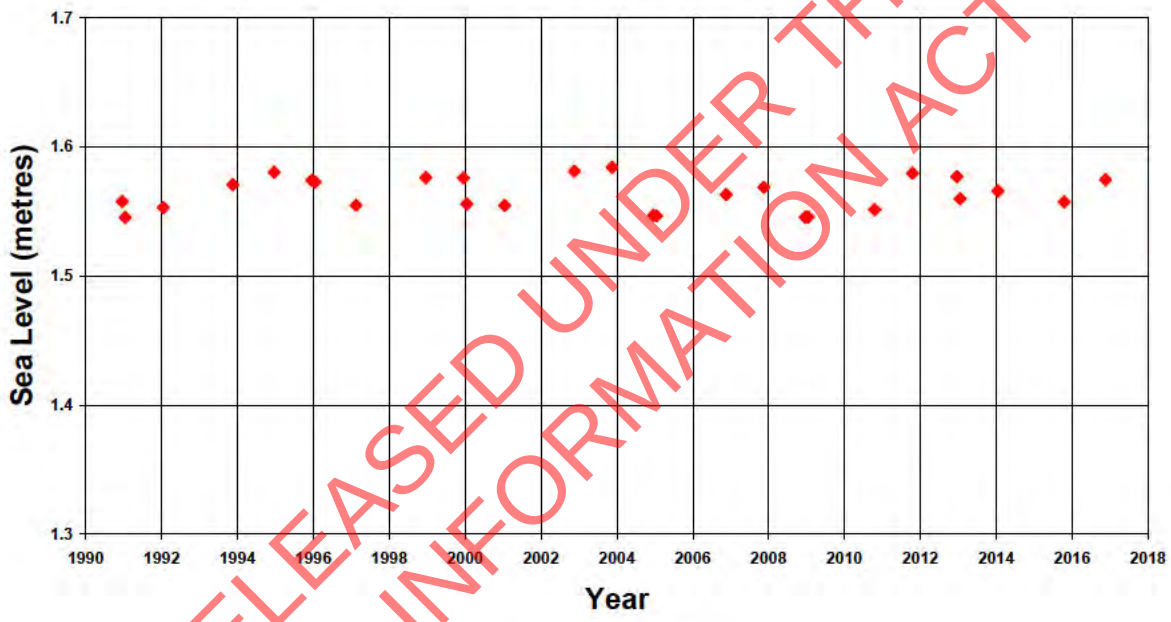

3.5. Monthly mean air temperature, water temperature and atmospheric pressure

The data summarised in Figures 20-22 follows the same format as the monthly sea level plot: the middle curve (green) represents the monthly mean, and the upper and lower curves show the highest and lowest values recorded each month.

Compared to the more equatorial sites, Port Vila undergoes much greater seasonal temperature variations. The summertime highs are normally recorded in January or February. The mean air temperature over the duration of the record is 25.1°C. The minimum air temperature of 15.2°C was reached on 10th of August 2006, and a maximum of 33.3°C was reached on 24th of January 2002.

Figure 20

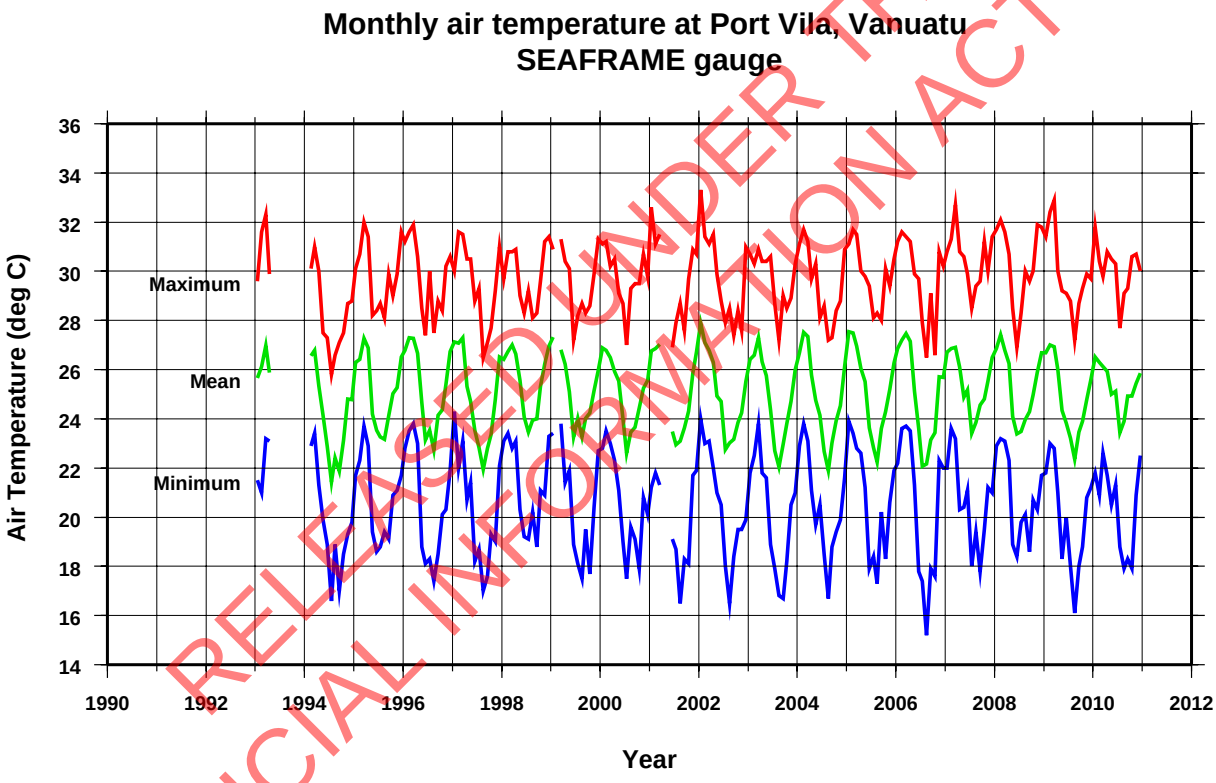

Water temperature also undergoes seasonal oscillations, which are virtually in phase with those of air temperature. Interestingly, in several years the maxima in air and water temperature come a month or two after the sea level maxima. The mean water temperature over the duration of the record is 27.2°C. The maximum water temperature of 31.7°C was recorded on 15th of February 2000, and the minimum of 23.3°C recorded on 8th of September 1994.

Figure 21

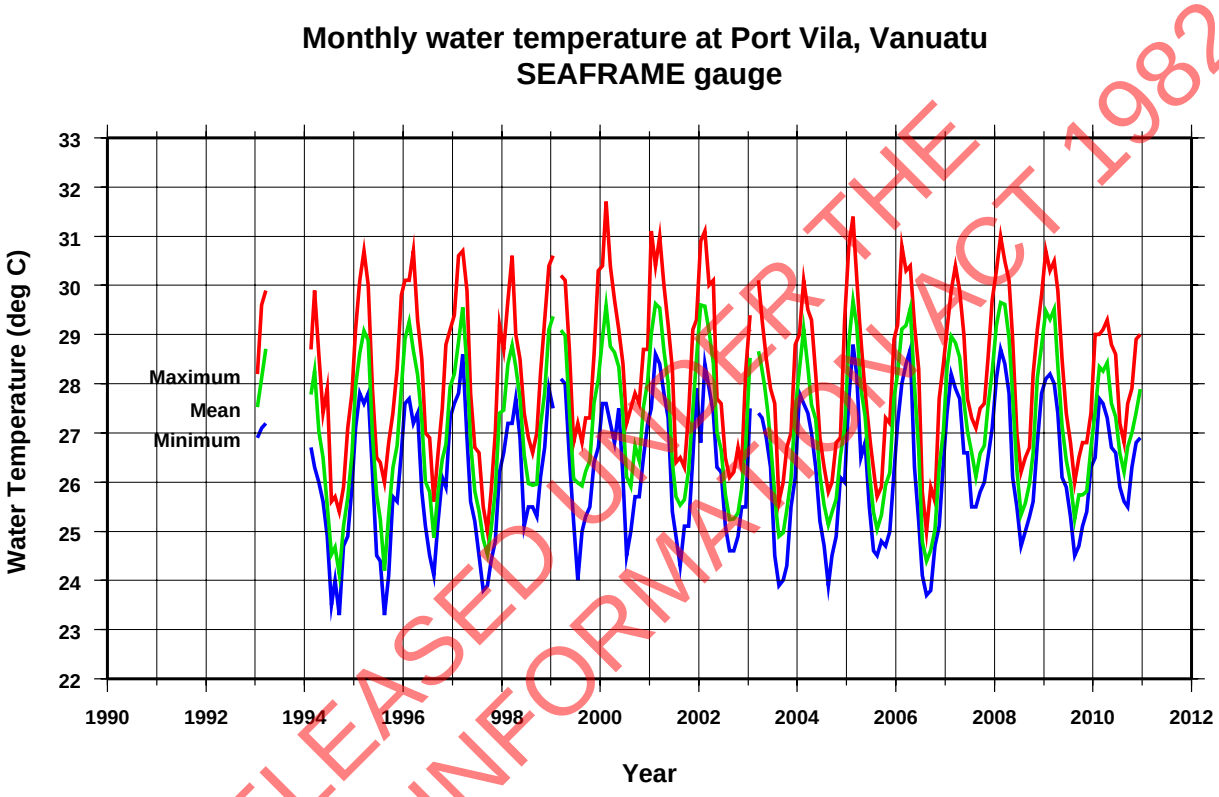

The sea level also responds to changes in barometric pressure. As a rule of thumb, a 1 hPa fall in the barometer, if sustained over a day or more, produces a 1 cm rise in the local sea level (within the area beneath the low pressure system). The seasonal (summertime) high sea levels at Port Vila are highly correlated with low barometric pressure systems. This is particularly the case for the very low pressure events (cyclones), most of which coincide with the highest sea levels for the year (since summer is also cyclone season). The mean barometric pressure over the duration of the record is 1010.6 hPa. The highest pressure recorded was 1021.1 hPa on 10th of November 1997, while the lowest was 961.7 hPa on 26th of February 2004 as a result of Tropical Cyclone Ivy.

Figure 22

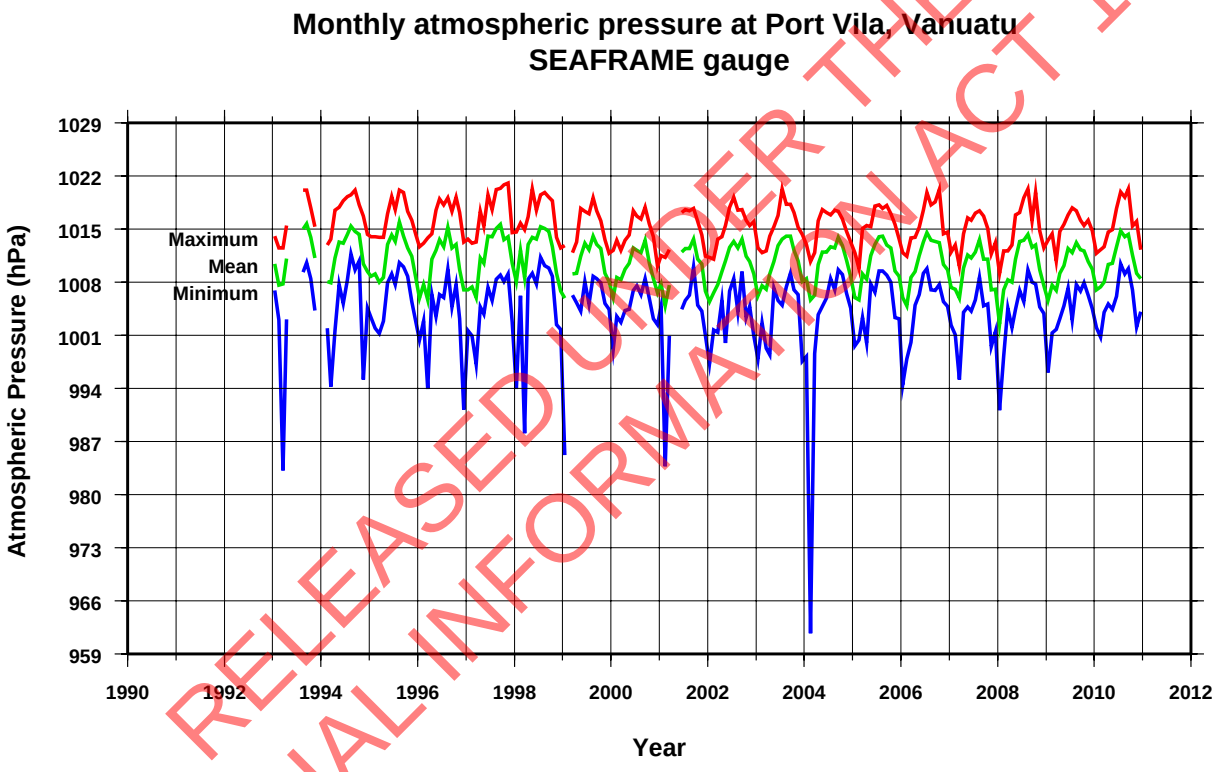

3.6. Precise Levelling Results for Vanuatu

While the SEAFRAME gauge exhibits a high degree of datum stability, it is essential that the datum stability be checked periodically by precise levelling to an array of deep-seated benchmarks located close to the tide gauge. For example, a wharf normally supports the SEAFRAME, and wharf pilings are often subject to gradual vertical adjustment, which in turn can raise or lower the SEAFRAME.

Precise levelling is carried out on a regular 18-monthly cycle between the SEAFRAME Sensor Benchmark and an array of at least six deep benchmarks. The nearest stable benchmark is designated the “Tide Gauge Benchmark (TGBM)”, and the others are considered the “coastal array”.

Figure 23 summarises the most important survey information being the movement of the SEAFRAME Sensor benchmark relative to the TGBM, as well as recent movement relative to the CGPS station. The graph does not include the results for the other benchmarks on the coastal array. The first two surveys in 1993 and 1994 are not shown because in 1995 the SEAFRAME Sensor benchmark was repositioned and a new zero value established after damage to the installation. Each survey is plotted relative to the 1995 survey, thus in 1997 the SEAFRAME Sensor benchmark had *risen* relative to the TGBM by 1.5 mm. An earthquake in January 2002 caused a substantial fall of the SEAFRAME sensor but the sea level record has been corrected for this. Over the duration of the project the SEAFRAME Sensor has risen at an average rate of +0.1 mm/year.

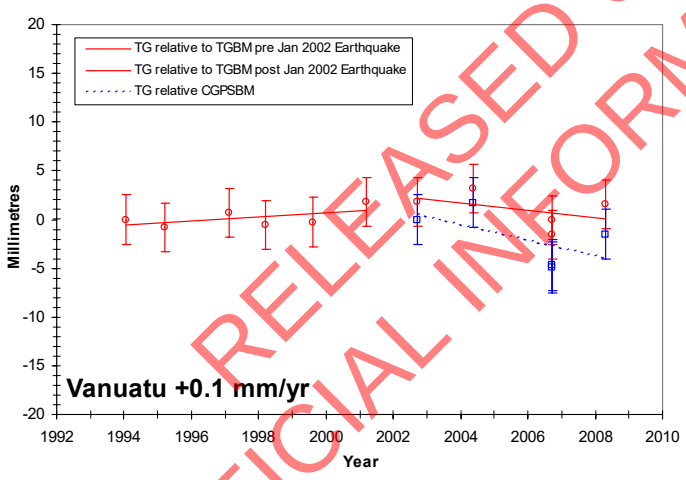

Figure 23. Movement of the SEAFRAME Sensor relative to the Tide Gauge Bench Mark and CGPS station.

Levelling of SEAFRAME Sensor benchmark. Photo credit: Steve Turner, NTC.

Appendix

A.1. Definition of Datum and other Geodetic Levels at Port Vila, Vanuatu

Newcomers to the study of sea level are confronted by bewildering references to "Chart Datum", "Tide Staff Zero", and other specialised terms. Frequent questions are, "how do NTC sea levels relate to the depths on the marine chart?" and "how do the UH sea levels relate to NTC's?".

Regular surveys to a set of coastal benchmarks are essential. If a SEAFRAME gauge or the wharf to which it is fixed were to be damaged and needed replacement the survey history would enable the data record to be "spliced across" the gap, thereby preserving the entire invaluable record from start to finish.

Figure 24

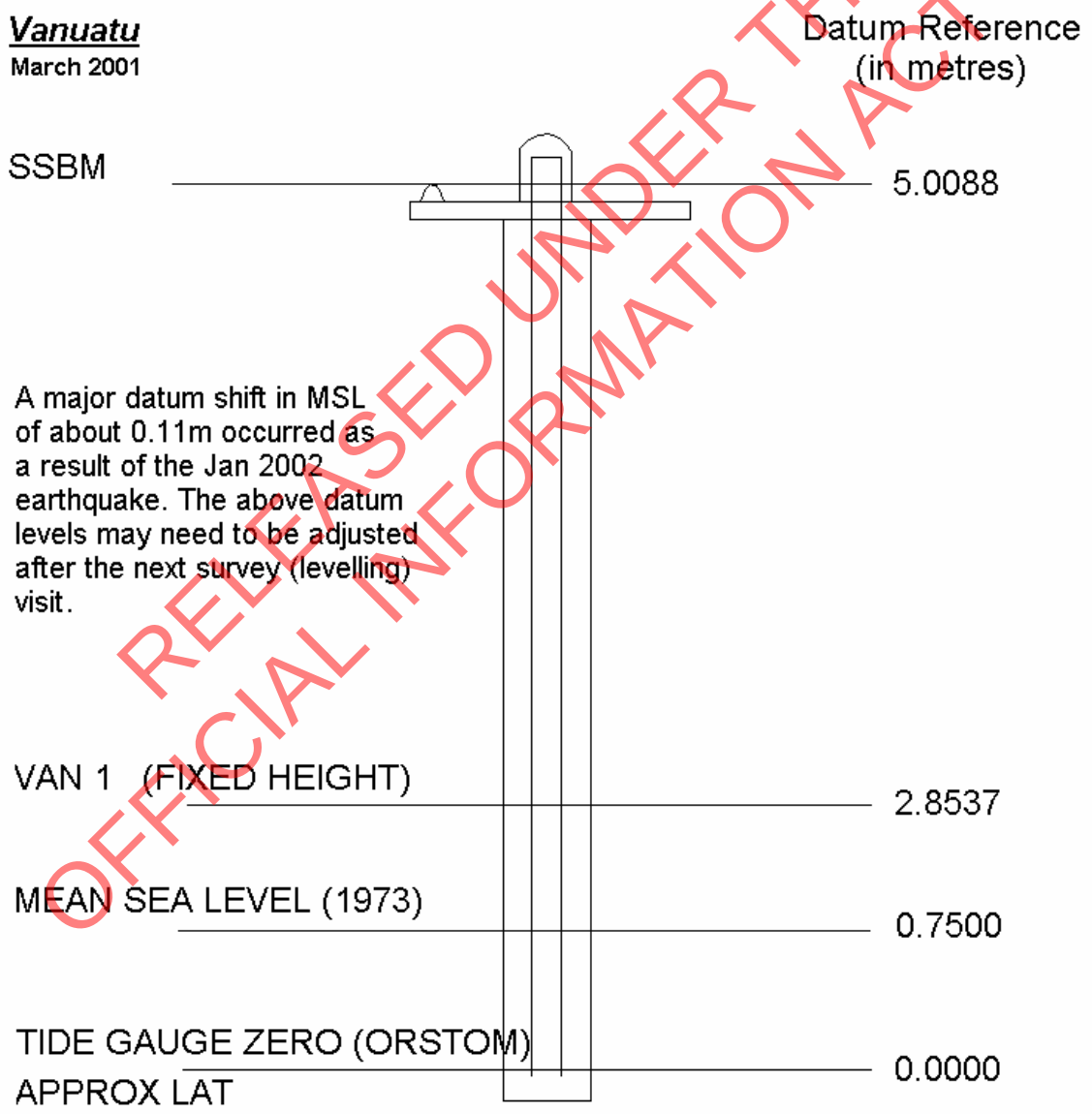

The word “datum” in reference to tide gauges and nautical charts means a reference level. Similarly, when you measure the height of a child, your datum is the floor on which the child stands.

Where possible, “sea levels” in the NTC data are normally reported relative to “Chart Datum” (CD), thus enabling users to relate the NTC data (such as shown in the figure above) directly to depth soundings shown on marine charts – if the NTC sea level is +1.5 metres, an additional 1.5 metres of water may be added to the chart sounding. At Port Vila, “LAT” (see below) provides an “equivalent” datum.

Mean Sea Level (MSL) in Figure 24 is the average recorded level at the gauge over the year 1973. The MSL at Port Vila is 0.75 metres above CD.

Lowest Astronomical Tide, or “LAT”, is based purely on tidal predictions over a 19 year period. In this case, LAT is 0.0 metres, meaning that if the sea level were controlled by tides alone, the sea level reported by NTC would drop to 0.0 metres just once in 19 years.

International Journal of Atmospheric and Oceanic Sciences
2019; 3(1): 13-26
http://www.sciencepublishinggroup.com/j/ijaos
doi: 10.11648/j.ijaos.20190301.13
ISSN: 2640-1142 (Print); ISSN: 2640-1150 (Online)

Human CO_2 Emissions Have Little Effect on Atmospheric CO_2

Edwin X Berry

Climate Physics LLC, Bigfork, USA

Email address:
ed@edberry.com

To cite this article:
Edwin X Berry. Human CO_2 Emissions Have Little Effect on Atmospheric CO_2. *International Journal of Atmospheric and Oceanic Sciences*. Vol. 3, No. 1, 2019, pp. 13-26. doi: 10.11648/j.ijaos.20190301.13

Received: May 13, 2019; **Accepted**: June 12, 2019; **Published**: June 4, 2019

Abstract: The United Nations *Intergovernmental Panel on Climate Change* (IPCC) agrees human CO_2 is only 5 percent and natural CO_2 is 95 percent of the CO_2 inflow into the atmosphere. The ratio of human to natural CO_2 in the atmosphere must equal the ratio of the inflows. Yet IPCC claims human CO_2 has caused all the rise in atmospheric CO_2 above 280 ppm, which is now 130 ppm or 32 percent of today's atmospheric CO_2. To cause the human 5 percent to become 32 percent in the atmosphere, the IPCC model treats human and natural CO_2 differently, which is impossible because the molecules are identical. IPCC's Bern model artificially traps human CO_2 in the atmosphere while it lets natural CO_2 flow freely out of the atmosphere. By contrast, a simple Physics Model treats all CO_2 molecules the same, as it should, and shows how CO_2 flows through the atmosphere and produces a balance level where outflow equals inflow. Thereafter, if inflow is constant, level remains constant. The Physics Model has only one hypothesis, that outflow is proportional to level. The Physics Model exactly replicates the 14C data from 1970 to 2014 with only two physical parameters: balance level and e-time. The 14C data trace how CO_2 flows out of the atmosphere. The Physics Model shows the 14 CO_2 e-time is a constant 16.5 years. Other data show e-time for 12CO_2 is about 4 to 5 years. IPCC claims human CO_2 reduces ocean buffer capacity. But that would increase e-time. The constant e-time proves IPCC's claim is false. IPCC argues that the human-caused reduction of 14C and 13C in the atmosphere prove human CO_2 causes all the increase in atmospheric CO_2. However, numbers show these isotope data support the Physics Model and reject the IPCC model. The Physics Model shows how inflows of human and natural CO_2 into the atmosphere set balance levels proportional to their inflows. Each balance level remains constant if its inflow remains constant. Continued constant CO_2 emissions do not add more CO_2 to the atmosphere. No CO_2 accumulates in the atmosphere. Present human CO_2 inflow produces a balance level of about 18 ppm. Present natural CO_2 inflow produces a balance level of about 392 ppm. Human CO_2 is insignificant to the increase of CO_2 in the atmosphere. Increased natural CO_2 inflow has increased the level of CO_2 in the atmosphere.

Keywords: Carbon Dioxide, CO_2, Climate Change, Anthropogenic

1. Introduction

The U.S. Global Change Research Program Climate Science Special Report (USGCRP) [1] claims,

This assessment concludes, based on extensive evidence, that it is extremely likely that human activities, especially emissions of greenhouse gases, are the dominant cause of the observed warming since the mid-20th century.

The United Nations Intergovernmental Panel on Climate Change (IPCC) [2] Executive Summary claims human emissions caused atmospheric CO_2 to increase from 280 ppm in 1750, to 410 ppm in 2018, for a total increase of 130 ppm.

IPCC and USGCRP claim there are "no convincing alternative explanations" other than their theory to explain the "observational evidence."

This paper presents a "convincing alternative explanation" that explains the data. A simple physics model explains the required first step of human-caused climate change: how human CO_2 changes atmospheric CO_2.

For simplicity, this paper uses levels in units of ppm (parts per million by volume in dry air) and flows in units of ppm per year. GtC (Gigatons of Carbon) units are converted into CO_2 units in ppm using:

$$1 \text{ ppm} = 2.12 \text{ GtC}$$

Authors who support the USGCRP [1] and IPCC [2, 3]

include Archer et al. [4], Cawley [5], Kern and Leuenberger [6], and Kohler [7].

Authors who conclude human CO_2 increases atmospheric CO_2 as a percentage of its inflow include Revelle and Suess [8], Starr [9], Segalstad [10], Jaworoski [11, 12], Beck [13], Rorsch, Courtney, and Thoenes [14], Courtney [15], Quirk [16], Essenhigh [17], Glassman [18], Salby [19-22], Humlum [23], Harde [24, 25], and Berry [26, 27].

2. The Science Problem

IPCC [2, 3] says nature emits about 120 GtC from land and 90 GtC from ocean for a total of 210 GtC per year. This is equivalent to about 98 ppm per year of natural CO_2 that flows into the atmosphere. IPCC admits its estimates of "gross fluxes generally have uncertainties of more than ±20%."

Boden [28] shows human CO_2 emissions in 2014 were 9.7 GTC per year, or 4.6 ppm per year. So, IPCC agrees that human inflow is less than 5% and nature is more than 95% of the total CO_2 inflow into the atmosphere. Yet IPCC assumes nature stayed constant since 1750 and human CO_2 causes 100 percent the increase in atmospheric CO_2 above 280 ppm, which today is 130 ppm or 32 percent of 410 ppm.

The Physics Model concludes the percent of human CO_2 in the atmosphere equals the percent of human CO_2 in the inflow.

Figure 1 shows how the predictions of the Physics Model and IPCC model differ regarding the composition of human CO_2 in the atmosphere.

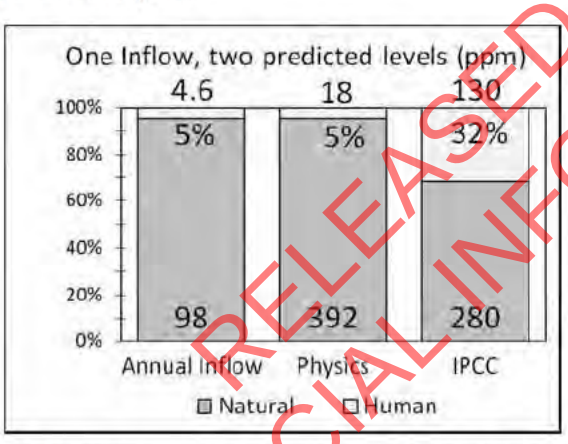

Figure 1. *The IPCC agrees the inflow of human CO_2 is less than 5 percent. The Physics Model says the percent of human CO_2 in the atmosphere equals the percent of its inflow. IPCC claims human CO_2 adds all atmospheric CO_2 above 280 ppm, which is now 32 percent of the total.*

If the IPCC model is correct, then the effect of human CO_2 emissions on atmospheric CO_2 is 100 percent. If the Physics Model is correct, then human CO_2 emissions do not cause climate change.

3. The Physics Model

3.1. How CO_2 Flows Through the Atmosphere

IPCC states, and much of the public believes, human emissions "add" CO_2 to the atmosphere. IPCC's view is the atmosphere is a garbage dump where human CO_2 is deposited and mostly stays forever.

However, nature must treat human and natural CO_2 the same because their molecules are identical. Nature has had millions of years to "add" to atmospheric CO_2. If nature's CO_2 "adds" to atmospheric CO_2, the CO_2 in the atmosphere would be much higher than it is today.

Therefore, natural and human CO_2 do not "add" CO_2 to the atmosphere. Both natural and human CO_2 "flow through" the atmosphere. As CO_2 flows through the atmosphere, it raises the level of atmospheric CO_2 just enough so CO_2 outflow equals CO_2 inflow. Nature balances CO_2 in the atmosphere when outflow equals inflow.

You pump air into a tire or inner tube that has a leak. As you pump air into the tube, air leaks out of the tube. The faster you pump air in, the faster air leaks out. If you pump air into the tube at a constant rate, the air pressure in the tube will find a level where outflow equals inflow.

River water flows into a lake or a pond and flows out over a dam. If inflow increases, the water level increases until outflow over the dam equals inflow from the river. Then, the water level will remain constant so long as inflow remains constant. The river does not "add" water to the lake. Water "flows through" the lake and finds a balance level where outflow equals inflow.

Similarly, human and natural CO_2 flow through the atmosphere. The inflow creates a balance level that remains constant so long as inflow remains constant.

3.2. Physics Model System Description

Figure 2 shows a bucket of water as an analogy to CO_2 in the atmosphere. Water flows into the bucket at the top and flows out through a hole in the bottom. An outside source (faucet) controls the inflow.

The water level and the hole size control the outflow. No matter what the inflow, the level and the size of the hole control the outflow. Inflow only serves to set a balance level.

This paper uses e-time rather than "residence" time because there are many definitions of residence time. E-time has a precise definition: the time for the level to move (1 – 1/e) of the distance from its present level to its balance level. The balance level is defined below.

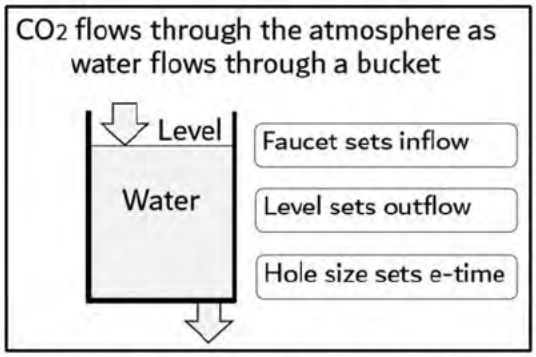

Figure 2. *A bucket of water is an analogy to the Physics Model for atmospheric CO_2. Water flows through the bucket as CO_2 flows through the atmosphere.*

The bucket analogy provides insight into e-time. If the hole in the bucket gets smaller, e-time increases. If the hole in the bucket gets larger, e-time decreases. The hole is an analogy to the ability of the oceans and land to absorb CO_2 from the atmosphere.

Figure 3 shows the Physics Model system for atmospheric CO_2. The system includes the level (concentration) of CO_2 in the atmosphere and the inflow and outflow of CO_2.

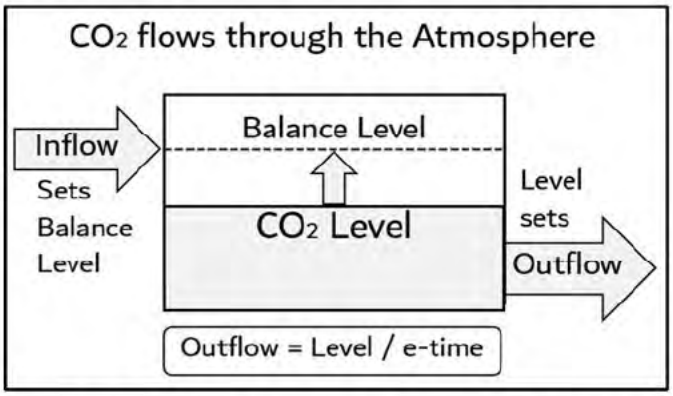

Figure 3. *The Physics Model system for atmospheric CO_2. Inflow and Outflow determine the change in level. The only hypothesis is Outflow = Level / e-time.*

The Physics Model applies independently and in total to all definitions of CO_2, e.g., to human CO_2, natural CO_2, and their sums, and to $12CO_2$, $13CO_2$, and $14CO_2$, and their sums.

The Physics Model is complete. It is not necessary to add separate inflows for human and natural CO_2 to the Physics Model. Just use a copy of the Physics Model for each CO_2 definition desired.

The Physics Model does not need to describe the details of the external processes. Inflow, outflow, and e-time include all the effects of outside processes. If the Physics Model were connected to land and ocean reservoirs, it would behave exactly as derived in this paper.

Kohler [7] claims Harde's [24] model and therefore the Physics Model is "too simplistic" and "leads to flawed results for anthropogenic carbon in the atmosphere."

Kohler is wrong. There is no such thing as a system being "too simplistic." A system should be as simple as possible to solve a problem. The Physics Model shows how inflow, outflow, and e-time affect the level of CO_2 in the atmosphere. The IPCC model cannot do this.

3.3. Physics Model Derivation

A system describes a subset of nature. A system includes levels and flows between levels. Levels set flows and flows set new levels. The mathematics used in the Physics Model are analogous to the mathematics used to describe many engineering systems.

The Physics Model derivation begins with the continuity equation (1) which says the rate of change of level is the difference between inflow and outflow:

$$dL/dt = Inflow - Outflow \quad (1)$$

Where

L = CO_2 level (concentration in ppm)

t = time (years)

dL/dt = rate of change of L (ppm/year)

Inflow = rate CO_2 moves into the system (ppm/year)

Outflow = rate CO_2 moves out of the system (ppm/year)

Following the idea from the bucket of water, the Physics Model has only one hypothesis, that outflow is proportional to level:

$$Outflow = L \ / \ Te \quad (2)$$

where Te is the "e-folding time" or simply "e-time."

Substitute (2) into (1) to get,

$$dL/dt = Inflow - L \ / \ Te \quad (3)$$

One way to replace *Inflow* in (3) is to set dL/dt to zero, which means the level is constant. Then *Inflow* will equal a balance level, Lb, divided by e-time. However, a more elegant way to replace *Inflow* is to simply define the balance level, Lb, as

$$Lb = Inflow * Te \quad (4)$$

Equation (4) shows how *Inflow* and Te set the balance level. Substitute (4) for *Inflow* into (3) to get,

$$dL/dt = -(L - Lb) \ / \ Te \quad (5)$$

Equation (5) shows the level always moves toward its balance level. At this point, both L and Lb are functions of time. Te can also be a function of time.

In the special case when Lb and Te are constant, there is an analytic solution to (5). Rearrange (5) to get

$$dL \ / \ (L - Lb) = -dt \ / \ Te \quad (6)$$

Then integrate (6) from Lo to L on the left side, and from 0 to t on the right side [29] to get

$$\text{Ln}\ [(L - Lb) \ / \ (Lo - Lb)] = -t \ / \ Te \quad (7)$$

where

Lo = Level at time zero ($t = 0$)

Lb = the balance level for a given inflow and Te

Te = time for L to move (1 – 1/e) from L to Lb

e = 2.7183

The original integration of (6) contains two absolute values, but they cancel each other because both L and Lo are always either above or below Lb.

Raise e to the power of each side of (7), to get the level as a function of time:

$$L(t) = Lb + (Lo - Lb) \exp(-t/Te) \quad (8)$$

Equation (8) is the analytic solution of (5) when Lb and Te are constant.

The hypothesis (2) that outflow is proportional to level creates a "balance level." Equation (4) defines the balance level in terms of inflow and e-time.

Figure 4 shows how the level always moves toward its

balance level according to (5). While outflow is always proportional to level, inflow sets the balance level.

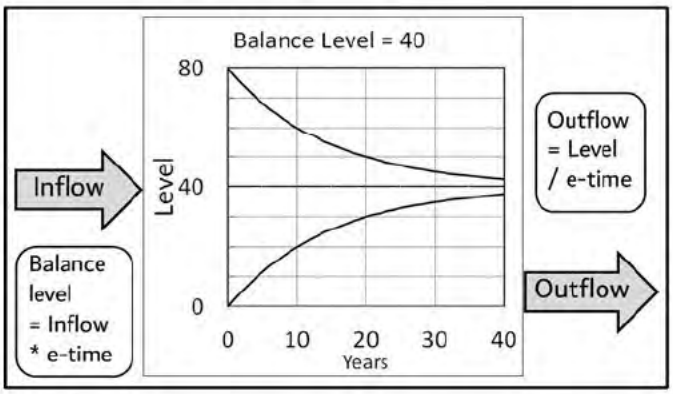

Figure 4. *Inflow sets the balance level. The level at any time t determines the outflow. Level always moves toward the balance level, whether the level is above or below the balance level.*

The Physics Model shows how CO_2 flows through the atmosphere. CO_2 does not "stick" in the atmosphere. A higher inflow merely raises the balance level. Then the level will rise until outflow equals inflow, which will be at the balance level.

3.4. Physics Model Consequences

All equations after (2) are deductions from hypothesis (2) and the continuity equation (1).

Equation (4) shows the balance level equals the product of inflow and e-time. Using IPCC numbers, and subscripts "p" to mean human (or people) and "n" to mean natural, the balance levels of human and natural CO_2 are 18.4 and 392 ppm:

$$Lbp = 4.6 \text{ (ppm/year)} * 4 \text{ (years)} = 18.4 \text{ ppm} \quad (9)$$

$$Lbn = 98 \text{ (ppm/year)} * 4 \text{ (years)} = 392 \text{ ppm} \quad (10)$$

The ratio of human to natural CO_2 is 4.6%. The percentage of human CO_2 to total CO_2 is 4.5%. Both are independent of e-time:

$$Lbp \ / \ Lbn = 4.6 \ / \ 98 = 4.6\% \quad (11)$$

$$Lbp \ / \ (Lbn + Lbp) = 4.6 \ / \ 102.6 = 4.5\% \quad (12)$$

Equation (9) shows present human emissions create a balance level of 18 ppm, independent of nature's balance level. If nature's balance level remained at 280 ppm after 1750, then present human emissions would have increased the CO_2 level 18 ppm from 280 ppm to 298 ppm.

Equation (10) shows present natural emissions create a balance level of 392 ppm. The human contribution of 18 ppm brings the total balance level to 410 ppm, which is close to the level in 2018.

Equation (11) shows the ratio of human to natural CO_2 in the atmosphere equals the ratio of their inflows, independent of e-time.

Equation (12) shows the percentage of human-produced CO_2 in the atmosphere equals its percentage of its inflow, independent of e-time.

Figure 5 illustrates these Physics Model conclusions when e-time is 4 years.

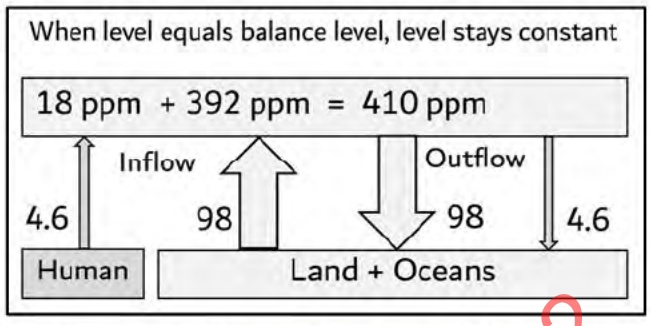

Figure 5. *For an e-time of 4 years, the human inflow of 4.6 ppm per year sets a balance level of 18 ppm, and the natural inflow of 98 ppm per year sets a balance level of 392 ppm. When the level equals the total balance level of 410 ppm, outflow will equal inflow and level will be constant.*

Equations (9) and (10) support the key conclusions of Harde [24, 25]:

Under present conditions, the natural emissions contribute 373 ppm and anthropogenic emissions 17 ppm to the total concentration of 390 ppm (2012).

4. The IPCC Bern Model

4.1. IPCC Bern Model Origin

In 1992, Siegenthaler and Joos [30] created the original Bern model. Their Figure 1 connects the atmosphere level to the upper ocean level, and the upper ocean level to the deep and interior ocean levels. They used 14C data to trace the flow of $12CO_2$ from the atmosphere to the upper ocean and to the deep and interior oceans. Using some physics constraints, they attempted without success to fit three versions of their model to available data.

Earlier, in 1987, Maier-Reimer and Hasselmann [31] used an ocean circulation model connected to a one-layer atmosphere to reproduce the main features of the CO_2 distribution in the surface ocean. They applied a mathematical curve fit to represent their conclusions. Their curve fit used a sum of four exponentials with different amplitudes and time constants, as in today's Bern model.

The use of four exponentials by [31] seems to result from their reconnection of both the deep and interior ocean levels directly to the atmosphere level. Such reconnection would be a serious modelling mistake. Other papers followed the model developed by [31].

Archer et al. [4] found the four-exponential models "agreed that 20–35% of the CO_2 remains in the atmosphere after equilibration with the ocean (2–20 centuries)."

Joos et al. [32] compared the response of such atmosphere-ocean models to a pulse emission of human CO_2. All the models predicted a "substantial fraction" of pulse would remain in the atmosphere and ocean for millennia.

The conclusions of [4, 30, 31, 32] must be questioned because:

1. Agreement among models does not prove they are

accurate.

2. All models treat human and natural CO_2 differently, which violates physics.
3. All models assume human CO_2 causes all the increase in atmospheric CO_2, which violates physics.
4. All models partition human CO_2 inflow into four artificial bins, which is unphysical.
5. All models lack a valid physics model for atmospheric CO_2.

Segalstad [10] notes that the models like [31] do not allow CO_2 to flow out of the atmosphere in linear proportion to the CO_2 level. Rather they use a non-linear constraint on the outflow that contradicts physics and chemistry.

Segalstad [10] concludes the alleged long residence time of 500 years for carbon to diffuse to the deep ocean is inaccurate because the 1000 GtC of suspended organic carbon in the upper 75 meters of the ocean can sink to the deep ocean in less than one year. That gives a residence time of 5 years rather than 500 years.

The IPCC Bern model that evolved from models like [31] artificially partitions human CO_2 into four separate bins. The separate bins prevent human CO_2 in one bin from moving to a bin with a faster e-time. This is like having three holes of different sizes in the bottom of a bucket and claiming the smallest hole restricts the flow through the largest hole.

The IPCC Bern model is unphysical. It begins with the assumption that human CO_2 causes all the increase in atmospheric CO_2. Then it creates a model that supports this assumption.

The Bern model fails Occam's Razor because it is unnecessarily complicated.

4.2. IPCC Bern Model Derivation

The Joos [33] Bern model is an integral equation rather than a level equation.

It is necessary to peer inside IPCC's Bern m del. To deconstruct the integral version of the Bern model, let inflow occur only in the year when "t-prime" equals zero. Then the integral disappears, and the Bern model becomes a level equation.

The Bern level equation is,

$$L(t) = Lo\,[A_0 \quad A_1 \exp(-t/T_1) + A_2 \exp(-t/T_2) + A_3 \exp(-t/T_3)] \qquad (13)$$

Where

t = time in years

Lo = level of atmospheric CO_2 in year $t = 0$

$L(t)$ = level of atmospheric CO_2 in year t

and the Bern TAR standard values, derived from curve-fitting the Bern model to the output of climate models, are,

$A_0 = 0.150$

$A_1 = 0.252$

$A_2 = 0.279$

$A_3 = 0.319$

$T_1 = 173$ years

$T_2 = 18.5$ years

$T_3 = 1.19$ years

The A-values weight the four terms on the right-hand side of (13):

$A_0 + A_1 + A_2 + A_3 = 1.000$

In (13), set t equal to infinity to get,

$$L = A_0\ Lo = 0.152\ Lo \qquad (14)$$

Equation (14) predicts a one-year inflow that sets Lo to 100 ppm, followed by zero inflow forever, will cause a permanent level of 15 ppm.

The four terms in (13) separate human (but not natural) CO_2 into 4 bins. Each bin has a different e-time. Only one bin allows human CO_2 to flow freely out of the atmosphere. Two bins trap human CO_2 for long times. One bin has no outflow and traps human CO_2 forever.

Figure 6 shows the size of the four Bern-model bins in percent and the amount of human CO_2 that remains in the atmosphere 8 years after an artificial pulse of human CO_2 enters the atmosphere.

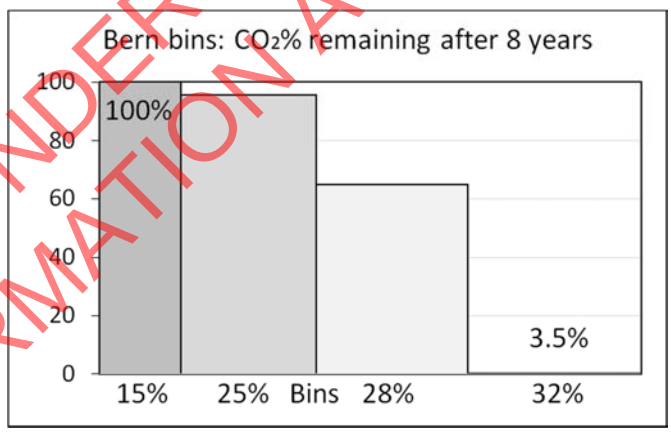

Figure 6. *The percent of human CO_2 left in each Bern model bin after 8 years.*

Bern (13) predicts 15 percent all human CO_2 entering the atmosphere stays in the atmosphere forever, 25 percent stays in the atmosphere almost forever, and only 32 percent flows freely out of the atmosphere.

4.3. How IPCC Gets 32 Percent

The burden of proof is upon the IPCC to explain how 5 percent human inflow becomes 32 percent in the atmosphere. IPCC cannot change the inflow. Therefore, IPCC must change the outflow. The IPCC Bern model restricts the outflow of human CO_2 while it lets natural CO_2 flow freely out of the atmosphere. The IPCC Bern model incorrectly treats human CO_2 differently than it treats natural CO_2. By doing so, it artificially increases human CO_2 in the atmosphere to 32 percent and beyond.

IPCC assumes its Bern model applies to human but not to natural CO_2. That assumption is unphysical because CO_2 molecules from human and natural sources are identical. All valid models must treat human and natural CO_2 the same.

If applied to natural CO_2, the Bern model predicts 15

percent of natural CO_2 sticks in the atmosphere. Then in 100 years, 1500 ppm of natural CO_2 sticks in the atmosphere. This clearly has not happened. Therefore, the Bern model is invalid.

For you mathematicians:

It is simple to prove the Bern model is unphysical. Take the derivative of (13) with respect to time. It is impossible to get rid of the exponential terms because the Bern model has more than one time constant in its exponentials. The Bern model dL/dt does not correspond to a physics formulation of a problem.

By contrast, it is straightforward to take the time derivative of the Physics Model (8) and reproduce its dL/dt form of (5).

The Physics Model began as a rate equation, as all physics models should. The Bern model began with a curve fit to an imaginary scenario for a level rather than as a rate equation for a level. The Bern model does not even include a continuity equation.

5. Theories Must Replicate Data

5.1. The 14C Data

The above-ground atomic bomb tests in the 1950s and 1960s almost doubled the concentration of 14C in the atmosphere. The 14C atoms were in the form of CO_2, called $14CO_2$.

After the cessation of the bomb tests in 1963, the concentration of $14CO_2$ decreased toward its natural balance level. The decrease occurred because the bomb-caused 14C inflow became zero while the natural 14C inflow continued.

The 14C data are in units of D14C per mil. The lower bound in D14C units is -1000. This value corresponds to zero 14C inflow into the atmosphere. In D14C units, the "natural" balance level, defined by the average measured level before 1950, is zero, 1000 up from -1000. [34]

Hua [34] processed 14C data for both hemispheres from 1954 to 2010. Turnbull [35] processed 14C data for Wellington, New Zealand, from 1954 to 2014. After 1970, $14CO_2$ were well mixed between the hemispheres and $14CO_2$ in the stratosphere were in the troposphere. The 14C data from both sources are virtually identical after 1970.

14C is an isotope of 12C. Levin et al. [36] conclude the C14 data provide "an invaluable tracer to gain insight into the carbon cycle dynamics."

5.2. Physics Model Replicates the 14C Data

The Physics Model (8) accurately replicates the $14CO_2$ data from 1970 to 2014 with e-time set to 16.5 years, balance level set to zero, and starting level set to the D14C level in 1970.

Figure 7 shows how the Physics Model replicates the 14C data.

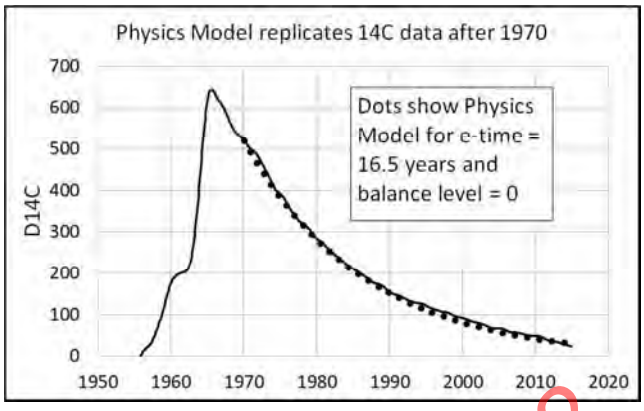

Figure 7. *The 14C data from Turnbull [35] using 721 data points. The dotted line is the Physics Model replication of the data.*

The Physics Model is not a curve fit with many parameters like the Bern model. The Physics model allows only 2 parameters to be adjusted: balance level and e-time, and they are both physical parameters. It is possible that the data would not allow replication by the Physics Model.

The replication of the 14C data begins by setting the Physics Model to the first data point in 1970. Then it is a matter of trying different balance levels and e-times until the model best fits the data. Although there is room for minor differences in the fit, the best fit seems to occur when the balance level is zero and e-time is 16.5 years.

The replication of the 14C data by the Physics Model has significant consequences. It shows the 14C natural balance level has remained close to zero and e-time has remained constant since 1970. If the e-time had changed since 1970, it would have required a variable e-time to make the Physics Model fit the data.

5.3. $12CO_2$ Reacts Faster Than $14CO_2$

Isotopes undergo the same chemical reactions but the rates that isotopes react can differ. Lighter isotopes form weaker chemical bonds and react faster than heavier isotopes [37].

Because $12CO_2$ is a lighter molecule than $14CO_2$, it reacts faster than $14CO_2$. Therefore, its e-time will be shorter than for $14CO_2$.

Equation (4) shows e-time equals *Level* divided by *Inflow*. Using IPCC numbers, e-time for $12CO_2$ is about 400 ppm divided by 100 ppm per year, or 4 years. Also, IPCC [3] agrees $12CO_2$ turnover time (e-time) is about 4 years. Segalstad [10] calculated 5 years for e-time.

Figure 8 shows the Physics Model (8) simulation of $12CO_2$ using an e-time of 4 years. For comparison, Figure 8 shows the 14C data from Hua [34] and the Physics Model replication of $14CO_2$ data with an e-time of 16.5.

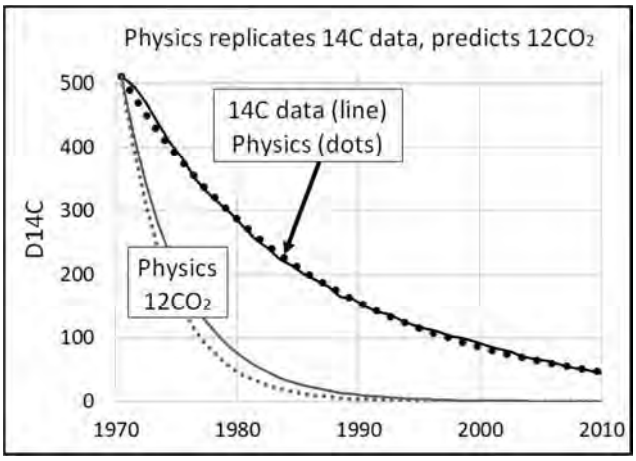

Figure 8. *This plot uses the 14C data from Hua [34] from 1970 to 2010. Hua data is in mid-years, so the fit begins in 1970.5. The Physics Model (dotted line) replicates the 14CO₂ data with an e-time of 16.5 years. The Physics Model simulates 12CO₂ for an e-time of 4 years (dotted line) and 5 years (solid line).*

5.4. IPCC Model Cannot Simulate 12CO₂

The Bern model claims to predict the outflow of $12CO_2$. Therefore, the Bern model should come close to predicting the outflow of $12CO_2$ as calculated by the Physics Model that replicates the 14C data.

Figure 9 shows the Bern model (13) predictions. The IPCC Bern model begins with a short e-time, then increases its e-time. The increased e-time causes the Bern line to cross the 14C line and thus conflicts with the 14C data. The Bern model traps 15 percent of human CO_2 in the atmosphere forever.

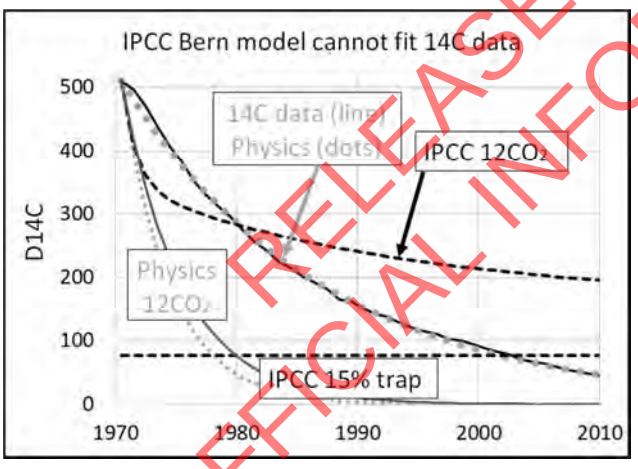

Figure 9. *The IPCC Bern model (dashed lines) is not consistent with the 12CO₂ simulation or with 14CO₂ data. The Bern model includes a trap for 15 percent of human CO₂.*

The IPCC Bern model is not just a failure to simulate data. The Bern model is a functional failure. It's e-time increases significantly with time when 14C data show e-time is constant. The only way the Bern model can increase with time is by using its history as a reference.

Figure 10 shows how the IPCC Bern model cannot even replicate itself when it is restarted at any point in its simulation.

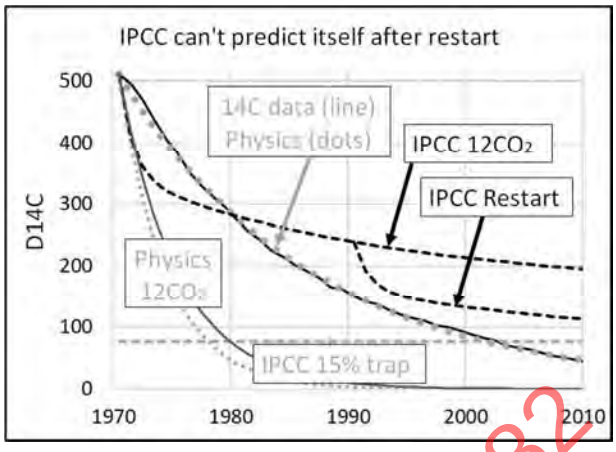

Figure 10. *The Bern model (dashed lines) cannot even replicate itself after a restart.*

The IPCC Bern model cannot continue its same prediction line if it is restarted at any point. The Bern model cannot properly restart because it depends upon its history, which makes it an invalid model.

A restart deletes the Bern model's history. This forces the Bern model to create a new history. In the real world, molecules do not remember their history. Molecules only know their present. Therefore, the IPCC Bern model fails the most basic test for a physical model.

Revelle and Suess [8] used 14C data to calculate correctly that human CO_2 would increase atmospheric CO_2 by only 1.2 percent as of 1957, based for an e-time of 5 years.

5.5. IPCC's Buffer Theory is Invalid

IPCC [3] claims:

> *The fraction of anthropogenic CO_2 that is taken up by the ocean declines with increasing CO_2 concentration, due to reduced buffer capacity of the carbonate system.*

Buffer capacity is the ability of the oceans to absorb CO_2.

Kohler et al. [7] claim human (but not natural) CO_2 has reduced the "buffer capacity" of the carbonate system:

> *The rise in atmospheric and oceanic carbon content goes along with an increase in the Revelle factor, a phenomenon which is already measurable. This implies that the oceanic uptake of anthropogenic carbon will become slower if we continue to increase anthropogenic CO_2 emissions. This is already seen in all CHIMP5 model simulations.*

Kohler's last sentence exhibits circular reasoning when it claims a model can prove what has been fed into the model.

All IPCC models use the buffer factor myth instead of Henry's Law to conclude human CO_2 causes all the rise in atmospheric CO_2 [10].

The problem for Kohler and IPCC is data. Where are the data that support their claim? They have only their models. Models are not data. Models must make predictions that replicate data. Their models cannot replicate data.

Ballantyne et al. [38] found "there is no empirical evidence" that the ability of the land and oceans to absorb atmospheric CO_2 "has started to diminish on the global scale."

The 14C data are the most accurate way to measure changes in the Revelle factor and "buffer capacity." Reduced buffer capacity, if it existed, would increase e-time. The 14C data prove e-time has been constant since 1970. Therefore, IPCC's buffer capacity has been constant.

IPCC's buffer capacity claim is absurd because it assumes only human CO_2 reduces the buffer capacity while natural CO_2 outflow does not. IPCC treats human and natural CO_2 differently, which is impossible.

Kohler [7] claims lower buffer capacity affects only $12CO_2$, not $14CO_2$. That claim violates chemistry and physics. Segalstad [10] previously showed Kohler's claim is impossible because "chemical and isotropic experiments show the equilibrium between CO_2 and water is obtained within a few hours."

The IPCC Bern model is based upon the invalid assumption that human CO_2 decreases buffer capacity.

5.6. Isotope Data Support the Physics Model

IPCC [3] writes:

> *Third, the observed isotropic trends of 13C and 14C agree qualitatively with those expected due to the CO_2 emissions from fossil fuels and the biosphere, and they are quantitatively consistent with results from carbon cycle modeling.*

Human fossil-fuel CO_2 is "14C-free" and the 14C balance level has decreased. IPCC [3] and Kohler [7] claim this proves human CO_2 caused all the rise in atmospheric CO_2.

But neither IPCC nor Kohler argue with numbers. Let's do the calculations to compare the results from both models with the data. IPCC [2] says human CO_2 comprises 32 percent of atmospheric CO_2 while the Physics Model (12) says human CO_2 is less than 5%. The question is whether the available isotope data support or reject either of the models.

RealClimate [39] says the 13C/12C ratio for human CO_2 is about 98 percent of the ratio in natural CO_2, and the 13C ratio has declined about 0.15 percent since 1850. RealClimate says this proves human CO_2 caused all the increase in atmospheric CO_2 since 1850.

Human CO_2 causes the new balance level of D14C and 13C/12C to be:

$$Lb = Ln\ Rn + Lh\ Rh \qquad (15)$$

Where

Lb = the new balance level (of D14C or 13C/12C)

Ln = the natural balance level (D14C = 0; 13C/12C = 100%)

Lh = the human balance level (D14C = –1000; 13C/12C = 98%)

Rn = the fraction of natural CO_2

Rh = the fraction of human CO_2

The Physics Model predicts for D14C:

$$Lb = (0)\ (0.955) + (-1000)\ (0.045) = -45 \qquad (16)$$

The IPCC model predicts for D14C:

$$Lb = (0)\ (0.68) + (-1000)\ (0.32) = -320 \qquad (17)$$

The Physics Model predicts for 13C/12C:

$$Lb = (100)\ (0.955) + (98)\ (0.045) = 99.91 \qquad (18)$$

The IPCC model predicts for 13C/12C:

$$Lb = (100)\ (0.680) + (98)\ (0.320) = 99.36 \qquad (19)$$

The 14C data

The Physics Model (16) predicts human CO_2 has lowered the balance level of 14C from zero to –45. The IPCC model (17) predicts human CO_2 has lowered the 14C balance level to –320.

Figure 11 compares the Physics and IPCC predicted levels for human CO_2 in the atmosphere.

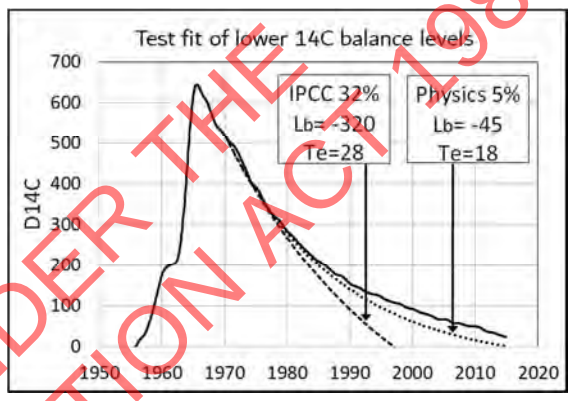

Figure 11. *The dotted lines show the Physics Model calculation for a balance level of –4. The dashed line shows the Physics Model calculation for the IPCC predicted balance level of -320.*

Figure 11 shows the Physics Model result of 5 percent human CO_2 in the atmosphere matches the 14C data much better than the IPCC model of 32 percent of human CO_2 in the atmosphere.

In summary, the 14C data support the Physics Model and reject the IPCC model.

The 13C data

The Physics Model (18) predicts human CO_2 has lowered the 13C ratio by 0.09. The IPCC model (19) predicts human CO_2 has lowered the 13C ratio by 0.64.

Figure 12 compares the Physics and IPCC predictions of the 13C/12C ratio to Real Climate's numbers.

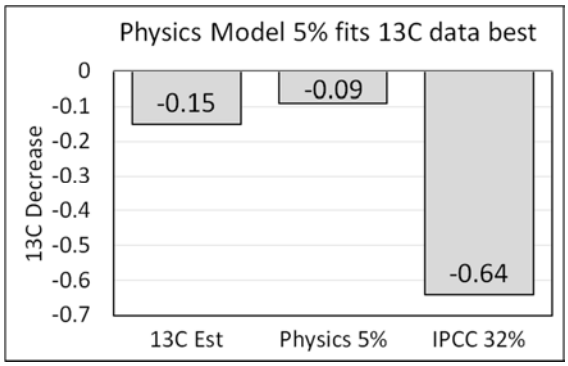

Figure 12. *Real Climate [39] says the 13C ratio has decreased by 0.15 since 1750. Physics predicts a decrease of 0.09 and IPCC predicts a decrease of 0.64.*

There seem to be no error bounds in the available 13C data. Nevertheless, even without error bounds the 13C data do not support the IPCC model over the Physics Model. So, the IPCC argument fails.

Segalstad [10] calculated similar results using permil units. He concluded the isotope data show human CO_2 cannot be more than 4 percent of atmospheric CO_2.

5.7. Mauna Loa Data

Some scientists argue that a viable CO_2 model must replicate the Mauna Loa CO_2 data. The Physics Model can simulate the Mauna Loa data for atmospheric CO_2 as well as any other model.

Spencer [40] has a model that fits the Mauna Loa data. Spencer assumes like the IPCC that the natural level of CO_2 is fixed at 280 ppm and human CO_2 causes all the increase in atmospheric CO_2. His model has many variables available to adjust so a fit to the Mauna Loa data is guaranteed.

The significance of the fit by the Physics Model is that it comes with physical constraints that the other models do not have. The Physics Model e-time must be 4 years and natural CO_2 must be 95 percent of atmospheric CO_2.

Figure 13 shows how the Physics Model fits the Mauna Loa data.

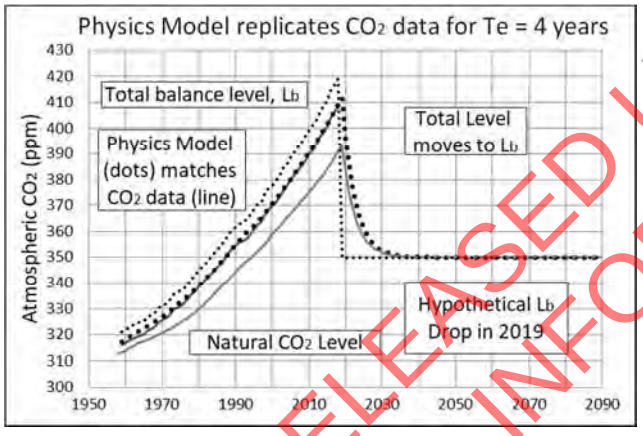

Figure 13. *The Physics Model replicates the Mauna Loa data with an e-time of 4 years and the requirement that natural CO_2 is 95 percent of atmospheric CO_2.*

In Figure 14, the total balance level is the sum of natural and human balance levels. The balance level continues to rise. Level follows the balance level with a lag of about 4 years (the e-time), after the year 2000. This lag keeps the level about 10 ppm below the its balance level. Human CO_2 adds to the natural level to produce the total level, about 15 ppm above the natural level.

In 2019, the balance level in Figure 14 is artificially reset to 350 ppm to test how fast the CO_2 level moves to the new balance level. The total CO_2 level falls to its new balance level of 350 ppm in about 10 years. No CO_2 remains stuck in the atmosphere.

5.8. Ice-core Data

IPCC claims "the observational CO_2 records from ice cores … show that the maximum range of natural variability about the mean of 280 ppm during the past 1000 years was small."

Using this invalid claim, IPCC assumes natural CO_2 emissions remained constant within about one percent. IPCC's invalid claim about ice-core data is the basis of IPCC's invalid claim that human CO_2 causes all the increase in atmospheric CO_2 above 280 ppm. This increase is presently 130 ppm or 32 percent.

Siegenthaler and Joos [30] observed that ice-core data show natural CO_2 increased by 17 ppm or 6 percent before 1900, when human CO_2 emissions totaled only 5 ppm. These ice-core data contradict IPCC's claim that natural CO_2 emissions stayed constant after 1750.

Jaworoski [12] explains why ice-core data do not properly represent past atmospheric CO_2. He concludes nature produces 97 percent of atmospheric CO_2.

Proxy ice-core values for CO_2 remained low for the past 650,000 years [10, 12]. If these ice-core values represent atmospheric CO_2, then atmospheric CO_2 did not cause any of the global warming in the last 650,000 years. And if CO_2 did not cause global warming in the past, then the IPCC has lost its claim that CO_2 causes present global warming [12].

Leaf stomata and chemical data prove the historical CO_2 level was much higher than derived from ice cores [12]. There is no evidence that the pre-industrial CO_2 level was 280 ppm as IPCC assumes.

Beck [13] reconstructed CO_2 from chemical data show the level reached 440 ppm in 1820 and again in 1945.

IPCC's claim that human CO_2 produces all the increase in atmospheric CO_2 above 280 ppm is invalid. In science, when data contradict a theory, the theory false. The IPCC, however, ignores how its theories contradict data.

6. Theories Must Be Logical

6.1. IPCC's Response Times Fail Physics

The Physics Model e-time has a precise definition: e-time is the time for the level to move (1 – 1/e) of the distance to its balance level.

Segalstad [10] observes IPCC [3] uses many definitions of lifetime — like residence time, transit time, response time, e-folding time, and adjustment time — in its quest to prove human CO_2 remains in the atmosphere for hundreds of years. Many investigators, from 1957 to 1992, have calculated the e-time of atmospheric CO_2 is about 5 years [10].

IPCC [3] defines "adjustment time (*Ta*)" as:

The time-scale characterising the decay of an instantaneous pulse input into the reservoir.

Cawley [5] defines "adjustment time (*Ta*)" as:

The time taken for the atmospheric CO_2 concentration to substantially recover towards its original concentration following a perturbation.

The word "substantially" is imprecise.

Cawley follows IPCC to define "residence time (*Tr*)" as:

The average length of time a molecule of CO_2 remains in the atmosphere before being taken up by the oceans or terrestrial

biosphere.

Some authors use "residence time" to mean "e-time" but other authors, such as Cawley and IPCC, have a different meaning for residence time. This paper uses e-time because its definition is precise.

In summary, IPCC uses two different response times when it should use only e-time:

1. When the level is far from its balance level (which can be zero), IPCC thinks e-time is an *adjustment* time because the level is moving rapidly toward its balance level.
2. When the level is close to its balance level, IPCC thinks e-time is a *residence* time because "molecules" are flowing in and out with little change in level.

Figure 14 illustrates how e-time relates to IPCC's adjustment and residence times.

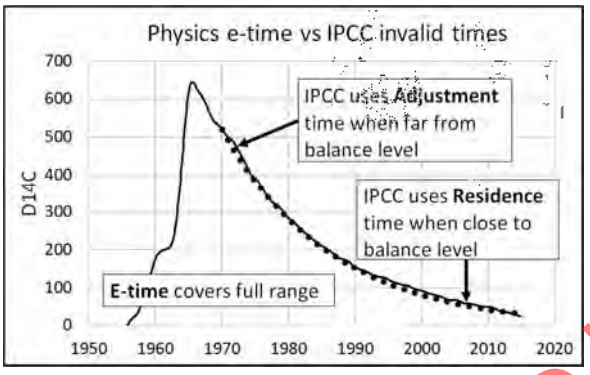

Figure 14. *E-time covers the full range of movement of level to a balance level. IPCC [3] adjustment and residence times apply to only each end of the range.*

IPCC defines "turnover time (*Tt*)" as:

The ratio of the mass M of a reservoir (e.g., a gaseous compound in the atmosphere) and the total rate of removal S from the reservoir: Tt = M/S.

IPCC's turnover time seems to be the same as e-time except "removal" is not the same as outflow. Near the balance level, IPCC sometimes interprets "removal" to mean the difference between outflow and inflow.

IPCC says when outflow is proportional to level (the Physics Model hypothesis) then adjustment time equals turnover time. IPCC claims:

In simple cases, where the global removal of the compound is directly proportional to the total mass of the reservoir, the adjustment time equals the turnover time: Ta = Tt.

The Physics Model's replication of the 14C data shows the $14CO_2$ outflow is proportional to level. Therefore, by IPCC's own definition, adjustment time equals e-time equals residence time.

IPCC says in further confusion:

In more complicated cases, where several reservoirs are involved or where the removal is not proportional to the total mass, the equality T = Ta no longer holds.

Carbon dioxide is an extreme example. Its turnover time is only about 4 years because of the rapid exchange between atmosphere and the ocean and terrestrial biota.

Although an approximate value of 100 years may be given for the adjustment time of CO_2 in the atmosphere, the actual adjustment is faster initially and slower later on.

IPCC agrees $12CO_2$ turnover time (e-time) is about 4 years. IPCC claims adjustment time is "fast initially and slower later on" which is why its Bern model cannot replicate the 14C data in Figure 9.

The 14C data show the e-time for $14CO_2$ is 16.5 years. This e-time is the upper bound for $12CO_2$ e-time. The IPCC claim of hundreds of years is based on IPCC's misunderstanding of e-time.

Unfortunately, there are many different definitions of residence time. Therefore, this paper uses e-time with its exact definition.

6.2. IPCC's First Core Argument Is Illogical

The IPCC [2] first core argument notes that human emissions from 1750 to 2013 totaled 185 ppm while atmospheric CO_2 increased by only 117 ppm. These numbers are OK. But IPCC claims this proves human CO_2 caused all the increase in atmospheric CO_2 above 280 ppm. IPCC's logic is faulty.

Figure 15 shows the IPCC first core argument.

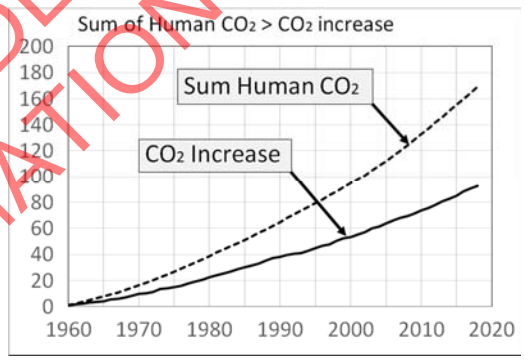

Figure 15. *The sum of human CO_2 year-by-year is larger than the increase in atmospheric CO_2.*

However, the fact that the sum of human emissions is greater than the increase does not prove human CO_2 caused the increase. The IPCC argument omits natural CO_2 which totaled about 6000 ppm during the same period, much larger than the sum of human CO_2.

Figure 16 shows the plot when the sum of natural CO_2 is included.

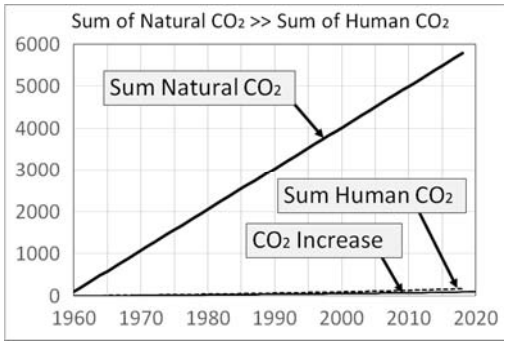

Figure 16. *The sum of natural CO_2 compared to the sum of human CO_2 and the increase in CO_2.*

The sum of natural CO_2 from 1959 to 2018 is 5700. The sum of human CO_2 over the same period is 170 ppm which is 3 percent of the natural CO_2 sum. IPCC's whole case depends upon its incorrect assumption that nature did not vary more that 3 percent since 1959 or since 1750. At the same time, IPCC admits it does not know nature's CO_2 emission within 50 percent.

The fundamental error in this IPCC argument is discussed in Section 3.1. The sums of inflows do not matter because inflows do not "add" to atmospheric CO_2. Inflows set balance levels. The human effect on the total balance level is less than 5 percent.

6.3. IPCC's Second Core Argument Is Illogical

IPCC [2] claims nature has been a "net carbon sink" since 1750, so nature could not have caused the observed rise in atmospheric carbon dioxide. Please refer to Figure 5 that shows the inflow and outflow of atmospheric CO_2.

Of course, nature is a "net carbon sink" because nature absorbs human CO_2 emissions. However, absorption of human CO_2 has no bearing whatsoever on how much natural CO_2 flows into the atmosphere. Nature can set its inflow as it pleases, no matter how much human inflow nature absorbs. The 98-ppm natural flow can double or reduce to one-half while nature continues to absorb the outflow of the human addition to atmospheric CO_2. So, the IPCC argument is absurd.

The Physics Model shows how CO_2 inflows set balance levels in atmospheric CO_2. At the balance level, outflow will equal inflow. No CO_2 gets trapped in the atmosphere.

6.4. Key IPCC Paper Makes Serious Errors

Kohler [7] uses Cawley [5] to "prove" the IPCC case. But Cawley fails physics and statistics.

Cawley [5] is a key paper for the IPCC theory. Cawley claims human CO_2 caused all the increase of atmospheric CO_2 above the 280 ppm in 1750. But Cawley's attempted proof fails physics.

Figure 17 shows three of Cawley's equations.

$$F_e = k_e C + F_e^0. \quad (3)$$

$$\frac{dC_A}{dt} = -\frac{C_A F_e}{C} \quad (7)$$

$$\frac{dC_N}{dt} = F_i^0 - \frac{C_N F_e}{C} \quad (8)$$

Figure 17. *Equations from Cawley [5].*

Cawley's equation (3) attempts to do the same job as Physics Model (2), namely, to represent how level sets outflow. But Cawley adds to his equation (3) a second term that represents a steady-state outflow that is independent of level. Cawley's added term is fictitious because his first term on the right side of his equation (3) is the true source of all outflow. As a result, all Cawley's equations after his (3) are wrong, which makes his whole paper wrong.

Cawley's equation (7) should include his Fa for human inflow. His equations (7) and (8) should omit his arbitrary Fe for outflow and set outflow equal to level (his C) divided by his residence time. His residence time is also inaccurate as shown in Section 6.1.

6.5. Statistical Correlation

Cawley [5] argues,

Lastly, the rise in atmospheric carbon dioxide closely parallels the rise in anthropogenic emissions ... which would be somewhat of a coincidence if the rise were essentially natural in origin!

IPCC [3] writes:

Second, the observed rate of CO_2 increase closely parallels the accumulated emission trends from fossil fuel combustion and from land use changes.

IPCC incorrectly claims this proves human CO_2 causes the increase in atmospheric CO_2.

A standard scientific test for the non-existence of cause and effect is to show the correlation of the assumed cause with the assumed effect, is zero.

For the IPCC to argue that human CO_2 causes climate change, the IPCC must show that the correlation of human emissions with the increase in atmospheric CO_2 is significantly greater than zero.

Proper statistics requires a detrended analysis of a time series to conclude cause and effect. Munshi [41] shows the "detrended correlation of annual emissions with annual changes in atmospheric CO_2" is zero. Chaamjamal [42] extended Munshi's calculations and found the correlations are zero for time intervals from one to five years.

Therefore, the standard statistical test for cause and effect proves human CO_2 is insignificant to the increase in atmospheric CO_2.

The ratio of annual change in atmospheric CO_2 to annual human CO_2 emissions that Munshi [41] tested is IPCC's "airborne fraction". Therefore, IPCC's airborne fraction has no useful meaning.

An estimate of the airborne fraction is about 2.5 ppm/year divided by 5 ppm/year, or 0.5. Since the increase in level is caused by an increase in natural CO_2 emissions, the airborne fraction has little physical meaning, and it would go to infinity if human emissions stopped.

7. Conclusions

The IPCC model and the Physics model compete to describe how human CO_2 emissions add to atmospheric CO_2. Both models agree that the CO_2 inflow into the atmosphere is less than 5 percent human CO_2 and more than 95 percent natural CO_2.

The IPCC model concludes that human CO_2 causes all the increase in atmospheric CO_2 above 280 ppm; that 15 percent of all human CO_2 emissions stays in the atmosphere forever; that 53 percent stays for hundreds of years; and only 32 percent flows freely out of the atmosphere like natural CO_2.

The Physics Model treats human CO_2 and natural CO_2 the

same because their CO_2 molecules are identical. The Physics model makes only one hypothesis: CO_2 outflow equals the level of CO_2 in the atmosphere divided by e-time.

The Physics Model concludes that inflow sets a balance level equal to inflow multiplied by e-time, and that continuing inflow does not continue to increase atmospheric CO_2. Rather inflow sets a balance level where outflow equals inflow and continuing inflow will not further increase the level of atmospheric CO_2 beyond the balance level.

The proper test of two theories is not to claim the IPCC theory explains "observational evidence." The proper test is the scientific method: if a prediction is wrong, the theory is wrong.

The 14C data following the cessation of the atomic bomb tests show how the level of CO_2 in the atmosphere returns to its balance level after inflow decreases. All valid models of atmospheric CO_2 must be able to replicate the 14C data.

The Physics Model exactly replicates the 14C data after 1970. This replication shows the e-time for $14CO_2$ is 16.5 years and that this e-time has been constant since 1970. The replication shows the Physics Model hypothesis — that outflow equals level divided by e-time — is correct.

The IPCC Bern model cannot replicate the 14C data. Its curve crosses the 14C data curve. The Bern model cannot even replicate itself if it is restarted at any point. This failure proves the IPCC Bern model does not have the mathematical structure for a valid model.

If natural CO_2 is inserted into the Bern model, as physics requires, the Bern model predicts that 15 percent of natural CO_2 inflow sticks in the atmosphere forever, which contradicts data and proves the Bern model is invalid.

The Physics Model concludes that the ratio of human to natural CO_2 in the atmosphere equals the ratio of their inflows independent of e-time, and that the e-times for both human and natural CO_2 are the same. Usin IPCC data, the e-time for $12CO_2$ is about 4 years.

The ratio conclusion means human CO_2 adds only about 18 ppm and natural CO_2 adds about 392 ppm to today's CO_2 level of 410 ppm. If all human CO_2 emissions stopped and natural CO_2 emissions stayed constant, then the level of atmospheric CO_2 would fall only to 392 ppm in about 10 years. Nothing would be gained by stopping human CO_2 emissions. There are no long-term effects of human CO_2 emissions. Continued constant CO_2 emissions do not add more CO_2 to the atmosphere. Continued constant CO_2 emissions simply maintain the balance level.

Acknowledgements

The author thanks Chuck Wiese, Laurence Gould, Tom Sheahen, Charles Camenzuli, and others who reviewed this paper and provided scientific critique and suggestions. The author thanks Daniel Nebert, Gordon Danielson, and Valerie Berry, who provided language and grammar suggestions.

This research did not receive any grant from funding agencies in the public, commercial, or not-for-profit sectors. This research was funded solely by the personal funds of the author.

Author's Contributions

The author declares he is the only contributor to the research in this paper.

Downloads

Download supporting files.

References

[1] USGCRP, 2017: Climate Science Special Report: Fourth National Climate Assessment, Volume I. U.S. Global Change Research Program, Washington, DC, USA, 470 pp; 2018. doi: 10.7930/J0J964J6. https://science2017.globalchange.gov/

[2] IPCC, 2001: Working Group 1: The scientific basis. The Carbon Cycle and Atmosphere CO_2. https://www.ipcc.ch/site/assets/uploads/2018/02/TAR-03.pdf

[3] IPCC, 2007: Climate Change 2007: The Physical Science Basis. https://www.ipcc.ch/site/assets/uploads/2018/05/ar4_wg1_full_report-1.pdf

[4] D. Archer, M. Eby, V. Brovkin, A. Ridgwell, L. Cao, U. Mikolajewicz, et al., "Atmospheric Lifetime of Fossil Fuel Carbon Dioxide". Annu. Rev. Earth Planet. Sci., 37, pp. 117–134; 2009. https://www.annualreviews.org/doi/pdf/10.1146/annurev.earth.031208.100206

[5] G. C. Cawley, "On the Atmospheric residence time of anthropogenically sourced CO_2". Energy Fuels 25, pp. 5503–5513; 2011. http://dx.doi.org/10.1021/ef200914u

[6] Z. Kern, M. Leuenberger, Comment on "The phase relation between atmospheric CO_2 and global temperature" by Humlum et al. Glob. Planet. Change 100: 51–69.: Isotopes ignored. Glob. Planet. Chang. 109, 1–2; 2013. https://dx.doi.org/10.1016/j.gloplacha.2013.07.002

[7] P. Kohler, J. Hauck, C. Volker, D. A. Wolf-Gladrow, M. Butzin, J. B. Halpern, et al. Comment on "Scrutinizing the carbon cycle andCO_2residence time in the atmosphere" by H. Harde, Global and Planetary Change; 2017. https://www.soest hawaii.edu/oceanography/faculty/zeebe_files/Publications/KoehlerGPC17.pdf

[8] R. Revelle, H. Suess, "CO_2 exchange between atmosphere and ocean and the question of an increase of atmospheric CO_2 during past decades". Tellus. 9: 18-27; 1957. http://onlinelibrary.wiley.com/doi/10.1111/j.2153-3490.1957.tb01849 x/abstract.

[9] C. Starr, "Atmospheric CO_2 residence time and the carbon cycle". Science Direct, 18, 12, pp. 1297-1310; 1992. https://www.sciencedirect.com/science/article/pii/0360544293900178

[10] T. V. Segalstad, "Carbon cycle modelling and the residence time of natural and anthropogenic atmospheric CO_2: on the construction of the "Greenhouse Effect Global Warming" dogma". In: Bate, R. (Ed.): *Global warming: the continuing debate*. ESEF, Cambridge, U. K. [ISBN 0952773422]: 184-219; 1998. http://www.CO_2web.info/ESEF3VO2.pdf

[11] Z. Jaworowski, "Climate Change: Incorrect information on pre-industrial CO_2". Statement written for the Hearing before the US Senate Committee on Commerce, Science, and Transportation. 2003. http://www mitosyfraudes.org/Calen5/JawoCO_2-Eng.html

[12] Z. Jaworowski, "CO_2: The Greatest Scientific Scandal of our Time". 21st CENTURY Science & Technology. 2007. https://21sci-tech.com/Articles%202007/20_1-2_CO_2_Scandal .pdf

[13] E. Beck, "180 Years of Atmospheric CO_2 Gas Analysis by Chemical Methods". Energy & Environment. Vol 18, No. 2. 2007. https://21sci-tech.com/Subscriptions/Spring%202008%20ON LINE/CO_2_chemical.pdf

[14] A. Rorsch, R.S. Courtney, D. Thoenes, "The Interaction of Climate Change and the CO_2 Cycle". Energy & Environment, Volume 16, No 2; 2005. https://journals.sagepub.com/doi/pdf/10.1260/0958305053749 589

[15] R.S. Courtney, "Limits to existing quantitative understanding of past, present and future changes to atmospheric CO_2 concentration". International Conference on Climate Change, New York. 2008. https://www.heartland.org/multimedia/videos/richard-courtney -iccc1

[16] T, Quirk, "Sources and sinks of CO_2". Energy & Environment. Volume: 20 Issue: 1, pp. 105-121. 2009. https://journals.sagepub.com/doi/10.1260/0958305097876891 23

[17] R. E. Essenhigh, "Potential dependence of global warming on the residence time (RT) in the atmosphere of anthropogenically sourced CO_2". Energy Fuel 23, pp. 2773-2784; 2009. https://pubs.acs.org/doi/abs/10.1021/ef800581r

[18] J. A. Glassman, "On why CO_2 is known not to have accumulated in the atmosphere and what is happening with CO_2 in the modern era". Rocket Scientist Journal; 2010. https://www.rocketscientistsjournal.com/2007/06/on_why_CO 2_is_known_not_to_hav.html#more

[19] M. L. Salby, "Physics of the Atmosphere and Climate". Cambridge University Press 2012. (ISBN: 978-0-521-76718-7) https://www.amazon.com/Physics-Atmosphere-Climate-Murr y-Salby/dp/0521767180/ref=mt_hardcover?_encoding=UTF8 &me=

[20] M. L. Salby, "Relationship Between Greenhouse Gases and Global Temperature". Video Presentation, April 18, 2013. Helmut-Schmidt-University Hamburg. https://www.youtube.com/watch?v=2ROw_cDKwc0

[21] M. L. Salby, "Atmosphere Carbon". Video Presentation, July 18, 2016. University College London. https://www.youtube.com/watch?v=3q-M_uYkpT0&feature= youtu.be

[22] M. L. Salby, "What is really behind the increase in atmospheric CO_2?" Video Presentation, October 10, 2018. Helmut-Schmidt-University Hamburg, Germany. https://www.youtube.com/watch?time_continue=10&v=rohF6 K2avtY

[23] O. Humlum, K. Stordahl, J.E. Solheim, "The phase relation between atmospheric CO_2 and global temperatures". Global and Planetary Change, 100, pp 51-69, 2013. https://www.sciencedirect.com/science/article/pii/S092181811 2001658

[24] H. Harde, "Scrutinizing the carbon cycle and CO_2 residence time in the atmosphere". Global and Planetary Change. 152, 19-26; 2017. https://www.sciencedirect.com/science/article/pii/S092181811 6304787.

[25] H. Harde, "What Humans Contribute to Atmospheric CO_2: Comparison of Carbon Cycle Models with Observations". Earth Sciences Vol. 8, No. 3, 2019, pp. 139-159. doi: 10.11648/j.earth.20190803.13 http://www.sciencepublishinggroup.com/journal/paperinfo?jo urnalid=161&doi=10.11648/j.earth.20190803.13, http://article.esjournal.org/pdf/10.11648.j.earth.20190803.13.p df

[26] E. X Berry, "A fatal flaw in global warming science". Basic Science of a Changing Climate. Porto University Portugal. Sep 7; 2018. https://www.portoconference2018.org/uploads/1/1/7/3/117342 822/11_edwinberryportosep7final.pdf

[27] E. X Berry, "Contradictions to IPCC's climate change theory". Annual meeting of the American Meteorological Society, Phoenix; 2019. https://ams.confex.com/ams/2019Annual/meetingapp.cgi/Pape r/349565

[28] T. Boden, B. Andres, (2017) Global CO_2 emissions from fossil-fuel burning, cement manufacture, and gas flaring: 1751-2014. http://cdiac.ornl.gov/ftp/ndp030/global.1751_2014.ems.

[29] H. B. Dwight, "Tables of Integrals and Other Mathematical Data" Item 90.1. MacMillian Company; 1955. https://www.amazon.com/Tables-Integrals-Other-Mathematica l-Data/dp/0023311703

[30] U. Siegenthaler, F. Joos, "Use of a simple model for studying oceanic tracer distributions and the global carbon cycle". Tellus, 44B, 186-207; 1992. https://onlinelibrary.wiley.com/doi/10.1034/j.1600-0889.1992. t01-2-00003 x/epdf

[31] E. Maier-Reimer, L. Hasselmann, "Transport and storage of CO_2 in the ocean – an inorganic ocean-circulation carbon cycle model". Climate Dynamics 2 (2):63–90; 1987. DOI: 10.1007/BF01054491

[32] F. Joos, R. Roth, J. S. Fuglestvedt, G. P. Peters, I. G. Enting, von Bloh, et al. "Carbon dioxide and climate impulse response functions for the computation of greenhouse gas metrics: a multi-model analysis". Atmospheric Chemistry and Physics 13 (5), doi: 10.5194/acpd-12-19799-2012. Atmos. Chem. Phys. 13, 2793-2825; 2013. https://www.atmos-chem-phys net/13/2793/2013/acp-13-2793 -2013.pdf https://www.researchgate net/publication/235431147_Carbon_ dioxide_and_climate_impulse_response_functions_for_the_co mputation_of_greenhouse_gas_metrics_A_multi-model_analy sis

[33] F. Joos, "Parameters for tuning a simple carbon cycle model". 2002. https://unfccc.int/resource/brazil/carbon html

[34] Q. Hua, M. Barbetti, A. Z. Rakowski. "Atmospheric radiocarbon for the period 1950–2010". RADIOCARBON, Vol 55, pp. 2059–2072. Table S2c. 2013. https://doi.org/10.2458/azu_js_rc.v55i2.16177

[35] J. C. Turnbull, S. E. Mikaloff Fletcher, I. Ansell, G. W. Brailsford, R. C. Moss, Norris, et al. "Sixty years of radiocarbon dioxide measurements at Wellington, New Zealand: 1954–2014". Atmos. Chem. Phys., 17, pp. 14771–14784. 2017. https://doi.org/10.5194/acp-17-14771-2017

[36] I. Levin, T. Naegler, B. Kromer, M. Diehl, R. Francey, A. Gomez-Pelaez, et al., "Observations and modelling of the global distribution and long-term trend of atmospheric $14CO_2$". Tellus B: Chemical and Physical Meteorology. 2010. https://www.tandfonline.com/doi/abs/10.1111/j.1600-0889.2009.00446 x

[37] Wikipedia: Isotopes. https://simple m.wikipedia.org/wiki/Isotope

[38] A. P. Ballantyne, C. B. Alden, J. B. Miller, P. P. Tans, J. W. C. White, "Increase in observed net carbon dioxide uptake by land and oceans during the past 50 years", Nature 488, pp. 70-73, 2012. doi:10.1038/nature11299. https://www.researchgate net/publication/230615762_Increase_in_observed_net_carbon_dioxide_uptake_by_land_and_oceans_during_the_past_50_years

[39] RealClimate, "How do we know that recent CO_2 increases are due to human activities?". 2004. http://www realclimate.org/index.php/archives/2004/12/how-do-we-know-that-recent-cosub2sub-increases-are-due-to-human-activities-updated/

[40] R. Spencer, "A simple model of the atmospheric CO_2 budget". 2019. http://www.drroyspencer.com/2019/04/a-simple-model-of-the-atmospheric-CO_2-budget/

[41] J. Munshi, "Responsiveness of atmospheric CO_2 to fossil fuel emissions: Updated". SSRN; 2017. https://papers.ssrn.com/sol3/papers.cfm?abstract_id=2997420

[42] Chaamjamal, "Fossil fuel emissions and atmospheric composition". Thongchai Thailand. 2019. https://tambonthongchai.com/2018/12/19/CO_2responsiveness/

GLOBAL WARMING *alias* CLIMATE CHANGE

[*the* NON-EXISTENT, *incredibly expensive,* THREAT TO US ALL, *including to our* GRANDCHILDREN]

by David Kear, 34 West End, Ohope, Whakatane, NZ

**(former Director-General, NZ DSIR;
United Nations consultant; & South Pacific geoscientist)**

INTRODUCTION

"Climate Change" has become an important international topic - one might almost say religion. It began life as "Global Warming".

So very many people, including politicians and "news people", appear to have been overwhelmed by it, and have led others to believe, and follow the doctrine.

It has sponsored a good deal of international co-operation, which can only have been good.

However, the cost of "Combating Carbon" has been extremely high, and the debt and economic consequences are being passed on to present citizens, and, worse still, to future generations, including all our grandchildren.

This booklet attempts to raise, in citizens' minds, questions regarding the enormous sums of money and effort being wasted on this topic.
Is it soundly based?
Will it "do good" or "do bad" for ordinary citizens?
Do those promoting it deserve our attention?

This booklet suggests that Global-Warming-alias-Climate-Change, as proposed by "Global Warmers" makes no sense. You, as the reader, must judge that for yourself - not to help the writer of this booklet, but to help you and your family.

Do you think after reading all this that the proponents are absolutely reliable?

Should you add your voice to those against it, or at least talk to your councillors and members of parliament and see how they feel?

.

THE ANCIENT ACCEPTABLE VIEW

Our Earth's climate is highly variable, and records show clearly that it always has been so. Animals and plants have had no option but *to accept what comes*, and to adapt life in *ways that suit best*. Evolution gave some help by introducing "*the Survival of the Fittest*"

Humans found early that their discussion and understanding were helped by a belief in some extraneous source being the cause of recorded changes of climate - perhaps with divine power. This booklet uses "Mother Nature" in that role to avoid wordy explanations.

Humans discovered that they could ameliorate climatic effects with buildings, clothing *and the rest*, and even create "microclimates" through windbreaks, forest clearing, artificial lakes, fossil fuel burning, *and the rest*. However, no-one originally thought seriously that man could change the basic influences to our climate – our Sun our Earth's rotation, the total quantity of our Planet's water, *and the rest*. Mother Nature is able to change all such things (and has been doing so for some 3,000,000,000 years), *but we are not*.

THE NEW BELIEF - THE NEW PROBLEM

Introduction

That ancient and acceptable view was amended in the minds of some people whom I call the "Global Warmers". I've heard nothing convincing about their so-called "Science"; but what they publish convinces me that it's close to nonsense. The most convincing evidence against it comes mostly from the Global Warmers themselves.

In this booklet, the beliefs of "Global Warming", and "Climate Change" have initial capital letters. That contrasts with natural warming, or natural changing of climate - indicated by lower case initial letters. The idea of a human cause is much less than 300 years old.

My interest in our changing climate and sea level

During fieldwork for a PhD thesis[c] I found a coastal exposure of soft sandstone at Ohuka Creek, south of Port Waikato. There were Pliocene fossils of marine shellfish *below* an extensive horizontal bedding plane. *Above* that plane were more fossils, but of cool-loving[a] plants. A finger could show the exact location of the abrupt change to the cooler climate at the onset of the first of the world-wide Pleistocene glaciations [Ice Ages]. Ice formed widely at the ultimate expense of sea water, so sea level fell. At Ohuka, sea bed had become land. Such changes are rarely seen in a continuous sequence, so I recorded it in a 1957 scientific paper[b]. That resulted in my joining an informal world-wide Group researching changing sea levels.

Most interest then was about the rate of sea level rise as the Earth warmed following the "Little Ice Age". That cool period, from about 1500 to 1700 AD, halted wine-making in England and taro cropping in New Zealand. Our Group determined the rate of sea level rise in many different World regions, from widely-available readings of tide gauges (less variable than those of thermometers). The average for us all was 125 mm/century ("***125***" here). Hence it would take 8 centuries for sea level to rise 1m – no serious threat to us.

Global Warming Dawns Subsequently, I attended many international science conferences representing DSIR, NZ or Pacific Nations. I noted the words "Global Warming" appearing increasingly in paper titles, and sensed a growing number of adherents. Those latter arranged a first-ever "Conference on Global Warming" in Vienna in 1985. Unlike most such meetings, where a communiqué summarising achievements was released on the final day, the full results of this one were delayed for over 2 years.

When they did appear (front page, *NZ Herald*, two days before Christmas 1987) a *World Declaration* included "Overseas scientists have estimated that the seas around New Zealand will rise by up to 1.4 m in the next 40 years". That article concentrated on the massive consequent problems, caused by our carbon dioxide (CO_2) emissions, but gave no adequate supporting science. That rate of rise was equivalent to ***3,500*** mm/century, 28 times faster than our ***125.*** Hence we stupidly ignored it, thinking no-one could possibly believe it. But the World did believe, and the Global Warming mirage was born. Had ***3,500*** been true, sea level should have risen by almost 1 m by today – it hasn't, not even closely.

This showed unambiguously that those "Overseas Scientists" were not true scientists. They ignored a most important basic rule of true science "*Thou shall not publish Science without first checking it.* A check against local tide gauges would have shown how wrong *1.4 m in 40 yrs* was; *they simply hadn't bothered to check.* That was a **First Grave Error.**

Australian government scientists were concerned about the effects on Pacific Island nations by any sea level rise of around ***3,500*** mm/century, and launched a project to determine the correct figure at that time. They announced the result at the 1992 meeting of SOPAC – a geoscientific organisation of South Pacific nations. Their figure was ***122*** mm/century, confirming the order of magnitude of our group's ***125*** average value.

Fooling the World The Global Warmers persisted with their use of pseudo-science and made further predictions. Understandably they too all proved wrong. At conferences I began to hear, regardless of the science involved, when a speaker wished to "rubbish" some scientific idea or research, he/she stated that conclusion firmly, and followed it by "*Just like Global Warming*". Clearly the Global Warmers heard that too. They didn't change their pseudo-science, but cleverly changed the name to 'Climate Change". [*One can disprove warming*, but the words *change of climate* can't be proved wrong].

The United Nations became interested – major sea level rise could cause havoc in low-lying areas or island groups. They established an *Intergovernmental Panel for Climate Change (IPCC)* and invited nations to send delegates. Not surprisingly those chosen were almost entirely Global Warmers, because *they clearly knew something about it.* But to do them credit the Panel members acted a little more like true scientists than those earlier.

They accepted that "*1.4 m in 40 yrs*" was wrong and re-evaluated it as "*0.49 m by 2100"*, [roundly a century ahead]. Thus they dropped ***3,500*** down to ***500*** mm/century – to 14% of the original. The cause remained unchanged – our CO_2 emissions to the atmosphere. In no other human activity would those involved retain a belief when the most crucial item involved was found to be 86% wrong ***by themselves.*** That was a **Second Grave Error.**

In spite of that, the World was taken in. Politicians were able to promise to save us from the consequences, and the Media had an unending "Field Day". It wasn't that people necessarily believed, but they lacked the courage to risk that it might come true, and that they might have to bear the terrible consequences that had been so forcibly promised.

The New Errors The new value of "0.49 m by 2100" became widely accepted. In New Zealand, District Councils were instructed by Government Departments, like Conservation and Environment, and by Regional Councils, that they must take full account of the risk that "0.49" implied for a sea level rise by 2100. Councils had to consider that in the same way as earthquake and volcanic risk. Yet that "0.49" value doesn't stand up to the most simple scientific scrutiny.

First, the rate is four times faster than the current sea level rise, as indicated by regional, widely-available tide gauges; *second*, no reason was given for quadrupling the value, and *third*, good science interprets "0.49" in this sense as being deliberately different from 0.48 and 0.50. Thus that effectively claims that those who determined that value know, for sure, where sea level will be a century ahead to ±5 mm. That was, and is, patently absurd

These were the **Third, Fourth & Fifth Grave Errors**

Further Damning Disclosures The United Nations appointed me personally to their UNCSTD **C**ommittee which assists small countries with their ability regarding **S**cience and **T**echnology **D**evelopment. Three or so of us would go to a central city to talk and discuss their options with delegates from regional countries. On one occasion we met in Prague, to assist countries on both sides of the "Iron Curtain". While there, we were invited to visit the World's only "Institute for Global Warming". It was founded and funded incredibly by the USA and Soviet Union jointly, at the height of their "Cold War" in an attempt to fund something "for the good of Mankind", rather than "for armaments". Some of its staff could have attended the 1985 Conference, and helped create the 1987 *World Declaration.*
I took the opportunity of asking to see copies of the documents that had been brought to that 1985 Meeting in neutral Austria. Several attendees brought their estimates for sea level rise due to Global Warming. The values, converted to mm/century, ranged from ***500*** minimum to ***3,500*** maximum. There can be no doubt that, to ensure that their 1987 World Declaration made the greatest impact, they published the maximum value - contravening the most sacred rule of acceptable science *Thou shall not publish items for monetary, political, or personal gain that are not clear un-biased un-inflated truths.*

The fact that "up to" was used, might be allowed in non-scientific areas, but not in Science. If World Media had distorted the message, the Warmers should immediately have denied what was wrongly claimed, and ensured that the proper statement got equal publicity. Using a maximum value for greatest effect was the **Sixth (and Worst) Grave Error.**

OLD SCIENTIFIC CONCLUSIONS ON CLIMATE IGNORED

19th Century science posed a important question. Why is our Earth's average temperature significantly higher than that calculated from the then-recent determinations of our Sun's distance and its radiation? Knowing my interests in climate, DSIR librarians found me a publication in German that answered that puzzle early. It had Scandinavian author(s), if I remember correctly. Its answer was that the CO_2 in our atmosphere acts like glass in a glasshouse. Both change the optical physical nature of the Sun's infra-red rays [that carry the warmth to us] such that they

may enter, but cannot then leave. *So we are warmed by the heat trapped below our CO_2; like the glasshouse below its glass.*

I surmise that the Global Warmers, along with Al Gore, noted correctly that CO_2 keeps us warm, but thought wrongly that *more* would make us *warmer*. The analogy with glass is important. Horticultural experiments long ago found that more (thicker) glass does not cause more warming, so more CO_2 probably doesn't either. The effect is like that of polarising spectacles, where the change takes place as light *begins* passing through the lenses. Thickness makes no difference. Polarisation is either 100%, or not at all.

A coincidence timed the Little Ice Age's end with the Industrial Revolution's start. The Warmers blamed the undoubted warming on the latter – ignoring the glasshouse evidence.

THE NEW CLIMATE REGIME

NIWA The National Institute of Water & Atmospheric Research (NIWA) retains New Zealand climate records. It has a history of persuading successive governments that Global Warming and Climate Change are both real. It often encouraged media headlines like *"We are Getting Warmer"*, when any news item sugges ed any higher temperature. Science progresses by new concepts and ideas being aired freely for scientific scrutiny. That has sometimes taken centuries to be completed. Although I don't agree with some of NIWA's views, it is proper that they should be aired for discussion, as in this booklet.

One announcement (that surely originated from NIWA) was very important to me and all citizens, and was a credit to NIWA itself. At the close of 2007, it stated that the decade just finishing was the warmest since New Zealand records began. The announcement added that, of those 10 years, 1998 was the warmest ever since records began. I was grateful to NIWA, and concluded that 2007 was no warmer than 1998, and probably cooler. I could assume therefore that warming at our ***125*** rate finished in 1998. In the roundest of figures, the Little Ice Age lasted for some 200 years. There would be no conflict with accepting that the following warming should similarly last for some 200 years.

As always in Science one seeks confirmation whenever possible. I have seen many items that lead to that same view of "no warming since 1998". The best was a written debate in the *Imperial Engineer* of autumn 2008. [*That scientific journal is produced for engineering graduates of Imperial College, London – arguably UK's top university in engineering.*] The debate was on whether Humans were to blame for current changes of climate. Prof Joanna Haigh blamed Humans, Lord Monckton blamed Mother Nature. The only point on which they both agreed was that there had been no warming since 1998. That confirmed NIWA's statement perfectly, along with several comparable pronouncements.

My conclusion is that warming since the Little Ice Age's end is now almost certainly finished. That was supported further by NIWA's release at the end of 2012, concerning the Eastern Bay of Plenty. Their report was that 2012 had been drier *and colder* than 2011. Citizens also notice that warming seems to be over. Skiing seasons are extended, winter fires are needed earlier, and some of us travelling overseas have been asked by those from Queensland, even Hawaii, whether we in New Zealand feel colder generally – *as they do*. I conclude that the New Zealand climate has not been warming since 1998.

THE AFFECTS ON CITIZENS

Astronomical Cost of Major Measures to Combat a Non-Existent Threat:
Politicians and the Media have listened to the proponents of Global-Warming-Climate-Change, but don't seem to have made any critical assessment of it all. Perhaps they were bemused by the Global Warmers constantly naming themselves and associates as "Scientists". As has been shown, those people disregarded the basic rules of true Science. Their political and media audiences innocently believed the statements ***- which contained grave errors***.

Innocents in politics and the media were badly mis-led. They gladly supported projects to combat the non-existent threat of Global-Warming-Climate-Change. The projects were ***unnecessary*** because there was no threat*;* ***extremely costly*** in money time and effort; ***full of praise*** *where ridicule was deserved* ***misleading*** *about benefits & options; and a*bove all ***diversionary*** away from today's real problems.

A huge international bureaucratic industry was born - with Cabinet Ministers, government departments, company sections, travel, conferences, treaties, carbon credits, and carbon trading, and very much more. The challenge was often heard that we must curb our carbon emissions or sacrifice our grandchildren's well-being. In truth, those children were being saddled with a gigantic debt to pay for everything encompassed by the Warmers' "carbon footprints", including the salaries and expenses of the loudest proponents.

Perhaps the saddest part has been that the essential and innocent gas, carbon dioxide, has been demonised and criminalised. It is essential in creating plant growth using chlorophyll and photo-synthesis. It is thus **essential for our very existence**. Crops grow better in a CO_2-enriched and warmer atmosphere, when heated by an old-fashioned vertical kerosene heater. It gives off "carbon emissions" that are valuable to us all.

Costs and Dangers of Local Measures to combat the Non-Existent Threat:
Local authorities were compelled to adop measures designed to combat the non-existent threat. Typically maps were drawn showing the coastline's position now, and in the year 2100 with intermediate zone(s), assuming that sea level would rise 0.49 m in the next 100 years. Onerous restrictions have been emplaced within the zones that were thus defined.

Many regions have vast quantities of sand transported by rivers to their coast, released by the erosion of hills and mountains, continuously raised by Mother Nature. Their coastline extends seawards steadily. Citizens in such regions have long noted (with surveys and photos) that the coastline has a net ***seawards*** movement. It contrasts with many Councils' imposed belief in "0.49" which demands ***landwards*** movement ("inundation").

Councils seem unable to accept their citizens' constant and loud protests about all this. They seem to feel that higher authorities insist that they must ignore such views. It is not just (a) the absurdity of restrictions about where houses may be erected (only inland of certain lines), etc.; or (b) the increasing costs to those building their first home. At the other end of the scale there are enforced dangers; a requirement for higher floor levels, leading to more steps, with unnecessary risks to elderly folk falling, when using them.

The fact that sea level is no longer rising is a new extra factor for councils to ignore. In the example of Ohope Beach, a Commission of enquiry, set up by Council, backed the Council's view of ***landwards*** inundation. That rejected all citizens' factual

evidence of ***seawards*** net movement for periods ranging from 50 to 5,000 years. Council also rejected the advice, supporting the Citizens, by one who was highly qualified in engineering and science and had had long and successful experience in coastal work.

Much worse, the Council's own appointed consultants provided an additional report based on every coastal survey for which a record was available**. It showed a "retreat of the sea" [seaward shoreline movement, or accretion] at the only three Ohope sites, of 0.30-0.94 m/yr over 130 years** ***that was still ongoing in 2008. Clearly neither Council nor Commission had bothered to read that critical report, written by highly regarded consultants, who had been appointed for this project by the Council itself.***

The widespread obsession with Global-Warming-Climate-Change, in opposition to all factual evidence, is quite incredible. It leads to unfair treatment of some citizens, and a massive bill for all, for nothing useful. When will citizens revolt effectively against such callous disregard for their observations and wishes, by those who are essentially their elected employees? When will the perpetrators examine the basis of their ideology, and realise that it's based on unfounded unscientific beliefs, not on confirmed, widely-available investigations by real scientists who abide by the moral standards of their profession?

References to Kaawa-Ohuka

a) Couper RA & McQueen DR 1954: Pliocene and Pleistocene plant fossils of NZ and their climatic interpretation. *Trans Roy Soc NZ 77(3): 398-420*

b) Kear D 1957: Statigraphy of the Kaawa-Ohuka coastal area, West Auckland. *NZ J Sci Tech B 38 (8): 826-42*

c) *Kear D 1963: Geology of Te Akau, West Auckland & regional implications. PhD thesis, London University. 2 vols, 599 pp (copies at libraries of GNS, and of London, Auckland & Waikato Universities).*

ISBN 978-0-473-25154-3
July 2013

Earth Sciences
2019; 8(3): 139-159
http://www.sciencepublishinggroup.com/j/earth
doi: 10.11648/j.earth.20190803.13
ISSN: 2328-5974 (Print); ISSN: 2328-5982 (Online)

What Humans Contribute to Atmospheric CO_2: Comparison of Carbon Cycle Models with Observations

Hermann Harde

Experimental Physics and Materials Science, Helmut-Schmidt-University, Hamburg, Germany

Email address:
harde@hsu-hh.de

To cite this article:
Hermann Harde. What Humans Contribute to Atmospheric CO_2: Comparison of Carbon Cycle Models with Observations. *Earth Sciences.* Vol. 8, No. 3, 2019, pp. 139-159. doi: 10.11648/j.earth.20190803.13

Received: April 3, 2019; **Accepted**: May 11, 2019; **Published**: June 12, 2019

Abstract: The Intergovernmental Panel on Climate Change assumes that the inclining atmospheric CO_2 concentration over recent years was almost exclusively determined by anthropogenic emissions, and this increase is made responsible for the rising temperature over the Industrial Era. Due to the far reaching consequences of this assertion, in this contribution we critically scrutinize different carbon cycle models and compare them with observations. We further contrast them with an alternative concept, which also includes temperature dependent natural emission and absorption with an uptake rate scaling proportional with the CO_2 concentration. We show that this approach is in agreement with all observations, and under this premise not really human activities are responsible for the observed CO_2 increase and the expected temperature rise in the atmosphere, but just opposite the temperature itself dominantly controls the CO_2 increase. Therefore, not CO_2 but primarily native impacts are responsible for any observed climate changes.

Keywords: Carbon Cycle, Atmospheric CO_2 Concentration, CO_2 Residence Time, Anthropogenic Emissions, Fossil Fuel Combustion, Land Use Change, Climate Change

1. Introduction

Following the interpretation of the Intergovernmental Panel on Climate Change (IPCC) the inclining atmospheric CO_2 concentration over recent years is assumed to result almost exclusively from anthropogenic emissions, and as a consequence of the greenhouse effect this increase is made responsible for the rising temperature over the Industrial Era (see, 5th Assessment Report, AR5 [1]). These predictions are based on more or less refined theoretical models of the carbon cycle and their comparison with observations. But good agreement between calculations and observations is only a necessary, not sufficient prerequisite for reliable simulations, they must also be in conformity with all natural causalities. Because of the expected far reaching consequences of anthropogenic carbon on future climate changes this was motivation enough to critically scrutinize the main assumptions used in these carbon cycle models.

In this contribution we consider three theoretical approaches, which find favor with the IPCC and predominantly focus on the influence of human activities caused by Land Use Change (LUC) (see e.g., Le Quéré et al. [2]; CICERO [3]) and the Fossil Fuel Emissions (FFE) (CDIAC [4]), while environmental effects are supposed to have been constant over the last 270 yr. We show that the main consequence of isolating the anthropogenic carbon cycle from the natural cycle is to introduce a new time scale, the adjustment time, which differs significantly from the residence time, the latter characterizing the natural uptake of CO_2 from the atmosphere by extraneous reservoirs.

We compare respective simulations of these approaches with actual observations at Mauna Loa (Keeling et al. [5]; AR5 [1] Chap.6-Fig.6.3, p. 476), and we contrast them with our alternative description of the atmospheric carbon cycle (Harde [6]), which is based on a first order absorption process for the full cycle with only one time scale, the residence time, and additionally including temperature dependent natural variations of the emission and uptake of CO_2.

We do not model carbon in the complete Earth-Atmosphere System, we only focus upon CO_2 in the atmosphere, which is controlled by the governing Conservation Law.

Based on this fundamental relation of mass conservation and a first order absorption process, we show that human activities have a minor influence on the CO_2 increase in the

atmosphere, while the main contribution has to be explained by natural effects, particularly the temperature, which is responsible for more than 85% of the CO_2 increase since the Industrial Revolution. Therefore, not CO_2 but primarily native impacts control any observed climate changes.

2. Physical Concept

The basis of our considerations is the balance for the influx of CO_2 into the atmosphere and the outflux from the atmosphere to extraneous reservoirs, by which the CO_2 concentration C in the atmosphere is controlled. This can well be compared with a swimming pool (see also Salby [7]) with an influx f_{in} and an outflux f_{out}, for which the changing amount of water dm_W in the pool over the time interval dt is given by the difference of these fluxes:

$$\frac{dm_W}{dt} = f_{in} - f_{out} \,. \tag{1}$$

From a simple flux consideration we get the average turnover or residence time τ_R it takes to completely exchange the water in the pool. Under steady state conditions for $f_{in} = f_{out}$ then the total amount of water in the pool m_W is exchanged within

$$\tau_R = \frac{m_W}{f_{in}} = \frac{m_W}{f_{out}} \,, \tag{2}$$

and the other way round is this an important measure for the outflux rate

$$f_{out} = \frac{m_W}{\tau_R} \,. \tag{3}$$

In the same way as for the pool we can consider the balance for atmospheric CO_2 with a total emission rate $e_T(t)$ of CO_2 from the surface to the atmosphere, and reversely a total absorption rate $a_T(t)$ of the extraneous reservoirs (Figure 1). Generally the influx can be split into natural emissions with a rate $e_N(t)$ and an additional anthropogenic emission rate $e_A(t)$, which on its part results from fossil fuel emissions and land use changes. The outflux is determined by temporary or continuing absorption of CO_2 by oceans and the land. Incidentally the total absorption rate $a_T(t)$ is also separated into a fraction $a_N(t)$, characterizing an uptake that can be addressed to the amount of natural emissions, and another contribution, $a_A(t)$, caused by the additional anthropogenic emissions. This results in a total mass balance, the Conservation Law:

$$\begin{aligned} \frac{dC(t)}{dt} &= \frac{dC_N(t)}{dt} + \frac{dC_A(t)}{dt} = e_T(t) - a_T(t) \,, \\ &= e_N(t) + e_A(t) - a_N(t) - a_A(t) \end{aligned} \tag{4}$$

which governs the atmospheric CO_2 concentration.

Generally all these fluxes are changing with time and also depend on the actual concentration $C(t)$, which virtually may be considered to consist of a time dependent fraction $C_N(t)$, caused by native emissions, and of a time dependent anthropogenic portion $C_A(t)$, with $C(t) = C_N(t) + C_A(t)$. Thus, usually this equation has to be solved numerically.

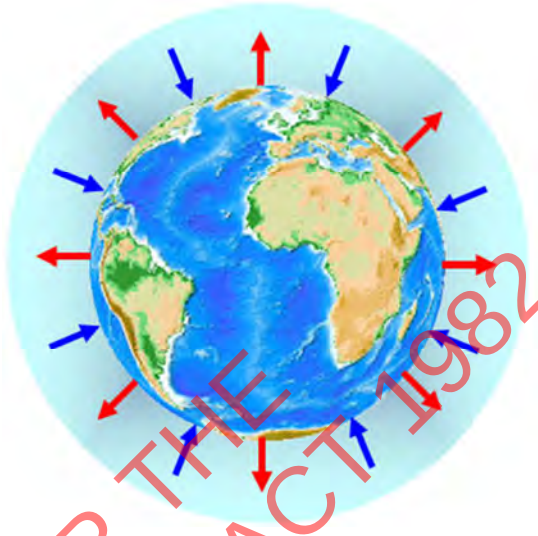

Figure 1. *Emissions of CO_2 from the surface to the atmosphere (Red Arrows) and absorption of CO_2 by the surface (Blue Arrows).*

In analogy to the pool example it follows that an exchange of CO_2 in the atmosphere takes the time

$$\tau_R = \frac{C(t)}{e_T(t)} = \frac{C(t)}{a_T(t)} \,, \tag{5}$$

the so called residence time of CO_2 in the atmosphere, and the absorption rate is

$$a_T(t) = \frac{C(t)}{\tau_R} \,. \tag{6}$$

With (4) we do not model the carbon cycle in the complete Earth-Atmosphere System (EASy). That would require a wider analysis, accounting for processes within extraneous systems and exchanges between them. Our analysis focuses upon CO_2 in the atmosphere, which is controlled by the governing conservation law. Incidentally this physical law is characterized as a flawed one-box description (see e.g., Köhler et al. [8]), because a single balance equation - so the argument - does not account for details in other reservoirs, systems that are extraneous to the atmosphere. As will be shown, such interpretation is confused. With the inclusion of surface fluxes e_T and a_T, which account for influences on the atmosphere, the balance equation (4) entirely determines the evolution of CO_2. Details of extraneous systems, which are largely unobservable, are then irrelevant.

Atmospheric CO_2 is fully described by this single equation for a reason. It follows from the 3-dimensional continuity equation, the physical law that governs the global distribution of atmospheric CO_2. In flux form, the continuity equation is given by

$$\frac{\partial c}{\partial t} + \nabla \cdot (\boldsymbol{v}\, c) = c \nabla \cdot \boldsymbol{v} \,, \tag{7}$$

where the local CO_2 concentration c is transported with velocity $\boldsymbol{v}$. When integrated over the volume of the atmosphere and subjected to the divergence theorem, (7) reduces to the governing balance equation (4) for globally averaged CO_2.

If this would be flawed, then so would be the fundamental physical law from which it follows.

The anthropogenic emissions $e_A(t)$ as the sum of the Land Use Change (LUC) (see e.g., Le Quéré et al. [2]; CICERO [3]) and the Fossil Fuel Emissions (FFE) (CDIAC [4]) are displayed in Figure 2. While LUC (Red-Brown) almost stays constant over the last 170 years, FFE (Blue) is rapidly increasing over recent years.

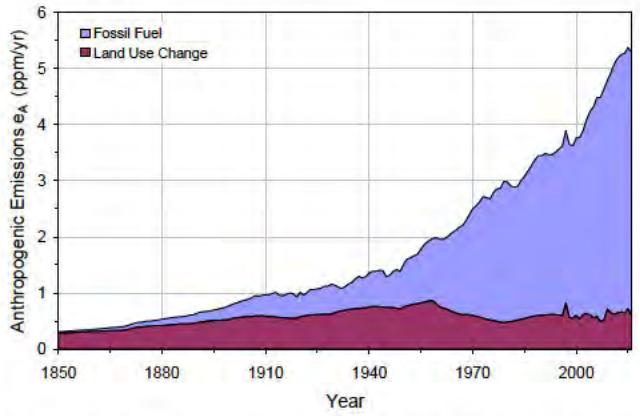

Figure 2. *Total anthropogenic emissions $e_A(t)$ due to land use change (Red-Brown) and fossil fuel emissions (Blue). Data from Le Quéré et al. [2] and CDIAC [4] displayed as stacked representation.*

Figure 3 shows again the total anthropogenic emissions (Red Squares) together with the temperature anomaly $\Delta T(t)$ (Blue Triangles) of the global annual station temperature data from the Goddard Institute for Space Studies (GISS) [9].

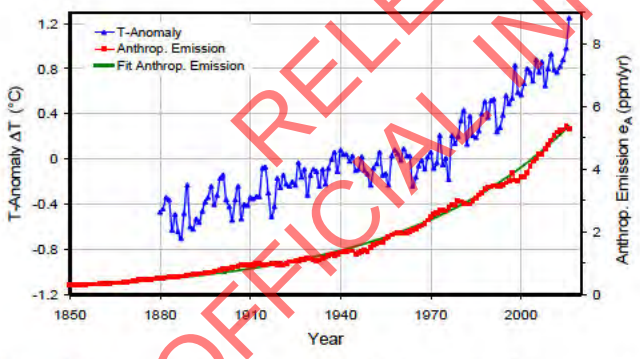

Figure 3. *Anthropogenic emissions $e_A(t)$ (Red Squares) with exponential fit (Green Graph) and global temperature anomaly (GISS-data, Blue Triangles).*

The anthropogenic emissions can be well approximated by an exponential of the form

$$e_A(t) = e_{A0} \cdot (e^{(t-t_0)/\tau_e} + b) \tag{8}$$

with parameters: $e_{A0} = 0.026$ *ppm/yr*, $\tau_e = 50$ *yr*, $t_0 = 1750$ *yr* and $b = 4$. The integral over the emission rate agrees within a few ‰ with the integral of the estimated observations.

On first glance the almost synchronous evolution of the fossil fuel emissions and temperature anomaly looks to be a strong indicator for the human influence as the driving force for a globally increasing temperature. But a closer look already reveals some systematic discrepancies, particularly between 1940 and 1970, where the emissions are further increasing, while the temperature stagnates or even slightly decreases. This has to be considered in some more detail, in particular by directly comparing model calculations of the CO_2 increase, based on the fossil fuel emissions and land use change, with the actual observations at Mauna Loa since 1958 (Keeling et al. [5]; AR5 [1] Chap.6-Fig.6.3, p. 476).

Therefore, in this contribution we first investigate the carbon cycle based on the IPCC's assumptions that the human emissions are the dominant cause of the CO_2 increase, before we extend the balance to the full carbon cycle also including natural variations with their temperature dependence (see also: Harde [6]; Salby [7], [10, 11]).

3. Anthropogenic Carbon Cycles

To explain the CO_2 increase over recent years and to predict its further progression, the IPCC assessment reports emanate from equation (4), but they are using some restricting assumptions (see AR5 [1] Chap.6), which can be summarized by the following statements:

1. Before 1750 and in first approximation also before 1850 steady state conditions are presupposed with a CO_2 concentration of $C_{N0}(1750) \approx 280$ *ppm*, which is determined by constant natural emission and absorption rates $e_{N0} = a_{N0}$ of about *93 ppm/yr* (AR5 [1] Chap.6-Fig.6.1).
2. At this concentration and with these fluxes it follows from (5) an average residence time τ_R (at pre-industrial times: τ_{R0}) of CO_2 in the atmosphere of

$$\tau_{R0} = \frac{C_{N0}}{e_{N0}} = \frac{C_{N0}}{a_{N0}} = 3.0 \ yr \cdot \tag{9}$$

Note: The same result is found from (4) for the in- and outfluxes in equilibrium and with an absorption rate equivalent to (6), which is scaling proportional to the concentration C_{N0}:

$$\frac{dC_{N0}}{dt} = e_{N0} - a_{N0} = e_{N0} - \alpha_{R0} \cdot C_{N0} = e_{N0} - \frac{C_{N0}}{\tau_{R0}}, \tag{10}$$

with $\alpha_{R0} = 1/\tau_{R0}$ as the absorptivity and τ_{R0} now as the e-folding residence time.

3. It is assumed that an increasing CO_2 concentration over the last 170 years is almost exclusively caused by anthropogenic emissions from fossil fuel combustion and land use change, while the natural emissions over this period are supposed to have been the same as in pre-industrial times.
The increasing concentration is attributed to only partial re-absorption of the anthropogenic emissions, from

which a fraction, the so-called Airborne Fraction $AF = \Delta e_A/e_A$, is assumed to remain in the atmosphere. Then

$$\Delta e_A(t) = AF \cdot e_A(t) \tag{11}$$

is the non-absorbed portion, which cumulates in the atmosphere and

$$a_A(t) = e_A(t) - \Delta e_A(t) = e_A(t) \cdot (1 - AF) \tag{12}$$

represents the absorbed fraction of the anthropogenic emissions. Actually the IPCC emanates from an airborne fraction of $AF = 44\%$ (AR5 [1] Chap.6, p. 495; Le Quéré et al. [12]).

4. To account for a changing uptake of extraneous reservoirs with increasing atmospheric concentration the absorption is supposed to consist of a series of different exponential decay terms representing the uptake of the different reservoirs with different time constants. This absorption is considered to be proportional to the human emissions, not the actual concentration C (see (12)).

Based on these assumptions more or less sophisticated approaches are known to explain the increasing CO_2 concentration in the atmosphere. Three of them will be briefly characterized and discussed in this contribution. They all emanate from the same basic concept to isolate the natural carbon exchange between atmosphere and extraneous reservoirs and only to consider the anthropogenic cycle.

3.1. Constant Airborne Fraction

With a constant natural emission and absorption rate over the Industrial Era ($e_{N0} = a_{N0}$) and also a constant airborne fraction over this period the balance equation (4) reduces to the simple form

$$\frac{dC(t)}{dt} = \Delta e_A(t) = AF \cdot e_A(t) \tag{13}$$

and changes synchronously with $e_A(t)$. The concentration as a function of time is found by simply integrating (13) over the Industrial Era:

$$C(t) = C(1750) + AF \cdot \int_{1750}^{t} e_A(t')\, dt' \cdot \tag{14}$$

From the carbon budget over the last 270 years we derive an airborne fraction of $AF = 42\%$ (see Le Quéré et al. [2], Table 9). Then, with an initial concentration of $C(1750) = C_{N0} = 280$ *ppm* this results in a progression as shown in Figure 4 (Green Line), which for the last 60 yr can directly be compared with measurements (Blue Diamonds) at Mauna Loa (Tans & Keeling [13]). This comparison shows generally too high concentrations, particularly for past periods. This might be caused by a too large initial concentration in 1750, but also the slope does not fit very well. More likely is a too large emission rate, especially due to LUC, which anyway is only known with an accuracy of about $\pm 50\%$.

A surprisingly good agreement can be found with an anthropogenic emission rate $e'_A(t)$, which as average over the considered period is reduced by *0.21 ppm/yr*, and using an airborne fraction of 48% (Green Crosses), 6% larger than the average fraction over the Industrial Era. The smooth shape of the fits is the result of an integration over the full anthropogenic emissions since 1750, where the soft increase of the curves is dominated by the 'average' emission rate, while even larger emission events are strongly flattened.

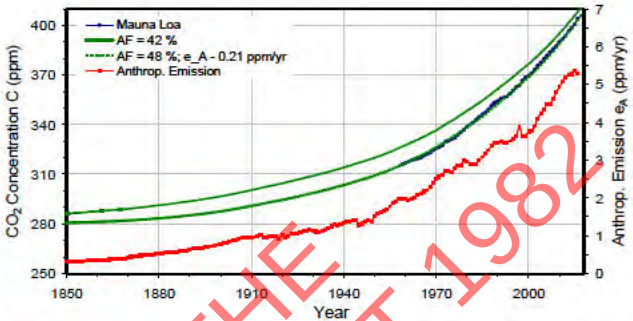

Figure 4. *Calculated CO_2 concentration with an airborne fraction of 42% (Green Line) compared with observations at Mauna Loa (Blue Diamonds). A simulation with AF = 48% and reduced emissions is plotted as Green Crosses. Also shown are the anthropogenic emissions $e_A(t)$ (Red Squares).*

3.2. Bern Model

A more advanced approach to describe the carbon cycle, is the so-called Bern Model of CO_2 absorption (e.g., Joos et al. [14]), a prototype of similar treatments in other models. It distinguishes between different sinks on different time scales and assumes a multi-exponential decay to re-equilibrate after a perturbation, e.g., caused by a transient spike of CO_2 added to the atmosphere. Using the five-term fit to the Bern carbon cycle model (Joos et al. [14]; Hansen et al. [15, 16]) the adjustment following a δ-pulse perturbation Δe_P from equilibrium emission e_{eq} is supposed to be:

$$\begin{aligned} R(t) &= (e(t) - e_{eq})/\Delta e_P \\ &= 0.18 + 0.14 \cdot e^{-t/420} + 0.18 \cdot e^{-t/70} \cdot \\ &\quad + 0.24 \cdot e^{-t/21} + 0.26 \cdot e^{-t/3.4} \end{aligned} \tag{15}$$

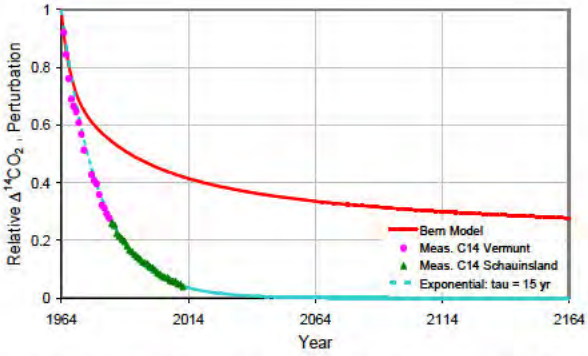

Figure 5. *Decay of perturbation predicted by the Bern Model (Red Graph) as calculated from (15). Also shown is the observed ^{14}C decay (Circles and Triangles) and an exponential fit with a decay time $\tau = 15$ yr (Dashed Blue).*

Figure 5 shows the adjustment of the relative perturbation $R(t)$ over 200 yr (Red). Also displayed is the observed $^{14}CO_2$ decay at Vermunt and Schauinsland (Levin et al. [17]) after the

stop of the atomic bomb tests, shown as relative fractionation-corrected ‰-deviation $\Delta^{14}CO_2$ from the Oxalic Acid standard. This decay is well represented by a single exponential with a decay constant of only 15 yr (Dashed Blue). Almost identical $\Delta^{14}CO_2$ decays of 16.5 yr can be found from the data of Hua et al. [18] and Turnbull et al. [19].

For calculating the atmospheric CO_2 concentration by the Bern Model (e.g., Joos [14]), the emission of anthropogenic CO_2 into the atmosphere is considered as a series of consecutive pulse inputs. Then the atmospheric CO_2 concentration $C(t)$ at time t is assumed to be the sum of earlier emissions $e_A(t')$ at time t' multiplied by the fraction, now a time dependent airborne fraction, which is still available in the atmosphere after the time $t - t'$ and which is given by the pulse response function $R(t - t')$ of (15). With an anthropogenic emission rate, which can well be approximated by (8) (see Figure 3), it follows:

$$\begin{aligned} C(t) &= C(t_0) + \int_{t_0}^{t} e_A(t') \cdot R(t-t') \cdot dt' \\ &= C(t_0) + e_{A0} \cdot \left[c_e \cdot e^{-(t-t_0)/\tau_e} - c_0 - c_1 \cdot e^{-(t-t_0)/\tau_1} \right. \\ &\quad - c_2 \cdot e^{-(t-t_0)/\tau_2} - c_3 \cdot e^{-(t-t_0)/\tau_3} \\ &\quad \left. - c_4 \cdot e^{-(t-t_0)/\tau_4} + 0.18 \cdot b \cdot (t-t_0) \right] \end{aligned} \tag{16}$$

with:

$$c_e = 0.18 \cdot \tau_e + 0.14 \cdot \tau_{e1} + 0.18 \cdot \tau_{e2} + 0.24 \cdot \tau_{e3} + 0.26 \cdot \tau_{e4};$$

$$c_0 = 0.18 \cdot \tau_e - b \cdot (0.14 \cdot \tau_1 + 0.18 \cdot \tau_2 + 0.24 \cdot \tau_3 + 0.26 \cdot \tau_4);$$

$$c_1 = 0.14 \cdot (\tau_{e1} + b \cdot \tau_1); \quad c_2 = 0.18 \cdot (\tau_{e2} + b \cdot \tau_2);$$

$$c_3 = 0.24 \cdot (\tau_{e3} + b \cdot \tau_3); \quad c_4 = 0.26 \cdot (\tau_{e4} + b \cdot \tau_4);$$

$$\tau_{ei} = \tau_e \cdot \tau_i / (\tau_e + \tau_i); \quad \tau_e = 50\,yr; \quad \tau_1 = 420\,yr;$$

$$\tau_2 = 70\,yr; \quad \tau_3 = 21\,yr; \quad \tau_4 = 3.4\,yr; \quad b = 4;$$

This approach also presupposes an equilibrium CO_2 concentration C_{eq} in 1750 of $C_{eq} = 280$ *ppm*, and it excludes any further variations in the natural emission rate over the Industrial Era.

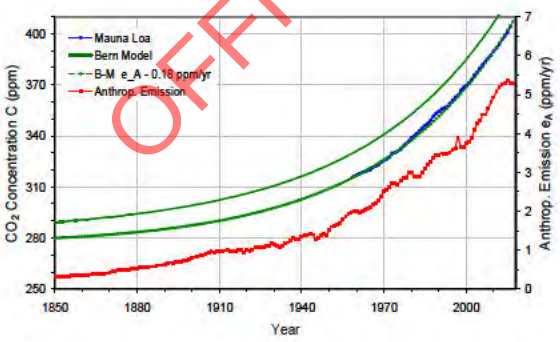

Figure 6. *Comparison of the Bern Model (Green Graph) with the Mauna Loa data (Blue Diamonds). A simulation with reduced emission $e_A(t)$ - 0.18 ppm/yr is displayed as Green Crosses. Also shown are the original data of anthropogenic emissions $e_A(t)$ (Red Squares).*

The calculated atmospheric CO_2 concentration as given by (16) is displayed in Figure 6 (Solid Green). The Bern Model shows the same tendency of too large calculated concentrations as this was already found for the much simpler model of constant airborne fraction (AF Model).

With a reduced average anthropogenic emission rate, in this case of *0.18 ppm/yr*, again a very good agreement with the Mauna Loa data can be observed.

But from basic causalities there exist some fundamental problems with the AF and the Bern Model:

1. Additional emissions to the atmosphere even at a constant rate will never attain a new equilibrium.
2. These emissions will further accumulate in the atmosphere, in the Bern Model 18%, in the simple AF Model even 48%, emissions which will stay for ever in the atmosphere.
3. This is a consequence of the defect, that these models essentially add up additional emissions deviating from pre-industrial times, and they only consider partial uptake, which is scaling *proportional with the emission rate* – and not with the concentration.
4. The Bern Model uses different time scales for the uptake, although the ^{14}C-decay shows a single exponential decay of only 15 yr or shorter.
5. Even natural year-to-year variations of only 1%, El Niños and volcanic activities comparable or even larger than the human emissions, will cumulate in the atmosphere, since only additional emissions but not adequate sinks are considered in these models.

To avoid some of these deficits another class of models uses a first order absorption process, but applies this only to concentration changes $C_A(t)$ caused by anthropogenic emissions.

3.3. Absorption Scales with Concentration

Since the anthropogenic absorption rate $a_A(t)$, by presumption, is proportional to the man-made emission rate $e_A(t)$ (see Eq.(12)) and this rate on its part directly determines the anthropogenically induced fraction of the CO_2 concentration $C_A(t)$, in analogy to (6) or (10) we infer:

$$a_A(t) = e_A(t) \cdot (1 - AF) \Rightarrow \frac{C_A(t)}{\tau_A}, \tag{17}$$

which converts the absorption term in (4) to a first order process scaling proportional to the anthropogenic fraction $C_A(t)$ of the concentration (for a similar approach see e.g.: Siegenthaler & Sarmiento [20]; Dietze [21]; Cawley [22]; Lüdecke & Weiss [23]). For $e_{N0} = a_{N0}$ this results in the balance equation:

$$\frac{dC(t)}{dt} = \frac{dC_A(t)}{dt} = e_A(t) - \frac{C_A(t)}{\tau_A} = e_A(t) - \frac{C(t) - C_{N0}}{\tau_A} \tag{18}$$

with τ_A as the respective absorption time of molecules in the atmosphere, which in the IPCC terminology controls the

'adjustment' of the atmosphere only due to anthropogenic emissions. From Figure 4 and with (17) we can estimate this 'adjustment' time, which for C_A = *(393-280) ppm = 113 ppm*, e_A = *4.7 ppm/yr* (all values averaged over 10 years from 2007-2016, see Le Quéré et al. [2], Table 7) and the fitted *AF = 48%* from Figure 4 gives

$$\tau_A = \frac{C_A(t)}{e_A(t)(1-AF)} = 46\,yr \cdot \tag{19}$$

Numerical integration of (18) with this 'adjustment' time, with the given emission rate $e_A(t)$ and a native concentration C_{N0} = *280 ppm* is shown in Figure 7 (Green Line). For a corrected emission rate $e'_A(t)$ = $e_A(t)$ - *0.3 ppm/yr* and the 'adjustment' time from (19) also this accounting scheme (Green Crosses) gives good agreement with the observations at Mauna Loa (Blue Diamonds). This absorption time is almost identical with an adjustment time of 48 yr as derived from a simple flux calculation presented in Harde [6], Eq. (9).

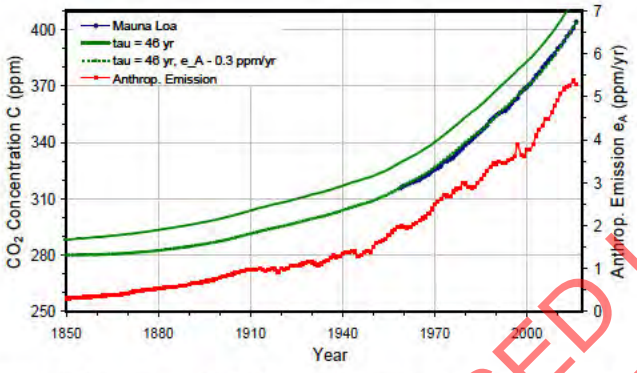

Figure 7. *Calculation of the CO_2 concentration for an adjustment time τ_A = 46 yr (Green Line) and comparison with observations at Mauna Loa (Blue Diamonds). A simulation with reduced emissions is displayed as Green Crosses. Also shown are the anthropogenic emissions $e_A(t)$ (Red Squares).*

3.4. Influence of Native Effects

So, with the right parameters all investigated approaches can reproduce the observations at Mauna Loa very well. But all these models are based on different hypotheses and boundary conditions, some of them are even in contradiction to each other. Therefore, only one or none of them may be right. Good conformity with observations alone is not a sufficient criterion for testing the validity of a model, it must also be in agreement with basic physical principles. They alone can give us the physically consistent explanations for a carbon cycle, which is dominated by more than 95% of native emissions and underlies continuous environmental impacts. It is also evident that this cycle is governed by the same principles at paleoclimatic times as today with human emissions.

Thus, for the further considerations it seems reasonable first to concentrate on three basic questions:

1. *How could nature be in equilibrium before the Industrial Era?*

Some climate scientists consider the natural carbon exchange as a closed cycle, which happened in this way unaffected over thousands of years without larger variations. But when looking to the glacial and interglacial periods or only to the Holocene we have to recognize that the atmospheric CO_2 concentration was always varying over longer and shorter periods. Slow variations per se are no sign of non-equilibrium, they can also result from varying emission strengths over time. But an adaptation to such natural variations is not possible, when emissions are only cumulating, as this is assumed in the AF and Bern Models for *anthropogenic* emissions, which never come to equilibrium. Thus, an adaptation to volcanic activities, temperature variations or even to the seasonal variations requires an absorption process for the *native* cycle, which behaves more or less proportional to the respective concentration $C_P(t)$ at pre-industrial times, in a similar way as considered in the 3rd model for the anthropogenic emissions.

So, it is close by to presuppose also a first order process for the native cycle, and the respective balance equation for pre-industrial times then assumes the form, analogous to (10):

$$\frac{dC_P(t)}{dt} = e_P(t) - \frac{C_P(t)}{\tau_{RP}} \tag{20}$$

with $e_P(t)$ as the emission rate and τ_{RP} as the residence time at pre-industrial times. Equilibrium is achieved when the left side of (20) is zero. Then the residence time becomes τ_{RP} = $C_P(t)/e_P(t)$.

The same relation was found from the simple flux model with a residence time τ_{R0} = *3 yr* at 1750. Such a residence or absorption time for the natural cycle is in good agreement with the observed seasonal variations and is also supported by the ^{14}C-decay as will be discussed in detail in subsection 5.7.3.

When CO_2 concentrations were continuously changing in pre-industrial times we also have to inquire:

2. *Can the natural cycle really be assumed to have been constant over the last 270 yr?*

Almost every day we recognize natural phenomena and processes in form of significant perturbations or variations, e.g., volcanic eruptions, earthquakes, El Niño - La Niña events, internal and external oscillations, global warming or seasonal variations.

All these phenomena have a direct influence on the naturally caused fraction $C_N(t)$ of CO_2 in the atmosphere. Therefore, the balance for the natural cycle also over the Industrial Era has to be expressed explicitly by a time dependent emission rate $e_N(t)$ and also a time dependent residence time $\tau_R(t)$. The latter can slightly be affected by internal or external variations, but should not significantly deviate from pre-industrial times or 1750. Otherwise the balance must obey the same principal relation as in pre-industrial times with:

$$\frac{dC_N(t)}{dt} = e_N(t) - \frac{C_N(t)}{\tau_R(t)}. \tag{21}$$

Finally we have to ask:

3. *Can the anthropogenic cycle be considered separately from a natural cycle?*

From the preceding discussion one may conclude that the total balance equation for the respective models looks like

$$\begin{aligned}\frac{dC(t)}{dt} &= \frac{dC_N(t)}{dt} + \frac{dC_A(t)}{dt} \\ &= \left(e_N(t) - \frac{C_N(t)}{\tau_R(t)}\right) + \begin{cases} e_A(t)\cdot AF & AF\,Model \\ e_A(t)\cdot R(t'-t) & Bern\,Model \\ e_A(t) - C_A/\tau_A & 1.\,Order\,Mod. \end{cases}\end{aligned} \tag{22}$$

In all cases is this equation controlled by two or more independent time scales, a fast scale with $\tau_R \approx 3\ yr$ for the absorption of natural emissions and a slow scale with an infinite decay for 48% of emissions in the AF Model, with 5 decay times for different sinks in the Bern Model, and an adjustment time of 46 yr in the 3rd model, all for the adaptation of the atmosphere to additional anthropogenic emissions.

At least here it gets obvious that naturally and human emitted molecules cannot be treated differently. As long as no saturation in the uptake is observed, which is not the case (see Appendix A), an additional emission by humans must underlie the same absorption process as the natural emissions. A separation is in startling contradiction to the Equivalence Principle, and as a consequence of this principle only one absorption time, τ_R, with the same absorption behavior for human and native emissions must exist.

4. Complete Carbon Cycle

The preceding considerations show that a realistic analysis of the CO_2 exchange between the atmosphere and its adjacent reservoirs has also to include natural variations due to temperature effects or temporal events. It has also to consider a common absorption of all natural and human contributions, which are scaling proportional to the apparent CO_2 concentration and which are represented by one unique decay time (see also: Essenhigh [24]; Salby [7, 10]; Harde [6]; Berry [25]).

We summarize the main deviations from the previously discussed accounting schemes by the following fundamental principles:

1. Changes in the natural carbon cycle, which are due to a continuous temperature increase over the Industrial Era, are included in the balance equation (4) by a temperature dependent term for the natural emissions and also a term for the temperature dependent absorption.
2. Perturbations from an equilibrium concentration C_{eq} due to natural changes or additional anthropogenic emissions are compensated for or controlled in the carbon cycle by an absorption rate, which changes proportional to the actual concentration C (first order process, see Eq. (6)).
3. Molecules emitted to the atmosphere can have a number of different sources, natural and man-made sources, but (up to now) they have only common natural sinks in form of the oceans and continents, which do not differentiate between the native or anthropogenic origin.
4. There exists no evidence that the absorption was suddenly saturating and the residence time τ_R jumping up by one or two orders of magnitude from τ_{R0} to τ_A, when the atmospheric concentration exceeded a level of *280 ppm*. τ_R can only have changed continuously from pre-industrial to present times from 3 to 4 yr, synchronously with the atmospheric concentration and in agreement with (5) and (9).
5. The observed exponential decay of ^{14}C in the atmosphere after the stop of the atomic bomb tests in 1963 is a strong indication for a first order absorption process of CO_2 by land and oceans with a unique time constant determined by the gross flux of CO_2 from the atmosphere to the reservoirs (see Figure 5). Only such an absorption ensures that the carbon cycle can stabilize and react adequately on any temporal perturbations like seasonal variations or volcanic activities.
6. For parallel absorption processes by the oceans, by the biosphere or rock weathering the absorptivity α is given as the sum of the individual channels α_i with $\alpha_R = \alpha_1 + \alpha_2 + \ldots + \alpha_N$ and $\tau_R = 1/\alpha_R$. The uptake is not restricted by the slowest process as assumed in the Bern Model, but by the sum of all processes with one unique absorptivity α_R for all molecules. The reciprocal of α_R is the residence time τ_R of CO_2 in the atmosphere.

These principles are incorporated in a balance equation, the General Conservation Law, which on the one side includes temperature dependent and, thus, time dependent natural and anthropogenic emissions, and on the other side considers a temperature dependent unique residence time τ_R, which describes the collective or net absorption of all molecules. It does not differentiate between a residence or adjustment time:

$$\frac{dC(t)}{dt} = e_N(T(t)) + e_A(t) - \frac{C(t)}{\tau_R(T(t))}. \tag{23}$$

In first order the natural emission rate and the residence time can be assumed to increase linearly with the temperature anomaly ΔT:

$$\begin{aligned} e_N(T(t)) &= e_{N0} + \beta_e \cdot \Delta T(t) \\ \tau_R(T(t)) &= \tau_{R0} + \beta_\tau \cdot \Delta T(t) \end{aligned}. \tag{24}$$

β_e and β_τ are the temperature coefficients of the natural emission and the absorption time. In the general case of a saturating uptake by the extraneous reservoirs τ_R will additionally change with C. But up to now any unequivocal saturation effects cannot be identified (see Appendix A).

With the temperature anomaly $\Delta T(t)$ and the anthropogenic emissions $e_A(t)$ as represented in Figure 3, Eq.(23) can be solved numerically.

Figure 8 shows the simulated CO_2 concentration in the atmosphere (Green Graph) over a time period 1880 - 2016, for which reliable temperature data are available (GISS [9]), whereas the direct CO_2 measurements at Mauna Loa (Blue Diamonds) started not before 1958. The temperature data were used as moving average over ±5 yr. We achieve good

agreement with the observations for a natural emission rate e_{N0} = *93.3 ppm/yr*, τ_{R0} = *3 yr* (both in agreement with (9)) and temperature coefficients β_e = *10 ppm/yr/°C* and β_τ = *0.37 yr/°C*. Similar good results are obtained with larger β_e (up to *24 ppm/yr/°C*) and smaller β_τ ($\rightarrow 0$) or vice versa with β_τ (up to *0.74 yr/°C*) and smaller β_e ($\rightarrow 0$). Thus, we have to assert that as long as the natural and anthropogenic emission rates and at least one of the temperature coefficients are not more accurately known, we can only determine a combination of these parameters, not their absolute values.

Figure 8 also displays a simulation for which the anthropogenic emissions were set to zero (Magenta).

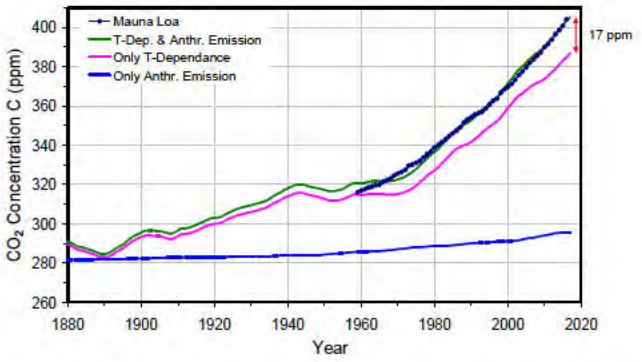

Figure 8. *Calculated CO_2 concentration with temperature-dependent emission and absorption (Green). Compared against the observed record of CO_2 from Mauna Loa (Blue Diamonds). Simulation without anthropogenic emissions (Magenta), and only human activities (Blue).*

The difference between both curves results from the human activities. These graphs evidently show that, based on (23), the anthropogenic contribution to the observed CO_2 increase over the last 150 years is significantly less than the natural influence. So, as an average over the period 2007- 2016 the anthropogenic emissions were contributing not more than 4.3% to the total concentration of 393 ppm and thus, their fraction to the atmospheric increase since 1750 of 113 ppm is not more than 17 ppm or 15%. The dominating contribution with 85% is determined by natural influences, in Figure 8 represented as difference of the Magenta Graph to the 280 ppm grid-line.

The pure anthropogenic contribution to the atmospheric concentration, which would result without temperature effects, is shown by the Blue Graph on a constant background of 280 ppm. With a residence time of τ_{R0} = *3 yr* human emissions cannot contribute more than 14.5 ppm, and with an increasing τ_R over the Industrial Era due to the temperature influence it will slightly increase to 17 ppm, as displayed by the difference between the Green and Magenta Graphs (see red arrow). *At equilibrium the relative contribution of human activities to the total CO_2 concentration is always determined by the anthropogenic to the total emission rate, independent of the actual residence time* (Eq.(23); Harde [6], Eq.(14)).

Note, a simulation without anthropogenic emissions, but slightly increased temperature coefficients (β_τ = *0.48 yr/°C* or β_e = *13.3 ppm/yr/°C*) lifts the Magenta curve to coincide almost exactly with the Green graph. Thus, the observed evolution at Mauna Loa could also be reproduced without involvement of $e_A(t)$, contrary to the IPCC interpretations.

Up to now we were only considering the seasonally averaged CO_2 measurements, but it is also worthwhile to look closer to the monthly data at Mauna Loa (see Keeling et al. [5]; AR5 [1] Chap.6-Fig.6.3, p. 476) as displayed in Figure 9 (Magenta Diamonds). The "sawtooth" curve is an obvious indication for the direct variation of the CO_2 emission and uptake rates, driven by the solar activity and the temperature over the seasons. Generally this modulation is attributed to the greater land mass on the Northern Hemisphere, where the uptake by photosynthesis predominantly occurs during the growing season, while CO_2 release by heterotrophic processes is more dominant over the other seasons.

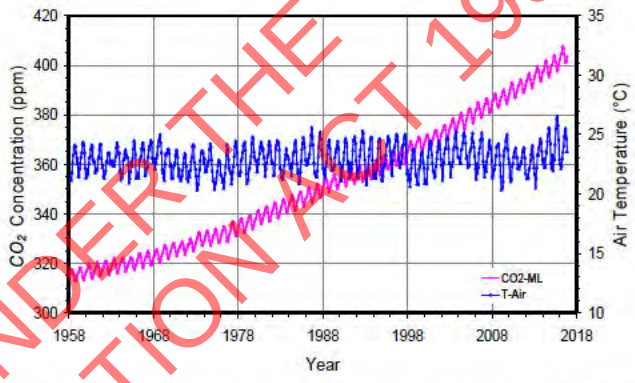

Figure 9. *Monthly time series of measured CO_2 concentration at Mauna Loa (Magenta Diamonds) and air temperature record at Hawaii (Blue Triangles).*

However, apparently also local effects have a direct influence on this record. Figure 9 shows also the monthly averaged air temperature at Hawaii (Blue Triangles) with seasonal variations of 3 - 4°C (NOAA [26]). Almost synchronous changes are found for the sea surface temperature (NOAA [27]). The CO_2 concentration follows these temperature variations with a delay of 6 - 7 months (see also Salby [7]).

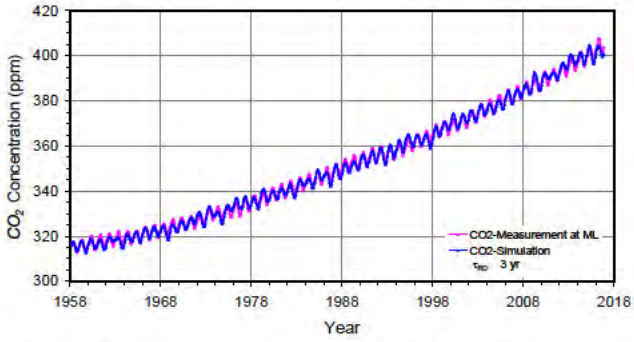

Figure 10. *Monthly CO_2 concentration integrated from the balance equation with temperature-dependent emission and absorption and an initial residence time of 3 years (Blue Triangles). Compared against the observed record of CO_2 from Mauna Loa (Magenta Diamonds).*

A calculation with human emissions included and using the modulated air temperature anomaly $\Delta T(t)$ at Hawaii (NOAA [26]) is shown in Figure 10 (Blue Diamonds). This excellent

agreement with the monthly Mauna Loa CO_2 measurements (Magenta Diamonds) is obtained by applying a linear response of the natural emissions to the modulated temperature anomaly, and assuming a residence time with an initial value of $\tau_{R0} = 3\ yr$ and an averaged slightly nonlinear temperature increase $\Delta T^{1.5}(t)$, which accounts for the nonlinear response of oceanic emissions and the uptake of CO_2 (see Subsection 5.6). It should be mentioned that the averaged air temperature at Hawaii is distinguished by a quite linear increase over time. Therefore, different to Figure 8 also smaller deviations at about 1970 are completely disappearing.

A detailed analysis of the Mauna Loa curve (Salby [7, 10, 11]) and independent cross-correlation investigations of thermally induced emission (Humlum et al. [28]) indicate that the actual absorption time of 3-4 yr, as derived from (9) and based on the IPCC's own estimates, may even be significantly shorter, as short as only 8–12 months, this at least over the vegetation growths' periods on land and in oceans, but also in areas such as the North Atlantic with cold downwelling waters. Under such conditions, in the same way as the residence time is getting shorter, the total emission rate gets larger (generally the most uncertain parameter of the guessed rates). As the admixture of human generated CO_2 is given by the percentage of anthropogenic to total emissions, also this fraction further decreases. So, with an absorption time of $\tau_{R0} = 1\ yr$ and a total emission rate of $e_T = 298\ ppm/yr$ the anthropogenic emissions of $4.7\ ppm/yr$ do not contribute more than 1.6% or 6 ppm to the atmospheric CO_2. However, for a more conservative assessment and in agreement with the IPCC's estimates (AR5 [1], Chap.6-Fig. 6.1) we further emanate from conditions as derived from the simulations of Figures 8 and 10 with $\tau_{R0} = 3\ yr$.

5. Discussion

All presented schemes for simulating the atmospheric CO_2 concentration are based on the balance equation considering the fluxes from extraneous reservoirs to the atmosphere and vice versa. However, as widely used in the literature, the approaches in Section 3 restrict these fluxes on anthropogenic emission-absorption cycles, whereas natural emissions and their uptake are supposed to be the same since 270 years, and thus, any changes in these fluxes are simply disregarded in the total balance. In addition, two of these approaches use a unilateral balance for this cycle, only controlled by the influxes and independent of the actual atmospheric concentration. These deficits have some fatal consequences in the further interpretation of the carbon cycle.

5.1. New Time Scale

Sole consideration of anthropogenic fluxes is identical with the introduction of a new time scale for the uptake of man-made emissions (see subsection 3.4). Since these emissions and also their changes are more than one order of magnitude too small to explain directly the observed concentration changes over recent years, carbon-cycle models just introduce an additional buffer factor, the 'adjustment' time. Such new time scale ensures a sufficiently long cumulation time of the molecules in the atmosphere to attain a concentration level, which is in agreement with the observations. But it looks quite dubious that 280 ppm, equivalent to the environmental fraction, are exchanged with extraneous reservoirs within 3-4 yr, and for about 45% of additional human emissions an accumulation over thousands of years in the atmosphere is assumed.

Effectively represents an 'adjustment' time τ_A nothing more than an amplification factor for the anthropogenic emission rate to fit with the observations. This is obvious for the approach described in subsection 3.3 (see Eqs.(18) and (19)), where the integrated net flux is proportional to $e_A(t)$ and τ_A. But implicitly this is also concealed in the other two schemes.

In the case of a constant airborne fraction the adjustment' time for the fraction $\Delta e_A = AF \cdot e_A(t)$, cumulating in the atmosphere, is even infinite. Under such conditions already any additional constant emission contributes to a linear increase of the concentration, whereas any changes in the emission rate only slightly affect the further shape of this increase. In such case - with an infinite lifetime of additionally emitted molecules in the atmosphere and a given emission rate for FFE from CDIAC [4] and for LUC from Le Quéré et al. [2] (see Figure 2) - AF is now the only free parameter controlling the size and steepness of the concentration growth rate (see (14)).

From a simple balance of the increasing concentration and the total emissions we derive a value for AF of 42%. A realistic model then should reproduce the observations with this airborne fraction. But our previous simulations (see Figure 4) showed that this does not fit in size and shape. The discrepancy would even further increase, when additional natural emissions due to a globally increasing temperature have to be considered. Good consistency can only be found with a reduced anthropogenic emission rate and a further adapted AF.

In the more elaborate Bern Model not only one, but even five new time scales are introduced. This is expressed by the response function with its five decay times (see (15)). While the last term in (15) is similar to the decay described by the residence time τ_R, the others shall represent the limited uptake by different extraneous reservoirs with different time constants, one also infinite. A simulation with this response function, which is equivalent with a time dependent airborne fraction, reproduces quite well the general trend of the increasing concentration (see Figure 6), but in direct analogy to 3.1 and 3.3 satisfactory agreement with the free-air measurements at Mauna Loa is only obtained when reducing the official anthropogenic emissions and neglecting any additional natural emissions.

5.2. First Order Absorption Process

Approaches 3.1 and 3.2 use a quite exceptional definition for the in- and outfluxes between the atmosphere and adjacent reservoirs. The respective absorption rates are considered to be independent of the actual atmospheric concentration, instead they are supposed to scale in direct proportion to the

emission rate either with fixed or time variable airborne fraction. As long as this emission is not zero, the atmospheric concentration further increases, independent of its actual level; and also at constant emissions the system never reaches steady state.

However, when such unusual correlation between emission and absorption rates would really exist, this cannot only be restricted to anthropogenic emissions and switched off for native emissions. Due to the equivalence principle it should be valid for both. *Also for times before 1750 the absorption process cannot have been completely different to that over the Industrial Era or was suddenly changing with the first anthropogenic emissions.*

The dramatic consequences when applying the Bern Model to the total emissions are illustrated in Figure 11. This would result in an exploding atmospheric CO_2 concentration (Green Line) up to levels found 500 Mio. yr ago, and it would never allow steady state conditions as supposed before 1750. In average such an increase over the last 270 yr is equivalent to an $AF = 35\%$.

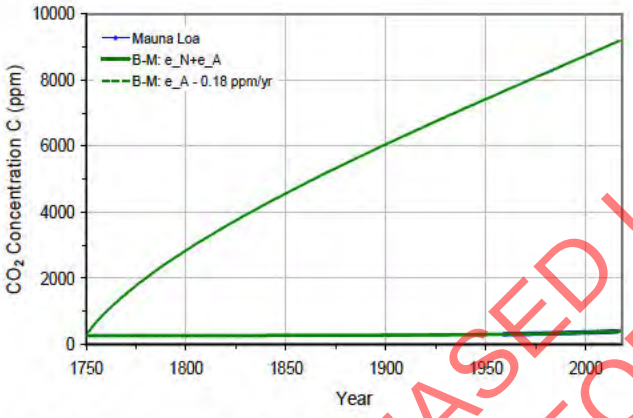

Figure 11. *Simulation of the CO_2 concentration based on the Bern Model assuming the total emissions (Green). Also shown is a calculation for only anthropogenic emissions (Green Crosses). Compared against the observed record of CO_2 from Mauna Loa (Blue Diamonds).*

An uptake process only scaling with the emission rate and not the concentration looks completely unrealistic (see also subsection 3.4). It must be dismissed, even when the simulation for the anthropogenic emissions alone (Green Crosses) pretends good agreement with the Mauna Loa observations (Blue Diamonds).

A balance which only adds up net emissions, and denies an increasing absorption rate with inclining atmospheric concentration, is in contradiction to real observations and hurts fundamental physical laws. CO_2 is not a noble gas, which indifferently accumulates in an open compartment after an emission, but it is dissolved in oceans and converted via photosynthesis to organic molecules. This uptake obeys a first order absorption process and scales with the actual concentration or the difference to an external reservoir[1]. It prevails as long as its concentration C or the difference remains nonzero, i.e., indefinitely.

Different to subsections 3.1 and 3.2 approach 3.3 already emanates from a first order absorption process, but it is also restricted only to anthropogenic concentration changes. Basically an 'ansatz' in (22), third case, and considering changes relative to some reference concentration is correct, when this also includes natural variations over the considered time period. But the fundamental flaw in 3.3 is to introduce a new, independent absorption constant, the adjustment time, for the uptake of the additional emissions instead of using the same absorption process, which already controls more than 95% of the carbon cycle, and this - due to physical causalities - at pre- industrial times in the same manner as over the Industrial Era.

5.3. Environment as a Net Sink

From the observations of the atmospheric concentration and estimates of anthropogenic emissions it is widely inferred that not natural but anthropogenic origin is responsible for the increasing atmospheric CO_2. Writing the global atmospheric carbon budget in the form (see e.g., Cawley [22])

$$\frac{dC}{dt} - e_A(t) = e_N - a_T < 0\,, \tag{25}$$

it is obvious that the net environmental flux, e_N - a_T can quite well be assessed without needing to know the absolute magnitudes of e_N or a_T, quantities which on their parts are highly uncertain. Since the concentration changes dC/dt are smaller than the anthropogenic emission rate, the left side of (25) is negative and thus, the environmental uptake a_T must be larger than the natural emissions e_N. From this correct statement that the environment has acted as a net sink throughout the Industrial Era, however, often wrong conclusions are derived that nature cannot be the reason for any observed CO_2 increase.

For a moment let us assume e_N may be the emission rate at which the system was in balance, and e_A may represent an additional rate of human or native emissions or of both. In reality and in all discussed models with airborne fraction or with first order uptake the concentration growth rate develops slower than these additional emissions and thus, a_T gets larger than e_N. So, with both sides of (25) getting negative this only means that with additional emissions, native or humans, nature also acts as a further increasing sink (compared to a previous equilibrium). As long as any arbitrary fraction of human emission is involved, the environment is always a net sink. This is true per definition, since up to now no artificial uptake exists. But this does not say anything about any additional native emissions over the Industrial Era, since emission and uptake are largely independent processes and the absorption does not impede nature from increasing its own emissions.

A similar strange logic is used by Richardson [29], who

[1] Diffusion processes which act proportional to the concentration difference between two reservoirs, can be assumed to consist of an outflux proportional to the atmospheric concentration C_a and an influx proportional to the concentration of the reservoir C_r.

considers mean values of the net atmospheric accumulation $\langle dC/dt\rangle = 1.7$ *ppm/yr* and of the human emissions $\langle dC_A/dt\rangle = e_A(t) = 3$ *ppm/yr* in a balance

$$\langle dC/dt\rangle - \langle dC_A/dt\rangle = \langle dC_N/dt\rangle < 0\,, \tag{26}$$

in which with $\langle dC_A/dt\rangle = e_A(t)$ a priori any anthropogenic absorptions are embezzled. From this relation it is also inferred that the average natural contribution $\langle dC_N/dt\rangle$ has been to remove CO_2 from the atmosphere, this with the same wrong conclusion as Cawley that the long term trend of rising CO_2 could not be explained by natural causes. This argument is disproved with Figures 8 and 10. The fact that the environment has acted as a net sink throughout the Industrial Era is a consequence of a dynamic absorption rate, which is only controlled by the total CO_2 concentration $C = C_N + C_A$. So, also with additional native emissions and/or temperature changes in the absorptivity the total uptake always tries - with some time delay - to compensate for the total emissions which, of course, also include the anthropogenic fraction. In other words: *Since nature cannot distinguish between native and human emissions, nature is always a net sink as long as human emissions are not zero.* Thus, except for shorter temporary events like volcanic activities the environment will generally act as a net sink even in the presence of increasing natural emissions.

To equate $\langle dC_A/dt\rangle$ in (26) exclusively with human emissions violates conservation of mass. Only when replacing $\langle dC_A/dt\rangle$ by $\langle e_A(t) - C_A/\tau_R\rangle$, eq.(26) satisfies the Conservation Law, and when additionally replacing $\langle dC_N/dt\rangle$ by $\langle e_N(t) - C_N/\tau_R\rangle$ eq.(26) converts to (23).

Again we emphasize that a separate treatment of the native and human cycle with their respective concentrations C_A and C_N is possible if and only if no contributions are missing and the two balances are linked together in one rate equation with only one unitary residence time.

5.4. Too Simple Model

Often climate scientists argue that changes of CO_2 in the atmosphere cannot be understood without considering changes in extraneous systems (see e.g., AR5 [1], Chap.6; Köhler et al. [8]), and they characterize the Conservation Law as a flawed 1-box description because, a single balance equation would not account for details in other reservoirs. In particular, they refer to carbonate chemistry in the ocean, where CO_2 is mostly converted to bicarbonate ions. As only about 1% remains in the form of dissolved CO_2, they argue that only this small fraction could be exchanged with the atmosphere. Due to this so-called Revelle effect, carbonate chemistry would sharply limit oceanic uptake of anthropogenic CO_2.

In regard to understanding changes of CO_2 in the atmosphere, changes in extraneous systems are only qualifiedly of interest. The governing law of CO_2 in the atmosphere (4) and in more elaborate form (23) is self contained. With the inclusion of the surface fluxes $e_T(t)$ and $a_T(t) = C/\tau_R(t)$, which account for influences of the adjacent reservoirs on atmospheric CO_2, details of other extraneous reservoirs of carbon are entirely irrelevant. This feature of the governing physics is not only powerful, but fortunate.

Concerning carbonate chemistry, it is noteworthy that, in the Earth's distant past, CO_2 is thought to have been almost 2000% as great as its present concentration (e.g., Royer et. al. [30]). Most of that was absorbed by the oceans, in which carbon today vastly exceeds that in the atmosphere. According to the IPCC, even in modern times the oceans account for 40% of overall absorption of CO_2 (AR5 [1], Fig.6.1). In relation to other sinks, their absorption of CO_2 is clearly not limited (see Appendix A). Of that 40%, over the Industrial Era anthropogenic CO_2 represents less than 1%. Contrasting with that minor perturbation in absorption is oceanic emission of CO_2. Through upwelling of carbon-enriched water, the oceans significantly enhance natural emission of CO_2 (Zhang [31]).

Different to our approach, which takes into account human and also naturally varying emissions and absorptions, the models in Section 3 emanate from such a simple and apparently flawed description that over thousands of years CO_2 was circulating like an inert gas in a closed system, and only with the industrial revolution this closed cycle came out of control due to the small injections by human emission.

5.5. Different Time Constants

The different time scales introduced with the models in Section 3 represent different absorption processes for the uptake of atmospheric CO_2 molecules by the extraneous reservoirs. From physical principles it is impossible that an absorption process would differentiate between naturally and anthropogenically emitted molecules. The temporal absorption or sequestration - except for smallest corrections due to isotopic effects - is for all molecules identical.

The absorption also cannot decline unexpectedly by more than one order of magnitude with the begin of the Industrial Era or because of an additional emission rate of a few %. Observations show that no noticeable saturation over recent years could be found (Appendix A).

Oceans and continents consist of an endless number of sources and sinks for CO_2 which act parallel, emitting CO_2 into the atmosphere and also absorbing it again. In the same way as the different emission rates add up to a total emission, the absorption rates with individual absorptivities α_i - and each of them scaling proportional to the actual CO_2 concentration - add up to a total uptake as a collective effect

$$\begin{aligned} a_T &= \alpha_1 C + \alpha_2 C + \ldots + \alpha_N C \\ &= (\alpha_1 + \alpha_2 + \ldots + \alpha_N)\cdot C = \alpha_R \cdot C \end{aligned}\,. \tag{27}$$

Collective absorption thus leads to exponential decay of perturbation CO_2 at a *single* rate

$$\alpha_R = 1/\tau_R = \alpha_1 + \alpha_2 + \ldots + \alpha_N\,. \tag{28}$$

This decay rate is faster than the rate of any individual sink

and it prevails as long as its concentration C or its difference to external reservoirs remains nonzero (see: Harde [6]; Salby [11]).

The above behavior is a consequence of the Conservation Law and in contrast to the Bern Model, where decay proceeds at *multiple* rates. A treatment of CO_2 with a multiple exponential decay obeys the following:

$$\begin{aligned} C &= C_{10}e^{-\alpha_1 t} + C_{20}e^{-\alpha_2 t} + ... + C_{N0}e^{-\alpha_N t} \\ &= C_1 + C_2 + ... + C_N \end{aligned} \quad . \tag{29}$$

Then differentiation gives:

$$\begin{aligned} \frac{dC}{dt} &= -\alpha_1 C_{10}e^{-\alpha_1 t} - \alpha_2 C_{20}e^{-\alpha_2 t} ... - \alpha_N C_{N0}e^{-\alpha_N t} \\ &= -\alpha_1 C_1 - \alpha_2 C_2 ... - \alpha_N C_N \\ &\neq -(\alpha_1 + \alpha_2 + ... + \alpha_N) \cdot C \end{aligned} \tag{30}$$

At multiple decay rates the corresponding sinks operate, not collectively, but independently. After a couple of their decay times, the fastest sinks become dormant. Overall decay then continues only via the slowest sinks, which remove CO_2 gradually. It is for this reason that such a treatment leaves atmospheric CO_2 perturbed for longer than a thousand years (Figure 5). In contrast, the behavior required by the Conservation Law decays as fast or faster than that of the fastest sink (see (28)).

The observed decay of ^{14}C shows that the corresponding absorption is determined by a single decay time and operates on a time scale of only about one decade (see Figure 5). This scale is the same for the natural carbon cycle as for the anthropogenic cycle. Therefore, it is unrealistic to differentiate between a residence time and different adjustment times.

In this context it should be noticed that due to re-emissions of $^{14}CO_2$ from extraneous reservoirs the real residence time of $^{14}CO_2$ in the atmosphere as well as that of the other isotopologues of CO_2 can only be shorter, even shorter than a decade (for details see subsection 5.7.3 and Appendix B).

5.6. Temperature Dependence

According to (9) or (10) we see that with increasing atmospheric concentration over the Industrial Era from 280 to 400 ppm either the residence time must be increased with temperature from 3 to about 4 yr, or τ_R is considered to be constant and the total emissions were rising from 93 to about 130 ppm/yr, synchronously increasing the concentration. Both these limiting cases are in agreement with a temperature anomaly of about 1.2 °C over this period (see GISS [9]), when we assume the maximum temperature coefficients $\beta_\tau = 0.74$ *yr/°C* or $\beta_e = 24$ *ppm/yr/°C*. However, generally both temperature induced natural emissions as well as temperature dependent absorptions together will dictate the inclining concentration in the atmosphere.

In any way, as we see from Figure 8, is the CO_2 concentration dominantly empowered by the temperature increase; with only one unique decay process not human activities but almost only natural impacts have to be identified as the main drivers for the observed CO_2 increase in the atmosphere and also for the continuous climate changes over the past and present times.

The various mechanisms, along with their dependence on temperature and other environmental properties, could not have remained constant during the pre-industrial era. This inconsistency invalidates the fundamental assumption, that natural emission and absorption during the pre-industrial period did remain constant. Even less this is valid over the Industrial Era, a period which is characterized by the IPCC as the fastest rise in temperature over the Holocene or even the last interglacial.

So, the CO_2 partial pressure in sea water approximately changes with temperature as $(pCO_2)_{sw}(T) = (pCO_2)_w(T_0)$* $exp[0.0433*(T-T_0)]$ (see: Takahashi et al. [32]) and thus, an increase of *1°C* causes a pressure change of about *18 µatm*, which amplifies the influx and attenuates the outflux. From observations over the North Atlantic Ocean (see, Benson et al. [33]) it can be estimated that a pressure difference ΔpCO_2 between the atmosphere and ocean of *1 µatm* contributes to a flux change of $\delta f_{in} \approx 0.075$ *mol/m²/yr = 3.3 g/m²/yr*. Therefore, with an Earth s surface of *320 Mio. km²* covered by oceans and a pressure change of $\Delta pCO_2 = 18$ *µatm,* under conventional conditions the native influx from oceans to the atmosphere already increases by $\Delta f_{in} \approx 19$ *Pg/yr* or *2.4 ppm/yr* for an average temperature incline of *1°C*. An even stronger variation can be expected for the land vegetation with an increased decomposition and reduced uptake of CO_2 at rising temperature (Lee [34]; Salby [11]).

Together this causes an incline of the atmospheric CO_2 level which is larger than all apparent human activities, but its contribution is completely neglected in the official accounting schemes.

Also melting permafrost and emissions of volcanoes on land and under water as well as any emissions at earthquakes are not considered. In addition, actual estimates of dark respiration suggest that under global warming conditions whole-plant respiration could be around 30% higher than existing estimates (Huntingford et al. [35]). This longer list of different native events and effects is completely embezzled in the favored IPCC models.

Equally inconsistent is the presumption that additional uptake of anthropogenic CO_2, which represents less than 1% of the total over the Industrial Era, has, somehow, exceeded the storage capacity of oceans and other surface and sub-surface reservoirs, capacity which is orders of magnitude greater. *A reduced absorption is rather the consequence of global warming than of saturation*. Due to Henry's law and its temperature dependence not only the partial pressure in sea water increases, but also the solubility of CO_2 in water declines exponentially with temperature and, thus, reduces the CO_2 uptake. Often is this effect incorrectly misinterpreted as saturation caused by a limited buffer capacity and dependent on the concentration level. But here we consider an uptake changing with temperature, as this is known for chemical reactions, where the balance is controlled by temperature. How strongly the biological pump (see Appendix A) and

photosynthesis on land is also controlled by temperature, is only incompletely known, but obviously they are also varying slightly exponentially with temperature (Lee [34]).

Figure 12 displays a scatter plot supporting the close correlation of the atmospheric CO_2 concentration with the land-ocean temperature anomaly (GISS [9]). The latter is controlled by more than 60% by the solar influence and less than 40% by CO_2 as greenhouse gas feedback (Harde [36, 37]).

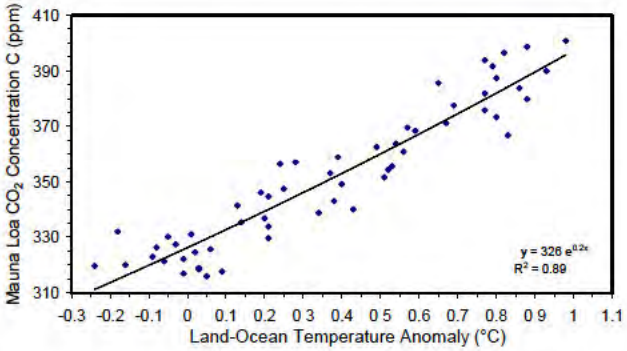

Figure 12. *Scatter plot of Mauna Loa CO_2 concentration (Blue Diamonds) and trend curve (Black Graph) versus land-ocean temperature anomaly.*

5.7. IPCC Arguments for a Human-Made CO_2 Increase

The preceding discussion has made clear that a consistent description of the carbon-cycle, which is in full agreement with all observations and physical relations, can only emanate from unitary treatment of all CO_2 molecules - native and human-caused ones. This means: the anthropogenic carbon cycle cannot be separated from the natural cycle; it exists only one single residence time of CO_2 molecules in the atmosphere; and the uptake of all these molecules obeys a first order principle.

But we still have to scrutinize how far this description is really in contradiction to the key arguments (lines of evidence) as adduced by the IPCC for a human caused CO_2 incline, or how far these arguments also hold for our alternative approach.

In AR5 [1], Subchap.6.3.2.3 we read:

"*With a very high confidence, the increase in CO_2 emissions from fossil fuel burning and those arising from land use change are the dominant cause of the observed increase in atmospheric CO_2 concentration.*"

IPCC then lists five arguments to support this conclusion (references in the following IPCC-citations are not listed as additional references in this article).

5.7.1. Decrease in Atmospheric O_2

The observed decrease in atmospheric O_2 content over past two decades and the lower O_2 content in the northern compared to the SH are consistent with the burning of fossil fuels (see Figure 6.3 and Section 6.1.3.2; Keeling et al., 1996; Manning and Keeling, 2006)."

This is barely a supporting argument for a dominantly man-made CO_2 increase, since this 'line of evidence' is in the same way valid for our approach, which evidently includes the same amount of anthropogenic emissions. Burning of fossil fuels removes oxygen from the atmosphere in a tightly defined stoichiometric ratio dependent on the fuel carbon content. This content is the same in our balance as in the IPCC models, therefore, the respective O_2 decay rate and on the other hand the CO_2 growth rate due to combustion is also the same, independent of any additional emissions of natural origin. The fundamental difference to the IPCC's assumption is that the anthropogenic emissions do not cumulate in the atmosphere for longer times or for ever. They have the same residence time as native CO_2, in average 4 yr or shorter, and therefore they only contribute 15% or even less to the observed increase since 1750.

In this context it should also be clear that CO_2 and O_2 behave just anti-cyclic in the photosynthesis and respiration cycle. Also the biochemical reactions in the atmosphere are completely different. CO_2 is a non-reacting gas in the atmosphere, while O_2 preferentially oxidizes other materials and is tied in chemical compounds. All these reactions are directly controlled by the temperature. Compared to the atmospheric oxygen content of about 21% a decrease of 80 ppm over 20 yr is relatively small, it is not more than 0.4‰. As long as this O_2 cycle is not better known, an observed decline in atmospheric oxygen gives only little evidence for a dominantly human caused CO_2 increase. At best it can confirm the CDIAC-data, which are the same in our approach as in the IPCC models.

5.7.2. Lower $^{13}C/^{12}C$ Isotope Ratio in Fossil Fuels

CO_2 from fossil fuels and from the land biosphere has a lower $^{13}C/^{12}C$ stable isotope ratio than the CO_2 in the atmosphere. This induces a decreasing temporal trend in the atmospheric $^{13}C/^{12}C$ ratio of atmospheric CO_2 concentration as well as, on annual average, slightly lower $^{13}C/^{12}C$ values in the NH (Figure 6.3). These signals are measured in the atmosphere."

Also this is no supporting argument for a dominantly man-made CO_2 increase, as with our approach we are also expecting such declining $^{13}CO_2$ concentration. The $^{13}C/^{12}C$ ratio in the atmosphere or its normalized ‰-difference $(\delta^{13}C)_{atm}$ is measured at Mauna Loa and at the South Pole atmospheric station (see AR5 [1], Figure 6.3). At Mauna Loa, e.g., it shows an average decrease of 0.7‰ from -7.6‰ in 1980 to -8.3‰ in 2010. Over these 30 years was the anthropogenic emission rate increasing by *1.8 ppm/yr* from *2.5 ppm/yr* in 1980 to *4.3 ppm/yr* in 2010 (CDIAC [4]). With respect to the total emission rate this corresponds to an increase of 1.8 %.

Owing to the equivalence principle fossil fuel emissions cannot cumulate in the atmosphere but will be absorbed with the same probability like naturally emitted CO_2 molecules. Thus, in first order the $^{13}C/^{12}C$ ratio in the atmosphere can only be diluted proportional to the leaner ^{13}C concentration and proportional to the fraction of the man-made flux to the total flux. Smaller corrections will result from the fractionation for lighter molecules and a slightly higher emission probability for molecules, which were just taken up (re-emission, see next

item).

Since the fossil fuel emissions have a leaner difference $(\delta^{13}C)_{fuel\text{-}atm}$ = -18 ‰ compared to the atmosphere, or $(\delta^{13}C)_{fuel\text{-}VPDB}$ = -25 ‰ with respect to the international VPDB carbonate standard (Coplen [38]), the rising human emissions over the 30 yr interval can only have contributed to a decline of $\Delta = (\delta^{13}C)_{fuel\text{-}atm} \times 1.8\% = -18‰ \times 1.8\% = -0.32$ ‰ or a $(\delta^{13}C)_{atm}$ = -7.92‰ in 2010. Thus, the difference to -8.3‰, which is more than 50%, in any case must be explained by other effects.

One possible explanation for a faster decline of $(\delta^{13}C)_{atm}$ to -8.3‰ can be - even with oceans as source and an $^{13}C/^{12}C$ ratio in sea water greater than in air (particularly in the surface layer) - that the lighter $^{12}CO_2$ molecules are easier emitted at the ocean's surface than $^{13}CO_2$, this with the result of a leaner ^{13}C concentration in air and higher concentration in the upper water layer (see also: Siegenthaler & Münnich [39]). From water we also know that its isotopologues are evaporated with slightly different rates.

Such behavior is in agreement with the observation that with higher temperatures the total CO_2 concentration in the atmosphere increases, but the relative $^{13}CO_2$ concentration decreases. This can be observed, e.g., at El Niño events (see: M. L. Salby [40], Figure 1.14; Etheridge et al. [41]; Friedli et al. [42]).

We also remind at the Mauna Loa curve, which shows for the total emissions a seasonal variation with an increasing CO_2 concentration from about October till May and a decline from June to September. The increase is driven by respiration and decomposition mainly on the Northern Hemisphere (NH) as well as the temperature on the Southern Hemisphere (SH) and also local temperature effects. The $(\delta^{13}C)_{atm}$ value is just anti-cyclic to the total CO_2 concentration (AR5 [1], Figure 6.3) with a minimum at maximum CO_2 concentration and with seasonal variations of 0.3 - 0.4‰, the same order of magnitude as the fossil fuel effect.

An increase of ^{13}C in the upper strata of oceans also results from an increased efficiency of photosynthesis for lighter CO_2. Plankton accumulates this form and sinks to lower layers, where it decomposes and after longer times is emitted in higher concentrations with stronger upwelling waters particularly in the Eastern Tropic Pacific. It is also known that the ^{13}C concentrations are by far not equally distributed over the Earth's surface. Thus it can be expected that with volcanic and tectonic activities different ratios will be released.

So, without any doubts fossil fuel emissions will slightly dilute the $^{13}CO_2$ concentration in air. But presupposing regular conditions for the uptake process (equivalence principle) they contribute less than 50% to the observed decrease. The difference has to be explained by additional biogeochemical processes. Particularly the seasonal cycles and events like El Niños are clear indications for a stronger temperature controlled modulation of the $(\delta^{13}C)_{atm}$ value. Therefore is an observed decline of the $^{13}C/^{12}C$ ratio over recent years by far not a confirmation of an anthropogenic global warming (AGW) theory.

Also the widely spread but wrong declaration that "*about half of the emissions remained in the atmosphere since 1750*" and "*the removal of all the human-emitted CO_2 from the atmosphere by natural processes will take a few hundred thousand years (high confidence)*" (see AR5 [1], Chap. 6-Summary and Box 6.1) can be simply refuted by the isotope measurements at Mauna Loa. If the *113 ppm* CO_2 increase since 1750 (28.8% of the present concentration of *393 ppm* - average between 2007 and 2016) would only result from human impacts and would have cumulated in the atmosphere, the actual $(\delta^{13}C)_{atm}$ value should have dropped by $\Delta = (\delta^{13}C)_{fuel\text{-}atm} \times 28.8\% = -18‰ \times 28.8\% = -5.2‰$ to $(\delta^{13}C)_{atm} \approx$ -7‰ -5.2‰ = -12.2‰, which by far is not observed. $(\delta^{13}C)_{atm}$ in 1750 was assumed to have been -7‰.

5.7.3. Fossil Fuels are Devoid of Radiocarbon

"Because fossil fuel CO_2 is devoid of radiocarbon (^{14}C), reconstructions of the $^{14}C/C$ isotopic ratio of atmospheric CO_2 from tree rings show a declining trend, as expected from the addition of fossil CO_2 (Stuiver and Quary, 1981; Levin et al., 2010). Yet nuclear weapon tests in the 1950s and 1960s have been offsetting that declining trend signal by adding ^{14}C to the atmosphere. Since this nuclear weapon induced ^{14}C pulse in the atmosphere has been fading, the $^{14}C/C$ isotopic ratio of atmospheric CO_2 is observed to resume its declining trend (Naegler and Levin, 2009; Graven et al., 2012)."

For ^{14}C we can adduce almost the same comments as listed for ^{13}C. Fossil CO_2 devoid of ^{14}C will reduce the $^{14}C/C$ ratio of the atmosphere, this is valid for our approach in the same manner as for the IPCC schemes. But, as no specific accumulation of anthropogenic molecules is possible (equivalence principle), this decline can only be expected proportional to the fraction of fossil fuel emission to total emission. Before 1960 this was not more than 1% and actually it is about 4.3%.

^{14}C is continuously formed in the upper atmosphere from ^{14}N through bombardment with cosmic neutrons, and then rapidly oxidizes to $^{14}CO_2$. In this form it is found in the atmosphere and enters plants and animals through photosynthesis and the food chain. The isotopic $^{14}C/C$ ratio in air is about $1.2 \cdot 10^{-12}$, and can be derived either from the radioactivity of ^{14}C, which with an average half-lifetime of 5730 yr decays back to ^{14}N by simultaneously emitting a beta particle, or by directly measuring the amount of ^{14}C in a sample by means of an accelerator mass spectrometer.

Fossil fuels older than several half-lives of radiocarbon are, thus, devoid of the ^{14}C isotope. This influence on radiocarbon measurements is known since the investigations of H. Suess [43] who observed a larger ^{14}C decrease (about 3.5%) for trees from industrial areas and a smaller decline for trees from unaffected areas. This so-called Suess or Industrial effect is important for reliable age assignments by the radiocarbon method and is necessary for respective corrections. But for global climate considerations it gives no new information, it only confirms the calculations based on the human to total emission rate (see above), and it clearly shows that an assumed accumulation of anthropogenic CO_2 in the

atmosphere contradicts observations.

More important for climate investigations is that after the stop of the nuclear bomb tests 1963 ^{14}C could be used as a sensitive tracer in the biosphere and atmosphere to study temporal carbon mixing and exchange processes in the carbon cycle. As the bomb tests produced a huge amount of thermal neutrons and almost doubled the ^{14}C activity in the atmosphere, with the end of these tests the temporal decline of the excess radiocarbon activity in the atmosphere can well be studied. This decline is almost completely independent of the radioactive lifetime, but practically only determined by the uptake through extraneous reservoirs.

Such decline has already been displayed in Figure 5 as fractionation-corrected ‰-deviations $\Delta^{14}CO_2$ from the Oxalic Acid activity corrected for decay, this for a combination of measurements at Vermunt and Schauinsland (Magenta Dots and Green Triangles; data from Levin et al. [17]). The decay is well represented by a single exponential with a decay constant of about 15 yr (Dashed Blue). For similar observations see also Hua et al. [18] and Turnbull et al. [19]. Thus, the decay satisfies the relation

$$\frac{dC'_{14}}{dt} = -\frac{1}{\tau_{14}} \cdot C'_{14}, \tag{31}$$

where C'_{14} represents the excess concentration of radiocarbon above a background concentration in the atmosphere. It corresponds to absorption that is proportional to instantaneous concentration with an apparent absorption time τ_{14} slightly more than a decade.

Because CO_2 is conserved in the atmosphere it can change only through an imbalance of the surface fluxes e_T and a_T. This holds for all isotopologues of CO_2 in the same way. For this reason, its adjustment to equilibrium must proceed through those influences. They are the same influences that determine the removal time of CO_2 in the atmosphere. If CO_2 is perturbed impulsively (e.g., through a transient spike in emission), its subsequent decay must track the removal of perturbation CO_2, C', which in turn is proportional to its instantaneous concentration. Determined by the resulting imbalance between e_T and a_T, that decay is governed by the perturbation form of the balance equation:

$$\frac{dC'}{dt} = -\frac{1}{\tau_R} \cdot C', \tag{32}$$

which is the same form as the observed decay of ^{14}C following elimination of the perturbing nuclear source. But there is still one important difference between these equations.

Eq.(32) is the perturbation form of (23) with a decay time τ_R, the residence time, because $1/\tau_R$ describes the rate at which CO_2 is removed from the atmosphere, this as the result of the balance between all absorption and emission processes.

In contrast to this describes (31) a decay process, which implicitly also considers some back-pumping of radiocarbon to the atmosphere (see Appendix B, (37)). So, from all ^{14}C that is removed from the atmosphere with the time constant τ_R - in the same way as all isotopes -, only some smaller fraction is completely sequestered beneath the Earth's surface by a single absorption process. A substantial fraction is therefore returned to the atmosphere through re-emission (e.g., through decomposition of vegetation which has absorbed that ^{14}C), and in average it takes several absorption cycles to completely remove that ^{14}C from the atmosphere. This simply modifies the effective absorption for radiocarbon, but with a resulting decay which remains exponential (see Figure 5). Unlike any dilution effect by fossil fuel emission, which is minor (see Appendix B), this re-emission slows decay over what it would be in the presence of pure absorption alone. Therefore is the apparent absorption time - as derived from the ^{14}C decay curve - longer than the actual absorption time.

In this context we emphasize that apart from some minor influence due to fractionation all CO_2 isotopologues are involved in the same multiple re-emission cycles. But in (23) or (32) this is already considered in the total balance via the emission rates, for which it makes no difference, if the same or meanwhile exchanged molecules are recycled to the atmosphere. In contrast to this are $^{14}CO_2$ isotopologues identified through their radioactivity, and in the worst case without any dilution or exchange processes in an external reservoir τ_{14} would approach the radioactive lifetime. On the other hand, at strong diffusion, dilution or sequestration of ^{14}C in such reservoirs τ_{14} would converge to τ_R. Consequently it follows from the observed ^{14}C decay shown in Figure 5 that this provides an upper bound on the actual absorption time τ_R, which can be only shorter. Both are tremendously shorter than the adjustment time requested by the IPCC.

The exponential decay of ^{14}C with only one single decay time proves models with multiple relaxation times to be wrong. At the same time it gives strong evidence for a first order absorption process as considered in Section 4.[2]

5.7.4. Higher Fossil Fuel Emissions in the Northern Hemisphere

"Most of the fossil fuel CO_2 emissions take place in the industrialised countries north of the equator. Consistent with this, on annual average, atmospheric CO_2 measurement stations in the NH record increasingly higher CO_2 concentrations than stations in the SH, as witnessed by the observations from Mauna Loa, Hawaii, and the South Pole (see Figure 6.3). The annually averaged concentration difference between the two stations has increased in proportion of the estimated increasing difference in fossil fuel combustion emissions between the hemispheres (Figure 6.13; Keeling et al., 1989; Tans et al., 1989; Fan et al., 1999)".

The strongest terrestrial emissions result from tropical forests, not industrial areas. The strongest oceanic emissions can be seen from the map of Takahashi et al. [32]. They are

[2] A calculation similar to Figure 8 but with a residence time of 15 yr as an upper bound would require to reduce the natural emissions at pre-industrial times from *93 ppm/yr* to *19 ppm/yr*. Then the anthropogenic contribution would supply *59 ppm*, which is 15% of the total atmospheric concentration or 52% of the increase since 1850.

between 10°N and 10°S in the Eastern Tropic Pacific. Nevertheless, there is no doubt that industrial emissions endow their fingerprints in the atmosphere and biosphere (Suess effect). The influence and size of these emissions has already been discussed above, and their different impact on the two hemispheres can be estimated from Figure 6.3c of AR5 [1] indicating a slightly faster decline of $(\delta^{13}C)_{atm}$ for the NH in agreement with predominantly located industrial emissions in this hemisphere. Even more distinctly this is illustrated by Figure 6.13 of AR5 [1] for the difference in the emission rates between the northern and SH with 8 PgC/yr, which can be observed as a concentration difference between the hemispheres of 3.8 ppm. But this is absolutely in no dissent to our result in Section 4 that from globally *4.7 ppm/yr* FFE and LUC (average emission over 10 yr) 17 ppm or 4.3 % contribute to the actual CO_2 concentration of *393 ppm* (average). This impact is of the same size as seasonal variations observed at Mauna Loa before flattening and averaging the measurements.

5.7.5. Human Caused Emissions Grew Exponentially

> *"The rate of CO_2 emissions from fossil fuel burning and land use change was almost exponential, and the rate of CO_2 increase in the atmosphere was also almost exponential and about half that of the emissions, consistent with a large body of evidence about changes of carbon inventory in each reservoir of the carbon cycle presented in this chapter".*

The size and influence of FFE and LUC on the atmospheric CO_2 concentration has extensively been discussed in the preceding sections. Only when violating fundamental physical principles like the equivalence principle or denying basic causalities like a first order absorption process with only a single absorption time, the CO_2 increase can be reproduced with anthropogenic emissions alone.

In contrast to that we could demonstrate that conform with the rising temperature over the Industrial Era and in conformity with all physical legalities the overwhelming fraction of the observed CO_2 increase has to be explained by native impacts. Such simulations reproduce almost every detail of the observed atmospheric CO_2 increase (see Figures 8 and 10). And from observations of natural emissions it can be seen that they are increasing slightly exponential with temperature (Takahashi et al. [32]; Lee [34]).

Thus, no one of the preceding lines of evidence can really support the above statement that "*fossil fuel burning and land use change are the dominant cause of the observed increase in atmospheric CO_2 concentration*." In fact, they apply in the same way for our concept, and thus they are useless to disfavour our approach. The isotopic studies rather confirm our ansatz of a first order absorption process with a single absorption time, which is significantly shorter than one decade, and they refute the idea of cumulating anthropogenic emissions in the atmosphere.

6. Conclusion

The increase of CO_2 over recent years can well be explained by a single balance equation, the Conservation Law (23), which considers the total atmospheric CO_2 cycle, consisting of temperature and thus time dependent natural emissions, the human activities and a temperature dependent uptake process, which scales proportional with the actual concentration. This uptake is characterized by a single time scale, the residence time of about 3 yr, which over the Industrial Era slightly increases with temperature. Only this concept is in complete conformity with all observations and natural causalities. It confirms previous investigations (Salby [7, 10]; Harde [6]) and shows the key deficits of some widespread but largely ad hoc carbon cycle models used to describe atmospheric CO_2, failures which are responsible for the fatal conclusion that the increase in atmospheric CO_2 over the past 270 years is principally anthropogenic.

For a conservative assessment we find from Figure 8 that the anthropogenic contribution to the observed CO_2 increase over the Industrial Era is significantly less than the natural influence. At equilibrium this contribution is given by the fraction of human to native impacts. As an average over the period 2007-2016 the anthropogenic emissions (FFE&LUC together) dominated not more than 4.3% to the total concentration of 393 ppm, and their fraction to the atmospheric increase since 1750 of 113 ppm is not more than 17 ppm or 15%. With other evaluations of absorption, the contribution from anthropogenic emission is even smaller. Thus, not really anthropogenic emissions but mainly natural processes, in particular the temperature, have to be considered as the dominating impacts for the observed CO_2 increase over the last 270 yr and also over paleoclimate periods.

Acknowledgements

The author thanks Prof. Murry Salby, formerly Macquarie University Sydney, for many stimulating discussions when preparing the paper, and Jordi López Fernández, Institute of Environmental Assessment and Water Studies Barcelona, for his support when searching for temperature data.

This research did not receive any specific grant from funding agencies in the public, commercial, or not-for-profit sectors.

Appendix

Appendix A

The absorption efficiency of extraneous reservoirs has been claimed to have decreased, based on changes in the arbitrarily-defined airborne fraction (e.g., Le Quéré et al. [12]; Canadell et al. [44]). Such claims are dubious because they rely on the presumption that changes of CO_2 are exclusively of anthropogenic origin. Nor are the claims supported by recent atmospheric CO_2 data. Gloor et al. [45] found that decadal changes of AF followed from changes in the growth of anthropogenic emissions - not from changes in absorption efficiency, which were comparatively small. Further, uncertainties in emission and absorption exceeded any

changes in AF. Ballantyne et al. [46] arrived at a similar conclusion. They used global atmospheric CO_2 measurements and CO_2 emission inventories to evaluate changes in global CO_2 sources and sinks during the past 50 years. Their mass balance analysis indicates that net CO_2 uptake significantly increased, by about 0.18 Pg/yr (0.05 GtC/yr) and, between 1960 and 2010, that global uptake actually doubled, from 8.8 to 18.4 Pg/yr. It follows that, without quantitative knowledge of changes in natural emission, interpretations based on AF are little more than speculative.

The uptake and outgassing of atmospheric CO_2 by oceans is simulated with complex marine models. How much CO_2 enters or leaves the ocean surface is calculated from the difference between atmospheric and surface concentrations of CO_2, modified by the Revelle factor. However, most of these models involve assumptions which are not in agreement with observed behavior (see, e.g., Steele [47]). They assume that the surface layer absorbs CO_2 through equilibrium with atmospheric concentration. On this premise, they calculate how much Dissolved Inorganic Carbon (DIC) will be added to the ocean based on increased atmospheric CO_2 since pre-industrial times. In reality, the surface layer is not at equilibrium with the atmosphere. A difference in concentration results from conversion of CO_2 into organic carbon by photosynthesis. Organic carbon produced then sinks into the deep ocean, where it is sequestered. This downward transport to the deep ocean is known as the biological pump. In the Northeastern Atlantic basin, e.g., Benson et al. [33] report on seasonal pressure differences between the ocean and atmosphere of $\Delta pCO_2 = -70\ \mu atm$ and an air-sea CO_2 flux *of* $220\ g/m^2/yr$. Only in those regions where strong upwelling of DIC from the deep ocean exceeds sequestration of carbon via photosynthesis can CO_2 be outgassed to the atmosphere. The latter is found primarily in the tropical oceans (Takahashi et al. [32]; Zhang et al. [31]). Several models es imate that, without the biological pump, atmospheric CO_2 would be 200 to 300 ppm higher than current levels (see also Evans [48]).

With increasing primary production, carbon export to depth also grows. Arrigo et al. [49] reported that since 1998, annual primary production in he Arctic has increased by 30%. Steinberg et al. [50] observed a 61% increase in meso-plankton between 1994 and 2006 in the Sargasso Sea. The North Atlantic coccolithophores h ve increased by 37% between 1990 and 2012 (Krumhardt et al. [51]). And Chavez et al. [52] found a dramatic increase in primary production in the Peru Current since the end of the Little Ice Age (LIA). Together, the increase in primary production and downward transport of organic carbon is sufficient to account for anthropogenic CO_2 that was absorbed from the atmosphere (Steele [47]).

Further, seasonal changes in surface CO_2 illustrate that absorption of CO_2 by the oceans and accumulation of DIC near the surface are determined, not by the Revelle factor, but by the biological pump. Evans et al. [48] found from buoy data off the coast of Newport, Oregon that each spring photosynthesis lowers ocean surface CO_2 to 200 ppm - far below current atmospheric concentrations and much lower than what would be expected from equilibrium with a pre-industrial atmosphere. Anthropogenic CO_2 in surface water is then quickly removed. It is also well known that higher concentrations of CO_2 magnify photosynthesis. At increased atmospheric CO_2, the plankton community consumed 39% more DIC (Riebesell et al. [53]). During summer and autumn, surface CO_2 can rapidly increase to 1000 ppm - more than twice the concentration of CO_2 in the atmosphere. Surface water then significantly enhances natural emission to the atmosphere. Conversely, during winter, surface CO_2 remains at about 340 ppm. Despite reduced photosynthesis, CO_2 in surface water then remains below equilibrium with the atmosphere, reflecting efficient removal through downward transport by the biological pump. It is noteworthy that these strong seasonal variations of CO_2 in surface water are manifest in the record of atmospheric CO_2 (see Figures 9 and 10).

Under steady state conditions, diffusion of CO_2 into the ocean is believed to require about 1 year to equilibrate with an atmospheric perturbation. But, when increased sunlight enhances photosynthesis, such equilibration is no longer achieved. Perturbation CO_2 is then simply transported to depth, where it is sequestered from surface waters (McDonnell et al. [54]). Under such conditions uptake of CO_2 is not restricted by the Revelle factor but by the biological pump.

The foregoing processes are controlled essentially by sunlight and temperature. There is no reason to believe that net primary production, the biological pump, and sequestration of CO_2 below surface waters would be the same today as 270 years ago, when temperature and atmospheric CO_2 were likely lower.

In simulating transport of carbon in the ocean, complex models assume behavior that is found in tracers like chlorofluorocarbons (CFCs). Because those species accumulate near the ocean surface, models assume DIC does as well. But unlike CFCs, which are inert, CO_2 entering sunlit waters is quickly converted to organic matter by photosynthesis (Steele [47]). Although dissolved CFCs and dissolved carbon are passively transported in the same manner, particulate organic carbon (alive or dead) behaves very differently. It rapidly sinks, removing carbon from surface water through mechanisms which do not operate on CFCs.

The removal of carbon from surface water depends on the sinking velocity and also on how rapidly organic matter is decomposed. After descending below the pycnocline (depths of 500-1000 meters), carbon is effectively sequestered - because water at those depths does not return to the surface for centuries (Weber et al. [55]). For the atmosphere, this long-term sequestration translates into removal that is effectively permanent. Before such carbon can return to the atmosphere, fossil fuel reserves will have long since been exhausted.

The combination of sinking velocities and sequestration depth suggests that a significant fraction of primary production is sequestered in a matter of days to weeks (Steele [47]). Therefore, increasing primary production leads to a proportionate increase and rapid export of carbon to depth. If marine productivity has increased since pre-industrial times, it will

have also sequestered the respective anthropogenic carbon into the deeper ocean. Observations from ocean basins suggest that, since the Little Ice Age, marine productivity and carbon export have indeed increased as the oceans warmed (Chavez et al. [52]; Abrantes et al. [56]).

Appendix B

The bomb radiocarbon signal in the atmosphere is a sensitive tracer to study the fluxes in the carbon cycle, in particular to determine an upper bound for the residence time of CO_2 in the atmosphere and its uptake through extraneous reservoirs. Carbon 14 obeys the balance equation

$$\frac{dC_{14}}{dt} = e_{14} - \frac{C_{14}}{\tau_{14}} \tag{33}$$

with e_{14} as the emission rate, which follows from background emission of ^{14}C as well as anthropogenic emission. The decay after the stop of the bomb tests in 1963 then satisfies the relation (see Subsection 5.7.3, (31))

$$\frac{dC'_{14}}{dt} = -\frac{1}{\tau_{14}} \cdot C'_{14}, \tag{34}$$

where C'_{14} represents the excess concentration of radiocarbon above background concentration in the atmosphere, and τ_{14} is the apparent absorption time of about 15 yr. Regularly not the absolute number of ^{14}C but its ratio to ^{13}C or ^{12}C is measured, either as radioactivity or by accelerator mass spectrometry.

As the total CO_2 concentration is not constant over the observed decay period and this directly affects the relative ^{14}C decay as well as the background level, the measured ^{14}C activity has to be corrected for these variations to obtain the true C'_{14} concentration. Such corrections are important for age dating of materials and also for atmospheric ^{14}C measurements. Without compensating for the varying total concentration, e.g., the ^{14}C-decay and the background would be modified by several ten ‰.

Mostly the corrected data are specified as fractionation-corrected ‰-deviations from the Oxalic Acid standard activity corrected for decay (see Stuiver&Polach [57]):

$$\Delta^{14}C = \left[\frac{A_{SN}}{A_{ABS}} - 1\right] \cdot 1000 \tag{35}$$

with A_{SN} as sampling activity normalized for isotope fractionation to ^{13}C, and A_{ABS} as the absolute international standard activity (Oxalic Acid standard). A_{SN} relates to the measured sample activity A_S as

$$A_{SN} = A_S\left[1 - \frac{2(25+\delta^{13}C}{1000}\right], \tag{36}$$

where $\delta^{13}C$ is specified in ‰ with respect to the ^{13}C VPDB standard.

This normalization procedure also accounts for fossil fuel emissions, which are devoid of ^{14}C and also have a leaner ^{13}C abundance. So, human emissions dilute the $^{14}C/^{12}C$ and $^{13}C/^{12}C$ ratio in the atmosphere. Such corrections are important for correct age assignments, but how much does this industrial effect and the observed dilution also affect the atmospheric ^{14}C decay?

To answer this question we compare the original $\Delta^{14}CO_2$ data of Vermunt and Schauinsland shown in Figure 5, with a hypothetical $\Delta^{14}CO_2$-distribution, which is found for a fixed $\delta^{13}C$-value over the full observation period, thus, assuming no further dilution. This requires first to recalculate the sampling activity A_S from (35) and (36) with the known $\delta^{13}C$-record, e.g., from Mauna Loa (AR5 [1], Chap6, Figure 6.3c, missing data from 1964-1976 can be extrapolated from this record), and then to simulate the decay curve with new A_S activities, which are derived for a constant $\delta^{13}C(1964) = -7.4‰$.

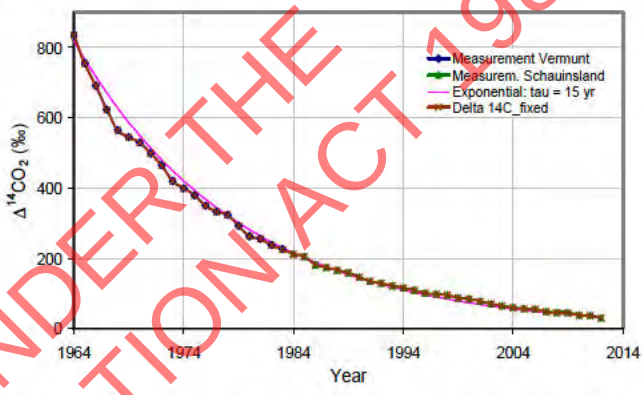

Figure 13. $\Delta^{14}CO_2$-evolution for Vermunt and Schauinsland (Magenta Dots and Green Triangles), compared with a recalculated decay neglecting dilution effects (Brown Crosses). Additionally shown is an exponential fit with an e-folding time of 15 yr (Magenta).

Figure 13 displays the normalized $\Delta^{14}CO_2$-values of Vermunt and Schauinsland (Blue Diamonds and Green Triangles; data from Levin et al. [17]) as reproduction of Figure 5 on a magnified scale.

It directly compares this with the hypothetical $\Delta^{14}CO_2$ decay curve (Brown Crosses). Deviations over the observed time period of 48 yr are smaller than 2‰ and the respective graphs completely coincide on this scale. They can well be approximated by a single exponential with a decay time of 15 yr (Magenta Line). Thus, any dilution effect of fossil fuel and natural emissions can well be neglected for the ^{14}C-decay.

Far more influential is re-emission of ^{14}C that was absorbed from the atmosphere. On the time scale of observed absorption, not all ^{14}C is directly sequestered beneath the Earth's surface, but needs several cycles before being removed from the atmosphere. This can be described by a perturbation balance, which different to (33) now considers the regular absorption (characterized by the residence time τ_R) and takes account of an emission rate e'_{14}, now for re-emitted ^{14}C from the upper Earth layer (e.g., through decomposition of vegetation which has absorbed that ^{14}C), before it is sequestered or distributed:

$$\frac{dC'_{14}}{dt} = e'_{14} - \frac{C'_{14}}{\tau_R} \approx \left(\frac{C'_{14}}{\tau_R} - \frac{C'_{E,14}}{\tau_{14}}\right) - \frac{C'_{14}}{\tau_R} \approx -\frac{C'_{14}}{\tau_{14}}. \tag{37}$$

Primed quantities are now referenced against unperturbed values before introduction of the nuclear source. From a balance for the Earth layer it follows that in good approximation e'_{14} opposes the atmospheric absorption rate C'_{14}/τ_R minus the sequestration rate $C'_{E,14}/\tau_{14}$, for which it is assumed that the concentration in the upper layer $C'_{E,14}$ is almost the same as the concentration C'_{14} in the atmosphere. Thus, re-emission simply modifies the effective absorption, which for ^{14}C is controlled by the apparent absorption time τ_{14} and not the residence time τ_R in agreement with (34).

Unlike the dilution effect, which is minor, this slows decay over what it would be in the presence of absorption alone. The apparent absorption time is therefore *longer* than the actual absorption time, which must even be shorter than a decade. Integration of (37) or (34) exactly reproduces a pure exponential decay in Figure 13 with an e-folding time $\tau_{14} = 15$ *yr*.

References

[1] AR5, In: Stocker, T. F., Qin, D., Plattner, G.-K., Tignor, M., Allen, S. K., Boschung, J., Nauels, A., Xia, Y., Bex, V., Midgley, P. M. (Eds.), "Climate Change 2013: The Physical Science Basis. Contribution of Working Group I to the Fifth Assessment Report of the Intergovernmental Panel on Climate Change", Cambridge University Press, Cambridge, United Kingdom and New York, NY, USA, 2013.

[2] C. Le Quéré et al., "Global Carbon Budget 2017", Earth Syst. Sci. Data Discuss., https://doi.org/10.5194/essd-2017-123 Open Access Earth System Science Data Discussions, Manuscript under review for journal Earth Syst. Sci. Data, 2017

[3] CICERO, Center for International Climate Research, Oslo, R Andrew: http://folk.uio no/roberan/GCP2017.shtml 2017.

[4] CDIAC, 2017: Carbon Dioxide Information Analysis Center http://cdiac.ornl.gov/trends/emis/glo_2014.html.

[5] C. D. Keeling, S. C. Piper, R. B. Bacastow, M. W hlen, T. P. Whorf, M. Heimann, H. A. Meijer, "Atmospheric CO_2 and $^{13}CO_2$ exchange with the terrestrial biosphere and oceans from 1978 to 2000: Observation and carbon cycle implications", In: Ehleringer, J. R., Cerling, T. E., Dearing, M. D. (Eds.), A History of Atmospheric CO2 and Its Effects on Plants, Animals, and Ecosystems. Springer Science+Business Media, New York, NY, USA, and Heidelberg, Germany, pp. 83–113 (actualized by Scripps-Institutes, USA), 2005.

[6] H. Harde, "Scrutinizing the carbon cycle and CO_2 residence time in the atmosphere", Global and Planetary Change 152, pp. 19–26, 2017. http://dx.doi.org/10.1016/j.gloplacha.2017.02.009.

[7] M. L. Salby, "Atmospheric Carbon", Video Presentation, July 18, 2016. University College London. https://youtu.be/3q-M_uYkpT0.

[8] P. Köhler, J. Hauck, C. Völker, D. A. Wolf-Gladrow, M. Butzin, J. B. Halpern, K. Rice, R. E. Zeebe, Comment on "*Scrutinizing the carbon cycle and CO2 residence time in the atmosphere*" by H. Harde, Global and Planetary Change 164, pp. 67-71, 2017. https://doi.org/10.1016/j.gloplacha.2017.09.015

[9] GISS, 2017: Goddard Institute for Space Studies: https://data.giss nasa.gov/gistemp/.

[10] M. L. Salby, "Relationship Between Greenhouse Gases and Global Temperature", Video Presentation, April 18, 2013. Helmut-Schmidt-University Hamburg https://www.youtube.com/watch?v=2ROw_cDKwc0.

[11] M. L. Salby, "What is Really Behind the Increase of Atmospheric CO_2"? Helmut-Schmidt-University Hamburg, 10. October 2018, https://youtu.be/rohF6K2avtY

[12] C. Le Quéré, M. R. Raupach, J. G. Canadell, G. Marland et al., "Trends in the sources and sinks of carbon dioxide", Nature Geosci., 2, pp. 831–836, 2009. doi:10.1038/ngeo689.

[13] P. Tans, NOAA/ESRL and R. Keeling, Scripps Institution of Oceanography (scrippsco2.ucsd.edu/), 2017. https://www.esrl noaa.gov/gmd/ccgg/trends/data html.

[14] F. Joos, M. Bruno, R. Fink, U. Siegenthaler, T. F. Stocker, C. Le Quéré, J. L. Sarmiento, "An efficient and accurate representation of complex oceanic and biospheric models of anthropogenic carbon uptake", Tellus B 48, pp. 397–417, 1996. doi:10.1034/j.1600-0889.1996.t01-2-00006.x.

[15] J. Hansen, M. Sato, P. Kharecha, G. Russell, D. W. Lea, M. Siddall, "Climate change and trace gases", Phil. Trans. R. Soc. A 365, pp. 1925–1954, 2007. doi:10.1098/rsta.2007.2052.

[16] J. Hansen, M. Sato, G. Russell, K. Pushker, "Climate sensitivity, sea level, nd atmospheric CO_2", Philos. Trans. R. Soc. A, 371, 20120294, 2013. doi:10.1098/rsta.2012.0294. https://www.nasa.gov/

[17] I. Levin, B. Kromer, and S. Hammer, "Atmospheric $\Delta^{14}CO_2$ trend in Western European background air from 2000 to 2012", Tellus B 65, pp. 1-7, 2013.

[18] Q. Hua, M. Barbetti, A. Z. Rakowski, "Atmospheric radiocarbon for the period 1950–2010". RADIOCARBON 55, pp. 2059–2072, (2013). Supplementary Material Table S2c, https://doi.org/10.2458/azu_js_rc.v55i2.16177

[19] J. C. Turnbull, S. E. Mikaloff Fletcher, I. Ansell, G. W. Brailsford, R. C. Moss, M. W. Norris, K. Steinkamp, "Sixty years of radiocarbon dioxide measurements at Wellington, New Zealand: 1954–2014", Atmos. Chem. Phys. 17, pp. 14771–14784, 2017. https://doi.org/10.5194/acp-17-14771-2017.

[20] U. Siegenthaler, J. L. Sarmiento, "Atmospheric carbon dioxide and the ocean", Nature 365, pp. 119-125, 1993.

[21] P. Dietze, IPCC's Most Essential Model Errors, 2001. http://www.john-daly.com/forcing/moderr.htm; (Carbon Model Calculations, http://www.john-daly.com/dietze/cmodcalc htm).

[22] G. C. Cawley, "On the Atmospheric Residence Time of Anthropogenically Sourced Carbon Dioxide", Energy Fuels 25, pp. 5503–5513, 2011. dx.doi.org/10.1021/ef200914u

[23] H.-J. Lüdecke, C. O. Weiss, "Simple Model for the Anthropogenically Forced CO_2 Cycle Tested on Measured Quantities", JGEESI, 8(4), pp. 1-12, 2016. DOI: 10.9734/JGEESI/2016/30532.

[24] R. E. Essenhigh, "Potential dependence of global warming on the residence time (RT) in the atmosphere of anthropogenically sourced carbon dioxide", Energy Fuel 23, pp. 2773–2784, 2009. http://pubs.acs.org/doi/abs/10.1021/ef800581r.

[25] E. Berry, "Human CO_2 has little effect on atmospheric CO_2", 2019. https://edberry.com/blog/climate-physics/agw-hypothesis/contradictions-to-ipccs-climate-change-theory/

[26] NOAA, 2017: https://www.esrl noaa.gov/psd/data/gridded/data ncep reanalysis html http://iridl.ldeo.columbia.edu/SOURCES/.NOAA/.NCDC/.GHCN/.v2/?bbox=bb%3A-161.488%3A16.360%3A-150.062%3A23.051%3Abb

[27] NOAA, 2018: http://iridl.ldeo.columbia.edu/SOURCES/.NOAA/.NCDC/.ERSST/.version2/.SST/index html http://iridl.ldeo.columbia.edu/SOURCES/.NOAA/.NCDC/.ERSST/.version2/.SST/X/%28164W%29VALUES/T/%28Jan%201938%29%28Dec%202009%29RANGEEDGES/Y/%2819N%29VALUES/datafiles.html

[28] O. Humlum, K. Stordahl, J. E. Solheim, "The phase relation between atmospheric carbon dioxide and global temperature", Global and Planetary Change 100, pp. 51-69, 2013.

[29] M. Richardson, Comment on "The phase relation between atmospheric carbon dioxide and global temperature" by Humlum, Stordahl and Solheim, Global and Planetary Change 107, pp. 226-228, 2013.

[30] D. L. Royer, R. A. Berner, I. P. Montañez, N. J. Tabor, D. J. Beerling, "CO_2 as a primary driver of Phanerozoic climate", GSA Today 14, no. 3, 2004. doi: 10.1130/1052-5173(2004)014<4:CAAPDO>2.0.CO;2.

[31] Y. G. Zhang, M. Pagani, J. Henderiks, H. Ren, "A long history of equatorial deep-water upwelling in the Pacific Ocean", Earth and Planetary Science Letters 467, pp. 1–9, 2017. http://dx.doi.org/10.1016/j.epsl.2017.03.016.

[32] T. Takahashi, S. C. Sutherland, R. Wanninkhof, C. Sweeney, R A. Feely et al., "Climatological mean and decadal change in surface ocean pCO_2 and net sea-air CO_2 flux over the global oceans", Deep-Sea Res. II, 56, pp. 554–577, 2009. doi:10.1016/j.dsr2.2008.12.009.

[33] N. U. Benson, O. O. Osibanjo, F. E. Asuquo, W. U. Anake "Observed trends of pCO_2 and air-sea CO_2 fluxes in the North Atlantic Ocean, Intern. J. Marine Science 4, pp. 1-7, 2014.

[34] J.-S. Lee, "Monitoring soil respiration using an automatic operating chamber in a Gwangneung temperate deciduous forest", J. Ecology & Field Biology 34(4), pp. 411-423, 2011.

[35] C. Huntingford, O. K. Atkin, A. Martinez de la Torre, L. M. Mercado, M. A. Heskel, A. B. Harper, K. J. Bloomfield, O. S. O'Sullivan, P. B. Reich, K. R. Wythers, E. E. Butler, M. Chen, K. L. Griffin, P. Meir, M. G. Tjoelker, M. H. Turnbull, S. Sitch, A. Wiltshire, Y. Malhi, "Implications of improved representations of plant respiration in a changing climate", NATURE COMMUNICATIONS 8, 1602, 2017. DOI: 10.1038/s41467-017-01774-z.

[36] H. Harde, "Radiation Transfer Calculations and Assessment of Global Warming by CO_2", International Journal of Atmospheric Sciences, Volume 2017, Article ID 9251034, pp. 1-30, 2017. https://doi.org/10.1155/2017/9251034.

[37] H. Harde, "Was tragen CO_2 und die Sonne zur globalen Erwärmung bei"? 12. Internationale EIKE Klima- und Energiekonferenz und 13th International Conference on Climate Change (ICCC-13), München, 23. u. 24. November, 2018, https://youtu.be/ldrG4mn_KCs.

[38] T. B. Coplen, "Reporting of stable hydrogen, carbon and oxygen isotopic abundances", Pure and Applied Chemistry 66, pp. 273-276, 1994.

[39] U. Siegenthaler, K. O. Münnich, "$^{13}C/^{12}C$ fractionation during CO_2 transfer from air to sea", *In:* Bolin, B. (Ed.): *Carbon cycle modelling (SCOPE 16),* John Wiley & Sons, pp. 249-257, 1981.

[40] M. L. Salby, "Physics of the Atmosphere and Climate", Cambridge University Press, Cambridge 2012. (ISBN: 978-0-521- 76718-7).

[41] D. M. Etheridge, L. P. Steele, R. L. Langenfelds, R. J. Francey, J.-M. Barnola, V. I. Morgan, "Natural and anthropogenic changes in atmospheric CO2 over the last 1000 years from air in Antarctic ice and firn", J. Geophys. Res. 101, pp. 4115-4128, 1996.

[42] Friedli H., H. Lötscher, H. Oeschger, U. Siegenthaler, B. Stauffer, 1986. Ice core record of the 13C/12C ratio of atmospheric CO2 in the past two centuries, Nature 324, pp. 237-238.

[43] H. Suess, "Radiocarbon Concentration in Modern Wood", Science 122, Issue 3166, pp. 415-417, 1955. DOI: 10.1126/science.122.3166.415-a

[44] J. G. Canadell, Le Quéré, C., Raupach, M. R., Field, C. B., Buitenhuis, E. T., Ciais, P., Conway, T. J., Gillett, N. P., Houghton, R. A., and Marland G., "Contributions to accelerating atmospheric CO_2 growth from economic activity, carbon intensity, and efficiency of natural sinks", P. Natl. Acad. USA. 104(47), 18866–18870, 2007, doi 10 1073/pnas 0702737104.

[45] M. Gloor, J. L. Sarmiento, and N. Gruber, "What can be learned about carbon cycle climate feedbacks from the CO_2 airborne fraction"? Atmos. Chem. Phys., 10, pp. 7739–7751, 2010. https://www.atmos-chem-phys net/10/7739/2010/, doi:10.5194/acp-10-7739-2010.

[46] A. P. Ballantyne, C. B. Alden, J. B. Miller, P. P. Tans, J. W. C. White, "Increase in observed net carbon dioxide uptake by land and oceans during the past 50 years", Nature 488, pp. 70-73, 2012. doi:10.1038/nature11299

[47] J. Steele, "How NOAA and Bad Modeling Invented an Ocean Acidification Icon", Part 2 – Bad Models, 2017. https://wattsupwiththat.com/2017/03/02/how-noaa-and-bad-modeling-invented-an-ocean-acidification-icon-part-2-bad-models/

[48] W. Evans, B. Hales, P. G. Strut, "Seasonal cycle of surface ocean pCO2 on the Oregon shelf", J. Geophys. Research 116, 2011, DOI: 10.1029/2010JC006625.

[49] K. R. Arrigo, G. L. van Dijken, "Continued increases in Arctic Ocean primary production", Progress in Oceanography 136, pp. 60-70, 2015, https://doi.org/10.1016/j.pocean.2015.05.002.

[50] D. K. Steinberg, M. W. Lomas, J. S. Cope, "Long-term increase in mesozooplankton biomass in the Sargasso Sea: Linkage to climate and implications for food web dynamics and biogeochemical cycling", Global Biogeochemical Cycle 26, 2012, DOI: 10.1029/2010GB004026.

[51] K. M. Krumhardt, N. S. Lovenduski, N. M. Freeman, N. R. Bates, "Apparent increase in coccolithophore abundance in the subtropical North Atlantic from 1990 to 2014", Biogeosciences 13, pp. 1163-1177, 2016. doi:10.5194/bg-13-1163-2016, http://www.biogeosciences net/13/1163/2016/.

[52] F. P. Chavez, M. Messié, J. T. Pennington, "Marine Primary Production in Relation to Climate Variability and Change", Annu. Rev. Mar. Sci. 3, pp. 227–260, 2011, doi:10.1146/annurev.marine.010908.163917.

[53] U. Riebesell, K. G. Schulz, R. G. J. Bellerby, M. Botros, P. Fritsche, M. Meyerhöfer, C. Neill, G. Nondal, A. Oschlies, J. Wohlers, E. Zöllner, "Enhanced biological carbon consumption in a high CO_2 ocean", Nature 450, pp. 545-548, 2007, doi:10.1038/nature06267.

[54] A. M. P. McDonnell, K. O. Buesseler, "Variability in the average sinking velocity of marine particles", Limnology and Oceanography 55, pp. 2085–2096, 2010. DOI:10.4319/lo.2010.55.5.2085.

[55] T. Weber, J. A. Cram, S. W. Leung, T. DeVries, C. Deutsch, "Deep ocean nutrients imply large latitudinal variation in particle transfer efficiency", PNAS 113 no. 31, pp. 8606–8611, 2016, doi: 10.1073/pnas.1604414113.

[56] F. Abrantes, P. Cermeno, C. Lopes, O. Romero, L. Matos, J. Van Iperen, M. Rufino, V. Magalhães, "Diatoms Si uptake capacity drives carbon export in coastal upwelling systems", Biogeosciences 13, pp. 4099–4109, 2016, https://doi.org/10.5194/bg-13-4099-2016

[57] M. Stuiver, H. A. Polach, "Discussion Reporting of ^{14}C Data", RADIOCARBON 19, No. 3, pp. 355-363, 1977.

On the decadal rates of sea level change during the twentieth century

S. J. Holgate[1]

Received 17 October 2006; accepted 21 November 2006; published 4 January 2007.

[1] Nine long and nearly continuous sea level records were chosen from around the world to explore rates of change in sea level for 1904–2003. These records were found to capture the variability found in a larger number of stations over the last half century studied previously. Extending the sea level record back over the entire century suggests that the high variability in the rates of sea level change observed over the past 20 years were not particularly unusual. The rate of sea level change was found to be larger in the early part of last century (2.03 ± 0.35 mm/yr 1904–1953), in comparison with the latter part (1.45 ± 0.34 mm/yr 1954–2003). The highest decadal rate of rise occurred in the decade centred on 1980 (5.31 mm/yr) with the lowest rate of rise occurring in the decade centred on 1964 (−1.49 mm/yr). Over the entire century the mean rate of change was 1.74 ± 0.16 mm/yr. **Citation:** Holgate, S. J. (2007), On the decadal rates of sea level change during the twentieth century, *Geophys. Res. Lett.*, *34*, L01602, doi:10.1029/2006GL028492.

1. Introduction

[2] In a previous paper, *Holgate and Woodwo th* [2004] (hereinafter referred to as HW04), rates of mean "global" sea level change (i.e., global coastal sea level change) were calculated from a large number of tide gauge records (177) for the period 1955–1998. HW04 found that the highest and lowest rates of change in the 1955–1998 period occurred in the last 20 years of the record. In this paper it is examined whether a few high quality tide gauge records can replace the many used by HW04. On the basis of these high quality records the work of HW04 is then extended back to the early twentieth century to examine whether the rates of sea level change experienced in recent decades are unusual.

[3] On a decadal timescale, the length scales of sea level change are very large (O(1000) km) though not necessarily global. As a result, many tide gauges in a given region are highly correlated with each other. This paper demonstrates that a few high quality records from around the world can be used to examine large spatial-scale decadal variability as well as many gauges from each region are able to.

2. Method

[4] When it comes to calculating long term global sea level means from tide gauge data, there are a number of problems. Firstly there is a bias in the distribution of tide gauges towards certain regions, notably Northern Europe and North America [*Douglas*, 1991]. Secondly there is the problem that not all tide gauge records are of equivalent quality. This can either be due to their location (being for example in an earthquake-prone region or an area of high glacial isostatic adjustment, GIA) or due to the quality of the instrumental record (being perhaps too discontinuous or lacking critical datum information to account for local vertical land movements).

[5] As a result of these two problems, there are very few high quality, long tide gauge records in different regions suitable for calculating global mean sea level change. An alternative approach is to make use of regional composites of shorter records as in HW04.

[6] In order to test whether a few high quality records could provide similar information to the composites, nine tide gauge records were carefully selected from the database of the Permanent Service for Mean Sea Level (PSMSL, available at http://www.p l.ac.uk/psmsl) [*Woodworth and Player*, 2003]: New York (1856–2003), Key West (1913–2003), San Diego (1906–2003), Balboa (1908–1996), Honolulu (1905–2003), Cascais (1882–1993), Newlyn (1915–2004) Trieste (1905–2004), and Auckland (1903–2000). The nine long records thus enable the study of HW04 into variability of decadal rates of sea level change to be extended over a much longer period. The locations of these tide gauge stations are shown in Figure 1.

[7] These tide gauge stations are part of the Revised Local Reference (RLR) data set of the PSMSL in which each time series is recorded relative to a consistent reference level on the nearby land. Annual values in the RLR data set of the PSMSL are only calculated if there are at least 11 months of data and each month must have less than 15 missing days. Hence the tide gauge data presented here is of the very highest quality available. All these records are almost continuous and are far away from regions with high rates of vertical land movement due to GIA or tectonics.

[8] Although most of these tide gauge records continue to the present, submissions of data to the PSMSL are often a year or two in arrears and hence most of these sea level records have data up until only 2003 or 2004. The current analysis begins in 1904 and ends in 2003 which ensures at least 70% completeness of the record in every decade.

[9] Following the method described in HW04, consecutive, overlapping decadal mean rates were calculated for each sea level record. The advantage of calculating decadal rates in this way is that the tide gauge records can then be combined into a single mean sea level time series, despite the different gauges having different datums. Furthermore, decadal rates remove any minor data discontinuities and introduce an element of smoothing. The rates of change at each station are corrected for GIA using the ICE-4G model of *Peltier* [2001] and for inverse barometer effects using the HadSLP2 air pressure data set [*Allan and Ansell*, 2006].

[10] The standard error of a sea level trend estimate, based on the assumption that each annual mean is inde-

[1]Proudman Oceanographic Laboratory, Liverpool, UK.

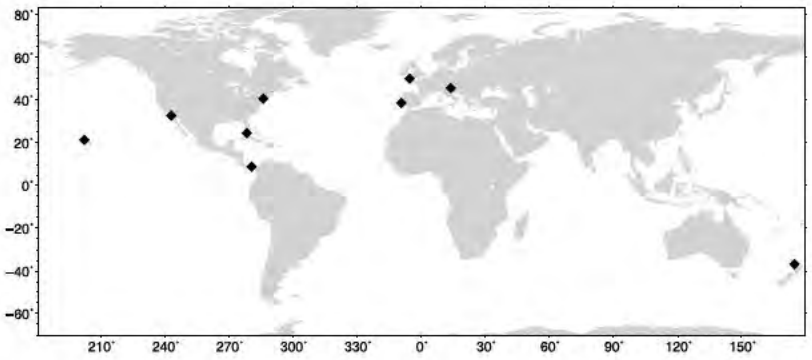

Figure 1. The distribution of the nine tide gauge records used in this study. Data are obtained from the Revised Local Reference data set of the Permanent Service for Mean Sea Level.

pendent, under-estimates the true error as the serial correlation is not accounted for [*Douglas*, 2001; *Nerem and Mitchum*, 2002]. Here serial correlation within each time-series is accommodated by reducing the number of degrees of freedom, using the lag-1 auto-correlation of the time-series [*World Meteorological Organization*, 1966; *Maul and Martin*, 1993]. The effect of calculating errors in this way increases one standard error for the trend over the 1904–2003 period from typically 0.02 mm/yr to 0.15 mm/yr.

3. Results

[11] Figure 2 compares the global decadal mean rates of change from the 177 stations of HW04 which were grouped into 13 regions (Figure 1 in HW04) with the global mean rates from the 9 long records. Although there are some differences between the two records, in particular the larger rate of rise in the 9 records during the 1950s, the two curves have overlapping error bars (based on one standard error). The global mean rates are similar for the second half of the 20th century (1953–97), 1.47 mm/yr and 1.41 mm/yr for the 177 and 9 stations respectively, with most of the disparity between the two due to differences in the 1950s. This comparison relies on using the HadSLP2 data set for pressure correction for both the 177 and 9 stations. HW04 used the NCEP pressure data set which gives a global mean rate for 177 stations of 1.64 mm/yr over the period 1953–97. Hence some uncertainty in the global mean rate of sea level rise is attributable to the commensurate uncertainty in the sea level pressure correction, which arises largely due to the difference in resolution between the two data sets (2.5° × 2.5° for NCEP and 5° × 5° for HadSLP2). Over the full 1904–2003 period, the mean global rate from the nine stations, corrected with HadSLP2, is 1.74 ± 0.16 mm/yr.

[12] Figure 3 shows that, not only is there considerable decadal variability in the individual sea level records, but there is generally little correlation between them. Stations which are in close proximity and which are affected by similar ocean and atmospheric processes show the greatest correlation. For example, Balboa and San Diego are both heavily influenced by the El Niño/Southern Oscillation (ENSO) and are similar (correlation of their decadal trends = 0.77), despite being over 4500 km apart. However, high correlation at a decadal scale does not imply that the long term trends are the same.

[13] The global mean sea level rates for the nine stations in Figure 2 show that the two highest decadal rates of change were recorded in the decades centred on 1980 (5.31 mm/yr) and 1939 (4.68 mm/yr) with the most negative decadal rates of change over the past 100 years during the decades centred on 1964 (−1.49 mm/yr) and 1987 (−1.33 mm/yr). There were also significant high decadal rates of change during the late 1910s, 1950s and 1990s. Negative decadal rates of change are seen in the early 1920s and early 1970s.

[14] Despite the high decadal rates of change in the latter part of the 20th century, it is found that the first half of the record (1904–1953) has a higher rate of rise overall (2.03 ± 0.35 mm/yr) than the 1954–2003 period which had a rate of 1.45 ± 0.34 mm/yr.

[15] The highest rates of sea level change over the common period for all gauges (1918–1996), occurred in New York (mean rate = 2.64 ± 0.44 mm/yr), San Diego (2.02 ± 0.31 mm/yr), Key West (2.00 ± 0.36 mm/yr) and

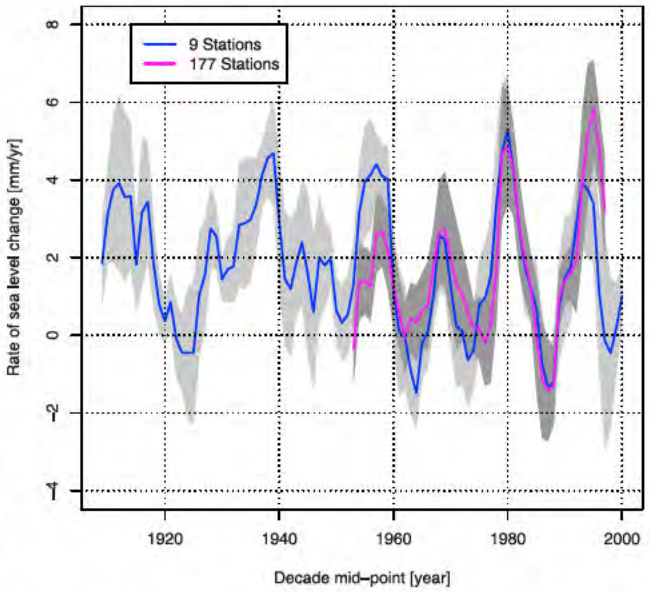

Figure 2. Comparison of the global mean decadal rates of sea level change based on the nine records with the rates from the 177 stations used in HW04. All rates are corrected for glacial isostatic adjustment and inverse barometer effects. The shaded region indicates ±1 standard error.

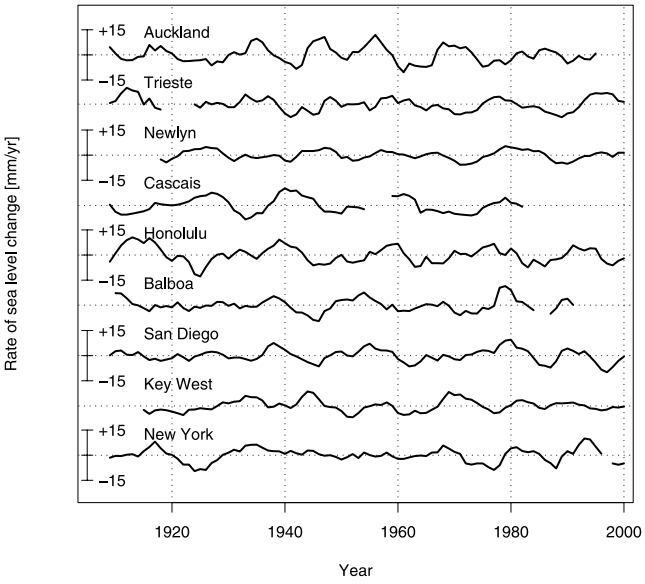

Figure 3. Comparison of the decadal rates of sea level change for each of the nine records. All rates are corrected for glacial isostatic adjustment and inverse barometer effects.

Cascais (1.85 ± 0.37 mm/yr). The smallest changes in sea level are seen in Trieste (1.25 ± 0.23 mm/yr) and Newlyn (1.46 ± 0.30 mm/yr).

[16] San Diego has the highest correlation with the global mean rates (r = 0.62) over the 1904–2003 period, followed by Honolulu (r = 0.58), New York (r = 0.56), Balboa (r = 0.55) and Trieste (r = 0.42). Cascais and Auckland have insignificant correlations at the 95% confidence level while the correlations with Newlyn (r = 0.29) and Key West (r = 0.25) are significant but low.

4. Discussion

[17] The nine stations selected here as high quality records capture the mean decadal rates of change described by the larger set of stations used in HW04 and also have a similar global mean rate over the common period of the two analyses (1953–1997). This provides confidence that the nine station set can be used to study decadal rates of global mean sea level change throughout the twentieth century.

[18] All the stations in this study show a significant increase in sea level over the period 1904–2003 with an average increase of 174 mm during that time (Figure 4). This mean rate of 1.74 mm/yr is at the upper end of the range of estimates for the 20th century in the Intergovernmental Panel on Climate Change, Third Assessment Report (IPCC TAR) [*Church et al.*, 2001], and consistent with other recent estimates [*Holgate and Woodworth*, 2004; *Church and White*, 2006].

[19] The rates for individual stations are consistent with those published by other authors [*Douglas*, 2001; *Peltier*, 2001; *Hannah*, 1990]. As has been noted previously [*Woodworth*, 1990], the rates for northern European tide gauges are consistently lower than the global mean. Trieste, along with other Mediterranean tide gauge stations, has shown a much lower rate of increase since 1960 [*Douglas*, 1997; *Tsimplis and Baker*, 2000]. However, the difference between the global mean and Trieste is 0.49 in comparison with the difference between the global mean and New York (the highest individual rate) which is 0.62. It would therefore seem that Trieste no more biases the mean low than New York biases the mean high. Nevertheless, excluding Trieste from the results would slightly increase the global mean from 1.74 to 1.80 mm/yr.

[20] Although the mean rate of change of global mean sea level is found to be greater in the first half of the twentieth century, the two rates are consistent with being the same at the 95% confidence level, given their individual standard errors. However, a greater rate of rise in the early part of the record is consistent with previous analyses of tide gauge records which suggested a general deceleration in sea level rise during the 20th century [*Woodworth*, 1990; *Douglas*, 1992; *Jevrejeva et al.*, 2006]. A twentieth century deceleration is consistent with the work of *Church and White* [2006] who, although finding evidence for a post-1870 acceleration based on an EOF reconstruction of global sea level, found that much of the overall acceleration occurred in the first half of the 20th century. *Church and White* [2006] suggested that the greater rate of sea level rise observed in the first half of last century was due to reduced volcanic emissions (and hence also lower variability in sea level) during the 1930s to 1960s. This idea is supported by results from the HadCM3 model which suggest that the simulated global mean sea level did not accelerate through the twentieth century due to the offsetting of anthropogenic warming by reduced natural forcing [*Gregory et al.*, 2006].

[21] The decadal rates of sea level change shown in Figure 2 are qualitatively similar to the corresponding rates in Figure 2 of *Church and White* [2006], with the exception of the period 1930–1940 which shows lower variability in the work of *Church and White* [2006]. The variability in the second half of the century is also similar to that found by

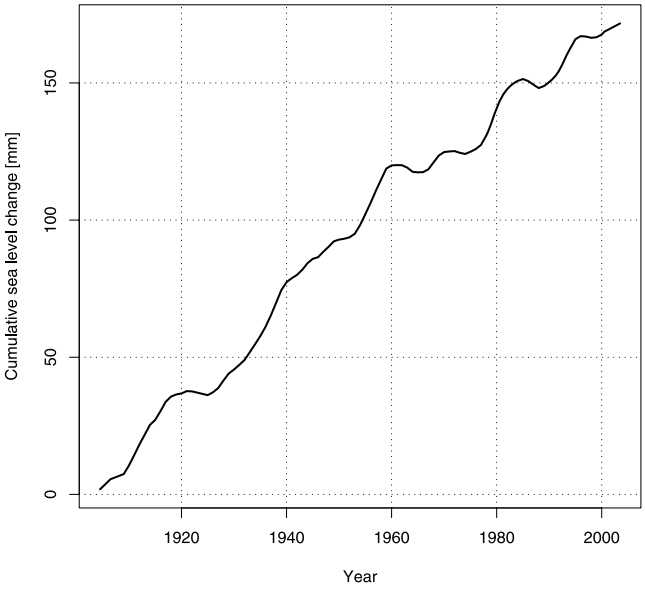

Figure 4. The mean sea level record from the nine tide gauges over the period 1904–2003 based on the decadal trend values for 1907–1999. The sea level curve here is the integral of the rates presented in Figure 2.

Chambers et al. [2002] though the lower number of gauges in the present study results in a greater level of variance.

5. Summary and Conclusions

[22] Based on a selection of nine long, high quality tide gauge records, the mean rate of sea level rise over the period 1904–2003 was found to be 1.74 ± 0.16 mm/yr after correction for GIA using the ICE-4G model [*Peltier*, 2001] and for inverse barometer effects using HadSLP2 [*Allan and Ansell*, 2006]. The mean rate of rise was greater in the first half of this period than the latter half, though the difference in rates was not found to be significant. The use of a reduced number of high quality sea level records was found to be as suitable in this type of analysis as using a larger number of regionally averaged gauges.

[23] Finally, in extending the work of HW04 to cover the whole century, it is found that the high decadal rates of change in global mean sea level observed during the last 20 years of the record were not particularly unusual in the longer term context.

[24] **Acknowledgments.** I'd like to thank Phil Woodworth, Simon Williams, and Svetlana Jevrejeva for discussion and comments which have helped to improve this paper.

References

Allan, R., and T. Ansell (2006), A new globally complete monthly historical mean sea level pressure data set (HadSLP2): 1850 2004, *J. Clim*, in press.

Chambers, D. P., C. A. Mehlhaff, T. J. Urban, D. Fujii, and R. S. Ner m (2002), Low-frequency variations in global mean sea level: 1950 2000, *J. Geophys. Res.*, *107*(C4), 3026, doi:10.1029/2001JC001089.

Church, J. A., and N. J. White (2006), A 20th century acceleration in global sea level rise, *Geophys. Res. Lett.*, *33*, L01602, doi:10.1029/2005GL024826.

Church, J. A., J. Gregory, P. Huybrechts, M. Kuhn, K. Lambeck, M. Nhuan, D. Qin, and P. Woodworth (2001), Changes in sea level, in *Climate Change 2001: The Scientific Basis: Contribution of Working Group to the Third Assessment Report of the Intergovernmental Panel on Climate Change*, edited by J. T. Houghton et al., chap. 11, pp. 639 694, Cambridge Univ. Press, New York.

Douglas, B. C. (1991), Global sea level rise, *J. Geophys. Res.*, *96*, 6981 6992.

Douglas, B. C. (1992), Global sea level acceleration, *J. Geophys. Res.*, *97*, 12,699 12,706.

Douglas, B. C. (1997), Global sea rise: A redetermination, *Surv. Geophys.*, *18*, 279 292.

Douglas, B. C. (2001), Sea level change in the era of the recording tide gauge, in *Sea Level Rise: History and Consequences*, *Int. Geophys. Ser.*, vol. 75, edited by B. C. Douglas, M. S. Kearney, and S. P. Leatherman, chap. 3, pp. 37 64, Elsevier, New York.

Gregory, J., J. Lowe, and S. Tett (2006), Simulated global-mean sea-level changes over the last half-millenium, *J. Clim.*, *19*, 4576 4591.

Hannah, J. (1990), Analysis of mean sea level data from New Zealand for the period 1899 1988, *J. Geophys. Res.*, *95*, 12,399 12,405.

Holgate, S. J., and P. L. Woodworth (2004), Evidence for enhanced coastal sea level rise during the 1990s, *Geophys. Res. Lett.*, *31*, L07305, doi:10.1029/2004GL019626.

Jevrejeva, S., A. Grinsted, J. C. Moore, and S. Holgate (2006), Nonlinear trends and multi-year cycles in sea level trends, *J. Geophys. Res.*, *111*, C09012, doi:10.1029/2005JC003229.

Maul, G. A., and D. M. Martin (1993), Sea level rise at Key West, Florida, 1846 1992: America's longest ins rument record?, *Geophys. Res. Lett.*, *20*, 1955 1958.

Nerem, R. S., and G. T. Mitchum (2002), Estimates of vertical crustal motion derived from differences of TOPEX/POSEIDON and tide gauge sea level measurements, *Geophys. Res. Lett.*, *29*(19), 1934, doi:10.1029/2002GL015037.

Peltier, W. (2001), Global glacial isostatic adjustment and modern instrumental records of relative s a level history, in *Sea Level Rise: History and Consequences*, *Int. Geophys. Ser.*, vol. 75, edited by B. C. Douglas, M. S. Kearney, a d S. P. Leath rman, chap. 4, pp. 65 95, Elsevier, New York.

Tsimplis, M. N., and T. F. Baker (2000), Sea level drop in the Mediterranean Sea: An indicator of deep water salinity and temperature changes?, *G phys. Res. Lett.*, *27*, 1731 1734.

Woodworth, P. (1990), A search for accelerations in records of European mean sea level, *Int. J. Climatol.*, *10*, 129 143.

Woodworth, P., and R. Player (2003), The Permanent Service for Mean Sea Level: An update to the 21st century, *J. Coastal Res.*, *19*(2), 287 295.

World Meteorological Organization (1966) Report of a working group on the commission for climatology, *Tech. Rep. 79*, 79 pp., World Meteorol. Organ., Geneva, Switzerland.

S. J. Holgate, Proudman Oceanographic Laboratory, Joseph Proudman Building, 6 Brownlow Street, Liverpool L3 5DA, UK. (simonh@pol.ac.uk)

Environment Pollution and Climate Change

Nikolov and Zeller, Environ Pollut Climate Change 2017, 1:2

Research Article OMICS International

New Insights on the Physical Nature of the Atmospheric Greenhouse Effect Deduced from an Empirical Planetary Temperature Model

Ned Nikolov* **and Karl Zeller**

Ksubz LLC, 9401 Shoofly Lane, Wellington CO 80549, USA

Abstract

A recent study has revealed that the Earth's natural atmospheric greenhouse effect is around 90 K or about 2.7 times stronger than assumed for the past 40 years. A thermal enhancement of such a magnitude cannot be explained with the observed amount of outgoing infrared long-wave radiation absorbed by the atmosphere (i.e. ≈ 158 W m^{-2}), thus requiring a re-examination of the underlying Greenhouse theory. We present here a new investigation into the physical nature of the atmospheric thermal effect using a novel empirical approach toward predicting the Global Mean Annual near-surface equilibrium Temperature (GMAT) of rocky planets with diverse atmospheres. Our method utilizes Dimensional Analysis (DA) applied to a vetted set of observed data from six celestial bodies representing a broad range of physical environments in our Solar System, i.e. Venus, Earth, the Moon, Mars, Titan (a moon of Saturn), and Triton (a moon of Neptune). Twelve relationships (models) suggested by DA are explored via non-linear regression analyses that involve dimensionless products comprised of solar irradiance, greenhouse-gas partial pressure/density and total atmospheric pressure/density as forcing variables, and two temperature ratios as dependent variables. One non-linear regression model is found to statistically outperform the rest by a wide margin. Our analysis revealed that GMATs of rocky planets with tangible atmospheres and a negligible geothermal surface heating can accurately be predicted over a broad range of conditions using only two forcing variables: top-of-the-atmosphere solar irradiance and total surface atmospheric pressure. The hereto discovered interplanetary pressure-temperature relationship is shown to be statistically robust while describing a smooth physical continuum without climatic tipping points. This continuum fully explains the recently discovered 90 K thermal effect of Earth's atmosphere. The new model displays characteristics of an emergent macro-level thermodynamic relationship heretofore unbeknown to science that has important theoretical implications. A key entailment from the model is that the atmospheric 'greenhouse effect' currently viewed as a radiative phenomenon is in fact an adiabatic (pressure-induced) thermal enhancement analogous to compression heating and independent of atmospheric composition. Consequently, the global down-welling long-wave flux presently assumed to drive Earth's surface warming appears to be a product of the air temperature set by solar heating and atmospheric pressure. In other words, the so-called 'greenhouse back radiation' is globally a result of the atmospheric thermal effect rather than a cause for it. Our empirical model has also fundamental implications for the role of oceans, water vapour, and planetary albedo in global climate. Since produced by a rigorous attempt to describe planetary temperatures in the context of a cosmic continuum using an objective analysis of vetted observations from across the Solar System, these findings call for a paradigm shift in our understanding of the atmospheric 'greenhouse effect' as a fundamental property of climate.

Keywords: Greenhouse effect; Emergent model; Planetary temperature; Atmospheric pressure; Greenhouse gas; Mars temperature

Introduction

In a recent study Volokin and ReLlez [1] demonstrated that the strength of Earth's atmospheric Greenhouse Effect (GE) is about 90 K instead of 33 K as presently assumed by most researchers [2-7]. The new estimate corrected a long-standing mathematical error in the application of the Stefan–Boltzmann (SB) radiation law to a sphere pertaining to Hölder's inequality between integrals. Since the current greenhouse theory strives to explain GE solely through a retention (trapping) of outgoing long-wavelength (LW) radiation by atmospheric gases [2,5,7-10], a thermal enhancement of 90 K creates a logical conundrum, since satellite observations constrain the global atmospheric LW absorption to 155–158 W m^{-2} [11-13]. Such a flux might only explain a surface warming up to 35 K. Hence, more than 60% of Earth's 90 K atmospheric effect appears to remain inexplicable in the context of the current theory. Furthermore, satellite- and surface-based radiation measurements have shown [12-14] that the lower troposphere emits 42-44% more radiation towards the surface (i.e. 341-346 W m^{-2}) than the net shortwave flux delivered to the Earth-atmosphere system by the Sun (i.e. 240 W m^{-2}). In other words, the lower troposphere contains significantly more kinetic energy than expected from solar heating alone, a conclusion also supported by the new 90 K GE estimate. A similar but more extreme situation is observed on Venus as well, where the atmospheric down-welling LW radiation near the surface (>15,000 W m^{-2}) exceeds the total absorbed solar flux (65–150 W m^{-2}) by a factor of 100 or more [6]. The radiative greenhouse theory cannot explain this apparent paradox considering the fact that infrared-absorbing gases such as CO_2, water vapor and methane only re-radiate available LW emissions and do not constitute significant heat storage or a net source of additional energy to the system. This raises a fundamental question about the origin of the observed energy surplus in the lower troposphere of terrestrial planets with respect to the solar input. The above inconsistencies between theory and observations prompted us to take a new look at the mechanisms controlling the atmospheric thermal effect.

We began our study with the premise that processes controlling the Global Mean Annual near-surface Temperature (GMAT) of Earth are also responsible for creating the observed pattern of planetary temperatures across the Solar System. Thus, our working hypothesis was that a general physical model should exist, which accurately describes equilibrium GMATs of planets using a common set of drivers. If true, such a model would also reveal the forcing behind the atmospheric thermal effect.

Instead of examining existing mechanistic models such as 3-D

***Corresponding author:** Ned Nikolov, Ksubz LLC, 9401 Shoofly Lane, Wellington CO 80549, USA, Tel: 970-980-3303, 970-206-0700; E-mail: nlconsulting@comcast.net

Received November 11, 2016; **Accepted** February 06, 2017; **Published** February 13, 2017

Citation: Nikolov N, Zeller K (2017) New Insights on the Physical Nature of the Atmospheric Greenhouse Effect Deduced from an Empirical Planetary Temperature Model. Environ Pollut Climate Change 1: 112.

GCMs, we decided to try an empirical approach not constrained by a particular physical theory. An important reason for this was the fact that current process-oriented climate models rely on numerous theoretical assumptions while utilizing planet-specific parameterizations of key processes such as vertical convection and cloud nucleation in order to simulate the surface thermal regime over a range of planetary environments [15]. These empirical parameterizations oftentimes depend on detailed observations that are not typically available for planetary bodies other than Earth. Hence, our goal was to develop a simple yet robust planetary temperature model of high predictive power that does not require case-specific parameter adjustments while successfully describing the observed range of planetary temperatures across the Solar System.

Methods and Data

In our model development we employed a 'top-down' empirical approach based on Dimensional Analysis (DA) of observed data from our Solar System. We chose DA as an analytic tool because of its ubiquitous past successes in solving complex problems of physics, engineering, mathematical biology, and biophysics [16-21]. To our knowledge DA has not previously been applied to constructing predictive models of macro-level properties such as the average global temperature of a planet; thus, the following overview of this technique is warranted.

Dimensional analysis background

DA is a method for extracting physically meaningful relationships from empirical data [22-24]. The goal of DA is to restructure a set of original variables deemed critical to describing a physical phenomenon into a smaller set of independent dimensionless products that may be combined into a dimensionally homogeneous model with predictive power. Dimensional homogeneity is a prerequisite for any robust physical relationship such as natural laws. DA distinguishes between measurement units and physical dimensions. For example, mass is a physical dimension that can be measured in gram, pound, metric ton etc.; time is another dimension measurable in seconds, hours, years, etc. While the physical dimension of a variable does not change, the units quantifying that variable may vary depending on the adopted measurement system.

Many physical variables and constants can be described in terms of four fundamental dimensions, i.e. mass [M], length [L], time [T], and absolute temperature [Θ]. For example, an energy flux commonly measured in W m^{-2} has a physical dimension [M T^{-3}] since 1 W m^{-2} = 1 J s^{-1} m^{-2} = 1 (kg m^2 s^{-2}) s^{-1} m^{-2} = kg s^{-3}. Pressure may be reported in units of Pascal, bar, atm., PSI or Torr, but its physical dimension is always [M L^{-1} T^{-2}] because 1 Pa = 1 N m^{-2} = 1 (kg m s^{-2}) m^{-2} = 1 kg m^{-1} s^{-2}. Thinking in terms of physical dimensions rather than measurement units fosters a deeper understanding of the underlying physical reality. For instance, a comparison between the physical dimensions of energy flux and pressure reveals that a flux is simply the product of pressure and the speed of moving particles [L T^{-1}], i.e. [M T^{-3}] = [M L^{-1} T^{-2}] [L T^{-1}]. Thus, a radiative flux F_R (W m^{-2}) can be expressed in terms of photon pressure P_{ph} (Pa) and the speed of light c (m s^{-1}) as $F_R = c\,P_{ph}$. Since c is constant within a medium, varying the intensity of electromagnetic radiation in a given medium effectively means altering the pressure of photons. Thus, the solar radiation reaching Earth's upper atmosphere exerts a pressure (force) of sufficient magnitude to perturb the orbits of communication satellites over time [25,26].

The simplifying power of DA in model development stems from the Buckingham Pi Theorem [27], which states that a problem involving n dimensioned x_i variables, i.e.

$$f(x_1, x_2, \ldots, x_n) = 0$$

can be reformulated into a simpler relationship of (n-m) dimensionless π_i products derived from x_i, i.e.

$$\phi(\pi_1, \pi_2, \ldots, \pi_{n-m}) = 0$$

where m is the number of fundamental dimensions comprising the original variables. This theorem determines the number of non-dimensional π_i variables to be found in a set of products, but it does not prescribe the number of sets that could be generated from the original variables defining a particular problem. In other words, there might be, and oftentimes is more than one set of (n-m) dimensionless products to analyze. DA provides an objective method for constructing the sets of π_i variables employing simultaneous equations solved via either matrix inversion or substitution [22].

The second step of DA (after the construction of dimensionless products) is to search for a functional relationship between the π_i variables of each set using regression analysis. DA does not disclose the best function capable of describing the empirical data. It is the investigator's responsibility to identify a suitable regression model based on prior knowledge of the phenomenon and a general expertise in the subject area. DA only guarantees that the final model (whatever its functional form) will be dimensionally homogeneous, hence it may qualify as a physically meaningful relationship provided that it (*a*) is not based on a simple polynomial fit; (*b*) has a small standard error; (*c*) displays high predictive skill over a broad range of input data; and (*d*) is statistically robust. The regression coefficients of the final model will also be dimensionless, and may reveal true constants of Nature by virtue of being independent of the units utilized to measure the forcing variables.

Selection of model variables

A planet's GMAT depends on many factors. In this study, we focused on drivers that are remotely measurable and/or theoretically estimable. Based on the current state of knowledge we identified seven physical variables of potential relevance to the global surface temperature: 1) top-of-the-atmosphere (TOA) solar irradiance (S); 2) mean planetary surface temperature in the absence of atmospheric greenhouse effect, hereto called a reference temperature (T_r); 3) near-surface partial pressure of atmospheric greenhouse gases (P_{gh}); 4) near-surface mass density of atmospheric greenhouse gases (ρ_{gh}); 5) total surface atmospheric pressure (P); 6) total surface atmospheric density (ρ); and 7) minimum air pressure required for the existence of a liquid solvent at the surface, hereto called a reference pressure (P_r). Table 1 lists the above variables along with their SI units and physical dimensions. Note that, in order to simplify the derivation of dimensionless products, pressure and density are represented in Table 1 by the generic variables P_x and ρ_x, respectively. As explained below, the regression analysis following the construction of π_i variables explicitly distinguished between models involving partial pressure/density of greenhouse gases and those employing total atmospheric pressure/density at the surface. The planetary Bond albedo (α_p) was omitted as a forcing variable in our DA despite its known effect on the surface energy budget, because it is already dimensionless and also partakes in the calculation of reference temperatures discussed below.

Appendix A details the procedure employed to construct the π_i variables. DA yielded two sets of π_i products, each one consisting of two

Planetary Variable	Symbol	SI Units	Physical Dimension
Global mean annual near-surface temperature (GMAT), the dependent variable	T_s	K	[Θ]
Stellar irradiance (average shortwave flux incident on a plane perpendicular to the stellar rays at the top of a planet s atmosphere)	S	W m^{-2}	[M T^{-3}]
Reference temperature (the planet's mean surface temperature in the absence of an atmosphere or an atmospheric greenhouse effect)	T_r	K	[Θ]
Average near-surface gas pressure representing either partial pressure of greenhouse gases or total atmospheric pressure	P_x	Pa	[M L^{-1} T^{-2}]
Average near-surface gas density representing either greenhouse-gas density or total atmospheric density	ρ_x	kg m^{-3}	[M L^{-3}]
Reference pressure (the minimum atmospheric pressure required a liquid solvent to exists at the surface)	P_r	Pa	[M L^{-1} T^{-2}]

Table 1: Variables employed in the Dimensional Analysis aimed at deriving a general planetary temperature model. The variables are comprised of 4 fundamental physical dimensions: mass [M], length [L], time [T] and absolute temperature [Θ].

dimensionless variables, i.e.

$$\pi_1 = \frac{T_s}{T_r}; \qquad \pi_2 = \frac{P_x^3}{\rho_x S^2}$$

and

$$\pi_1 = \frac{T_s}{T_r}; \qquad \pi_2 = \frac{P_x}{P_r}$$

This implies an investigation of two types of dimensionally homogeneous functions (relationships):

$$\frac{T_s}{T_r} = f\left(\frac{P_x^3}{\rho_x S^2}\right) \tag{1}$$

and

$$\frac{T_s}{T_r} = f\left(\frac{P_x}{P_r}\right) \tag{2}$$

Note that $\pi_1 = T_s/T_r$ occurs as a dependent variable in both relationships, since it contains the sought temperature T_s. Upon replacing the generic pressure/density variables P_x and ρ_x in functions (1) and (2) with either partial pressure/density of greenhouse gases (P_{gh} and ρ_{gh}) or total atmospheric pressure/density (P and ρ), one arrives at six prospective regression models. Further, as explained below, we employed two distinct kinds of reference temperature computed from different formulas, i.e. an effective radiating equilibrium temperature (T_e) and a mean 'no-atmosphere' spherical surface temperature (T_{na}). This doubled the π_i instances in the regression analysis bringing the total number of potential models for investigation to twelv

Reference temperatures and reference pressure

A reference temperature (T_r) characterizes the average thermal environment at the surface of a planetary body in the absence of atmospheric greenhouse effect; hence, T_r is different for each body and depends on solar irradiance and surface albedo. The purpose of T_r is to provide a baseline for quantifying the thermal effect of planetary atmospheres. Indeed, the T_s/T_r ratio produced by DA can physically be interpreted as a Relative Atmospheric Thermal Enhancement (RATE) ideally expected to be equal to or greater than 1.0. Expressing the thermal effect of a planetary atmosphere as a non-dimensional quotient instead of an absolute temperature difference (as done in the past) allows for an unbiased comparison of the greenhouse effects of celestial bodies orbiting at different distances from the Sun. This is because the absolute strength of the greenhouse effect (measured in K) depends on both solar insolation and atmospheric properties, while RATE being a radiation-normalized quantity is expected to only be a function of a planet's atmospheric environment. To our knowledge, RATE has not previously been employed to measure the thermal effect of planetary atmospheres.

Two methods have been proposed thus far for estimating the average surface temperature of a planetary body without the greenhouse effect, both based on the SB radiation law. The first and most popular approach uses the planet's global energy budget to calculate a single radiating equilibrium temperature T_e (also known as an effective emission temperature) from he average absorbed solar flux [6,9,28], i.e.

$$T_e = \left[\frac{S(1-\alpha_p)}{4\varepsilon\sigma}\right]^{0.25} \tag{3}$$

Here, S is the solar irradiance (W m^{-2}) defined as the TOA shortwave flux incident on a plane perpendicular to the incoming rays, α_p is he planetary Bond albedo (decimal fraction), ε is the planet's LW emissivity (typically $0.9 \leq \varepsilon < 1.0$; in this study we assume $\varepsilon = 0.98$ b sed on lun r regolith measurements reported by Vasavada et al. [29], and $\sigma = 5.6704 \times 10^{-8}$ W m^{-2} K^{-4} is the SB constant. The term $S(1-\alpha_p)/4$ represents a globally averaged shortwave flux absorbed by the planet-atmosphere system. The rationale behind Eq. (3) is that the TOA energy b l nce presumably defines a baseline temperature at a certain height in he free atmosphere (around 5 km for Earth), which is related to the planet's mean surface temperature via the infrared optical depth of the atmosphere [9,10]. Equation (3) was introduced to planetary science in the early 1960s [30,31] and has been widely utilized ever since to calculate the average surface temperatures of airless (or nearly airless) bodies such as Mercury, Moon and Mars [32] as well as to quantify the strength of the greenhouse effect of planetary atmospheres [2-4,6,9,28]. However, Volokin and ReLlez [1] showed that, due to Hölder's inequality between integrals [33], T_e is a non-physical temperature for spheres and lacks a meaningful relationship to the planet's T_s.

The second method attempts to estimate the average surface temperature of a planet (T_{na}) in the complete absence of an atmosphere using an explicit spatial integration of the SB law over a sphere. Instead of calculating a single bulk temperature from the average absorbed shortwave flux as done in Eq. (3), this alternative approach first computes the equilibrium temperature at every point on the surface of an airless planet from the local absorbed shortwave flux using the SB relation, and then spherically integrates the resulting temperature field to produce a global temperature mean. While algorithmically opposite to Eq. (3), this method mimics well the procedure for calculating Earth's global temperature as an area-weighted average of surface observations.

Rubincam [34] proposed an analytic solution to the spherical integration of the SB law (his Eq. 15) assuming no heat storage by the regolith and zero thermal inertia of the ground. Volokin and ReLlez [1] improved upon Rubincam's formulation by deriving a closed-form integral expression that explicitly accounts for the effect of subterranean heat storage, cosmic microwave background radiation (CMBR) and geothermal heating on the average global surface temperature of airless bodies. The complete form of their analytic Spherical Airless-Temperature (SAT) model reads:

$$T_{na} = \frac{2}{5}\left\{\frac{\left[(1-\eta_e)S(1-\alpha_e)+R_c+R_g\right]^{5/4}-\left(R_C+R_g\right)^{5/4}}{(1-\eta_e)S(1-\alpha_e)(\varepsilon\sigma)^{1/4}}+\frac{\left[0.754\eta_e S(1-\alpha_e)+R_c+R_g\right]^{5/4}-\left(R_C+R_g\right)^{5/4}}{0.754\eta_e S(1-\alpha_e)(\varepsilon\sigma)^{1/4}}\right\} \quad (4a)$$

where α_e is the effective shortwave albedo of the surface, η_e is the effective ground heat storage coefficient in a vacuum, $R_c = \sigma\, 2.725^4 = 3.13 \times 10^{-6}$ W m^{-2} is the CMBR [35], and R_g is the spatially averaged geothermal flux (W m^{-2}) emanating from the subsurface. The heat storage term η_e is defined as a fraction of the absorbed shortwave flux conducted into the subsurface during daylight hour and subsequently released as heat at night.

Since the effect of CMBR on T_{na} is negligible for $S > 0.15$ W m^{-2} [1] and the geothermal contribution to surface temperatures is insignificant for most planetary bodies, one can simplify Eq. (4a) by substituting $R_c = R_g = 0$ This produces:

$$T_{na} = \frac{2}{5}\left[\frac{S(1-\alpha_e)}{\varepsilon\sigma}\right]^{0.25}\left[(1-\eta_e)^{0.25}+0.932\eta_e^{0.25}\right] \quad (4b)$$

where $0.932 = 0.754^{0.25}$. The complete formula (4a) must only be used if $S \le 0.15$ W m^{-2} and/or the magnitude of R_g is significantly greater than zero. For comparison, in the Solar System, the threshold $S \le 0.15$ W m^{-2} is encountered beyond 95 astronomical unis (AU) in the region of the inner Oort cloud. Volokin and ReLlez [1] verified Equations (4a) and (4b) against Moon temperature data provided by the NASA Diviner Lunar Radiometer Experiment [29,36]. These authors also showed that accounting for the subterranean heat storage (η_e) markedly improves the physical realism and accuracy of the SAT model compared to the original formulation by Rubincam [34].

The conceptual difference between Equations (3) and (4b) is that T_e represents the equilibrium temperature of a blackbody d sk orthogonally illuminated by shortwave radiation with an in ensity equal to the average solar flux absorbed by a sphere having a Bond albedo α_p, while T_{na} is the area-weighted average temperature of a thermally heterogen ous airless sphere [1,37]. In other words, for spherical objects T_e is an abstract mathematical temperature, while T_{na} is the average kinetic temperature of an airless surface. Due to Hölder's inequality between integrals, one always finds $T_e >> T_{na}$ when us ng equivalent values of stellar irradiance and surface albedo in Equations (3) and (4b) [1].

To calculate the T_{na} temperatures for planetary bodies with tangible atmospheres, we assumed that the airless equivalents of such objects would be covered with a regolith of similar optical and thermo-physical properties as the Moon surface. This is based on the premise that, in the absence of a protective a mosphere, the open cosmic environment would erode and pulverize exposed surfaces of rocky planets over time in a similar manner [1]. Also, properties of the Moon surface are the best studied ones mong all airless bodies in the Solar System. Hence, one could further simplify Eq. (4b) by combining the albedo, the heat storage fraction and the emissivity parameter into a single constant using applicable values for the Moon, i.e. $\alpha_e = 0.132$, $\eta_e = 0.00971$ and $\varepsilon = 0.98$ [1,29]. This produces:

$$T_{na} = 32.44\, S^{0.25} \quad (4c)$$

Equation (4c) was employed to estimate the 'no-atmosphere' reference temperatures of all planetary bodies participating in our analysis and discussed below.

For a reference pressure, we used the gas-liquid-solid triple point of water, i.e. $P_r = 611.73$ Pa [38] defining a baric threshold, below which water can only exists in a solid/vapor phase and not in a liquid form. The results of our analysis are not sensitive to the particular choice of a reference-pressure value; hence, the selection of P_r is a matter of convention.

Regression analysis

Finding the best function to describe the observed variation of GMAT among celestial bodies requires that the π_i variables generated by DA be subjected to regression analyses. As explained in Appendix A, twelve pairs of π_i variables hereto called Models were investigated. In order to ease the curve fitting and simplify the visualization of results, we utilized natural logarithms of the constructed π_i variable rather than their absolute values, i.e. we modeled the relationship $\ln(\pi_1) = f(\ln(\pi_2))$ instead of $\pi_1 = f(\pi_2)$. In doing so we focused on monotonic functions of conservative shapes such as exponential, sigmoidal, hyperbolic, and logarithmic, for their fitting coefficients might be interpretable in physically meaningful terms. A key advantage of this type of functions (provided the existence of a good fit, of course) is that they also tend to yield reliable results outside the data range used to determine their coefficients. We specifically avoided non-monotonic functions such as polynomials because of thei bility to accurately fit almost any dataset given a sufficiently large number of regression coefficients while at the same time showing poor predictive skills beyond the calibration data range. Due to their highly flexible shape, polynomials can easily fit random noise in a d taset, an outcome we particularly tried to avoid.

The following four-parameter exponential-growth function was found to est m et our criteria:

$$y = a\exp(bx)+c\exp(dx) \quad (5)$$

where $x = \ln(\pi_2)$ and $y = \ln(\pi_1)$ are the independent and dependent variable respectively while *a, b, c* and *d* are regression coefficients. This function has a rigid shape that can only describe specific exponential patterns found in our data. Equation (5) was fitted to each one of the 12 planetary data sets of logarithmic π_i pairs suggested by DA using the standard method of least squares. The skills of the resulting regression models were evaluated via three statistical criteria: coefficient of determination (R^2), adjusted R^2, and standard error of the estimate (σ_{est}) [39,40]. All calculations were performed with SigmaPlot™ 13 graphing and analysis software.

Planetary data

To ensure proper application of the DA methodology we compiled a dataset of diverse planetary environments in the Solar System using the best information available. Celestial bodies were selected for the analysis based on three criteria: (*a*) presence of a solid surface; (*b*) availability of reliable data on near-surface temperature, atmospheric composition, and total air pressure/density preferably from direct observations; and (*c*) representation of a broad range of physical environments defined in terms of TOA solar irradiance and atmospheric properties. This resulted in the selection of three planets: Venus, Earth, and Mars; and three natural satellites: Moon of Earth, Titan of Saturn, and Triton of Neptune.

Each celestial body was described by nine parameters shown in Table 2 with data sources listed in Table 3. In an effort to minimize the effect of unforced (internal) climate variability on the derivation of our temperature model, we tried to assemble a dataset of means representing an observational period of 30 years, i.e. from 1981 to 2010. Thus, Voyager measurements of Titan from the early 1980s suggested an average surface temperature of 94 ± 0.7 K [41]. Subsequent observations by the Cassini mission between 2005 and 2010 indicated a mean global temperature of 93.4 ± 0.6 K for that moon [42,43]. Since

Parameter	Venus	Earth	Moon	Mars	Titan	Triton
Average distance to the Sun, r_{au} (AU)	0.7233	1.0	1.0	1.5237	9.582	30.07
Average TOA solar irradiance, S (W m^{-2})	2,601.3	1,360.9	1,360.9	586.2	14.8	1.5
Bond albedo, α_p (decimal fraction)	0.900	0.294	0.136	0.235	0.265	0.650
Average absorbed shortwave radiation, $S_a = S(1-\alpha_p)/4$ (W m^{-2})	65.0	240.2	294.0	112.1	2.72	0.13
Global average surface atmospheric pressure, P (Pa)	9,300,000.0 ± 100,000	98,550.0 ± 6.5	$2.96 \times 10^{-10} \pm 10^{-10}$	685.4 ± 14.2	146,700.0 ± 100	4.0 ± 1.2
Global average surface atmospheric density, ρ (kg m^{-3})	65 868 ± 0.44	1.193 ± 0.002	$2.81 \times 10^{-15} \pm 9.4 \times 10^{-15}$	$0.019 \pm 3.2 \times 10^{-4}$	5.161 ± 0.03	$3.45 \times 10^{-4} \pm 9.2 \times 10^{-5}$
Chemical composition of the lower atmosphere (% of volume)	96.5 CO_2 3.48 N_2 0.02 SO_2	77.89 N_2 20.89 O_2 0.932 Ar 0.248 H_2O 0.040 CO_2	26.7 ^{4}He 26.7 ^{20}Ne 23.3 H_2 20.0 ^{40}Ar 3.3 ^{22}Ne	95.32 CO_2 2.70 N_2 1.60 Ar 0.13 O_2 0.08 CO 0.021 H_2O	95.1 N_2 4.9 CH_4	99.91 N_2 0.060 CO 0.024 CH_4
Molar mass of the lower atmosphere, M (kg mol^{-1})	0.0434	0.0289	0.0156	0.0434	0.0274	0.0280
GMAT, T_s (K)	737.0 ± 3.0	287.4 ± 0.5	197.35 ± 0.9	190.56 ± 0.7	93.7 ± 0.6	39.0 ± 1 0

Table 2: Planetary data set used in the Dimensional Analysis compiled from sources listed in Table 3. The estimation of Mars' GMAT and the average surface atmospheric pressure are discussed in Appendix B. See text for details about the computational methods employed for some parameters.

Planetary Body	Information Sources
Venus	[32,44-48]
Earth	[12,13,32,49-55]
Moon	[1,29,32,48,56-59]
Mars	[32,48,60-63], Appendix B
Titan	[32,41-43,64-72]
Triton	[48,73-75]

Table 3: Literature sources of the planetary data presented in Table 2.

Saturn's orbital period equals 29.45 Earth years, we averaged th above global temperature values to arrive at 93.7 ± 0.6 K as an estimate of Titan's 30-year GMAT. Similarly, data gathered in the late 1970s by the Viking Landers on Mars were combined with more recent Curiosity-Rover surface measurements and 1999-2005 remote observations by the Mars Global Surveyor (MGS) spacecraft to derive representative estimates of GMAT and atmospheric urface pressure for the Red Planet. Some parameter values reported in the literature did not meet our criteria for global representativeness nd/or physical plausibility and were recalculated using available bservations a described below.

The mean solar irradiances of all bodies were calculated as $S = S_E r_{au}^{-2}$ where r_{au} is the body's average distance (semi major axis) to the Sun (AU) and S_E = 1,360.9 W m^{-2} is the Earth's new lower irradiance at 1 AU according to recent satellite observations reported by Kopp and Lean [49]. Due to a design flaw in earlier spectrometers, the solar irradiance at Earth's distance has been overestimated by ≈ 5 W m^{-2} prior to 2003 [49]. Consequently, our calculations yielded slightly lower irradiances for bodies such as Venus and Mars compared to previously published data. Our decision to recalculate S was based on the assumption that the orbital distances of planets are known with much greater accuracy than TOA solar irradiances. Hence, a correction made to Earth's irradiance requires adjusting the 'solar constants' of all other planets as well.

We found that quoted values for the mean global temperature and surface atmospheric pressure of Mars were either improbable or too uncertain to be useful for our analysis. Thus, studies published in the last 15 years report Mars' GMAT being anywhere between 200 K and 240 K with the most frequently quoted values in the range 210–220 K [6,32,76-81]. However, in-situ measurements by Viking Lander 1 suggest that the average surface air temperature at a low-elevation site in the Martian subtropics does not exceed 207 K during the summer-fall season (Appendix B). Therefore, the Red Planet's GMAT must be lower than 207 K. The Viking records also indicate that average diurnal temperatures bove 210 K can only occur on Mars during summertime. Hence, all uch v lues must be significantly higher than the actual mean annual temp rature at any M rtian latitude. This is also supported by results from a 3-D global circulation model of the Red Planet obtained by Fenton et al. [82]. The surface atmospheric pressure on Mars varies appreciably with season and location. Its global average value has p eviously been reported between 600 Pa and 700 Pa [6,32,78,80,83,84], a range that was too broad for the target precision of our study. Hence our decision to calculate new annual global means of near-surface temperature and air pressure for Mars via a thorough analysis of available dat from remote-sensing and *in-situ* observations. Appendix B details our computational procedure with the results presented in Table 2. It is noteworthy that our independent estimate of Mars' GMAT (190.56 ± 0.7 K), while significantly lower than values quoted in recent years, is in perfect agreement with spherically integrated brightness temperatures of the Red Planet derived from remote microwave measurements in the late 1960s and early 1970s [85-87].

Moon's GMAT was also not readily extractable from the published literature. Although lunar temperatures have been measured for more than 50 years both remotely and *in situ* [36] most studies focus on observed temperature extremes across the lunar surface [56] and rarely discuss the Moon's average global temperature. Current GMAT estimates for the Moon cluster around two narrow ranges: 250–255 K and 269–271 K [32]. A careful examination of the published data reveals that the 250–255 K range is based on subterranean heat-flow measurements conducted at depths between 80 and 140 cm at the Apollo 15 and 17 landing sites located at 26°N; 3.6°E and 20°N; 30.6°E, respectively [88]. Due to a strong temperature dependence of the lunar regolith thermal conductivity in the topmost 1-2 cm soil, the Moon's average diurnal temperature increases steadily with depth. According to Apollo measurements, the mean daily temperature at 35 cm belowground is 40–45 K higher than that at the lunar surface [88]. The diurnal temperature fluctuations completely vanish below a depth of 80 cm. At 100 cm depth, the temperature of the lunar regolith ranged from 250.7 K to 252.5 K at the Apollo 15 site and between 254.5 K and 255.5 K at the Apollo 17 site [88]. Hence, reported Moon average temperatures in the range 250-255 K do not describe surface conditions. Moreover, since measured in the lunar subtropics, such temperatures do not likely even represent Moon's global thermal environment at these depths. On the other hand, frequently quoted Moon global temperatures of ~270 K have actually been calculated from Eq. (3) and are not based on surface measurements. However, as demonstrated by Volokin and ReLlez [1],

Eq. (3) overestimates the mean global surface temperature of spheres by about 37%. In this study, we employed the spherical estimate of Moon's GMAT (197.35 K) obtained by Volokin and ReLlez [1] using output from a NASA thermo-physical model validated against Diviner observations [29].

Surprisingly, many publications report incorrect values even for Earth's mean global temperature. Studies of terrestrial climate typically focus on temperature anomalies and if Earth's GMAT is ever mentioned, it is often loosely quoted as 15 C (~288 K) [2-4,6]. However, observations archived in the HadCRUT4 dataset of the UK Met Office's Hadley Centre [50,89] and in the Global Historical Climatology Network [51,52,90,91] indicate that, between 1981 and 2010, Earth's mean annual surface air temperature was 287.4 K (14.3 C) ± 0.5 K. Some recent studies acknowledge this more accurate lower value of Earth's absolute global temperature [92]. For Earth's mean surface atmospheric pressure we adopted the estimate by Trenberth et al. [53] (98.55 kPa), which takes into account the average elevation of continental landmasses above sea level; hence, it is slightly lower than the typical sea-level pressure of ≈ 101.3 kPa.

The average near-surface atmospheric densities (ρ, kg m^{-3}) of planetary bodies were calculated from reported means of total atmospheric pressure (P), molar mass (M, kg mol^{-1}) and temperature (T_s) using the Ideal Gas Law, i.e.

$$\rho = \frac{P\,M}{R\,T_s} \tag{6}$$

where R = 8.31446 J mol^{-1} K^{-1} is the universal gas constant. This calculation was intended to make atmospheric densities physically consistent with independent data on pressure and temperature utilized in our study. The resulting ρ values were similar to previously published data for individual bodies. Standard errors of the air-density estimates were calculated from reported errors of P and T_s for each body using Eq. (6).

Data in Table 2 were harnessed to compute several intermediate variables and all dimensionless π_i products necessary for the regression analyses. The results from these computations are shown in Table 4.

Greenhouse gases in planetary atmospheres represented by the major constituents carbon dioxide (CO_2), methane (CH_4) and water vapor (H_2O) were collectively quantified via three bulk parameters: average molar mass (M_{gh}, kg mol^{-1}), combined partial pressure (P_{gh}, Pa) and combined partial density (ρ_{gh}, kg m^{-3}). These parameters were estimated from reported volumetric concentrations of individual greenhouse gases (C_x, %) and data on total atmospheric pressure and density in Table 2 using the formulas:

$$M_{gh} = \left(0.044 C_{CO2} + 0.016 C_{CH4} + 0.018 C_{H2O}\right) / C_{gh} \tag{7}$$

$$P_{gh} = P\left(0.01 C_{gh}\right) \tag{8}$$

$$\rho_{gh} = \rho\left(0.01 C_{gh}\right)\left(M_{gh} / M\right) \tag{9}$$

where $C_{gh} = C_{CO2} + C_{CH4} + C_{H2O}$ is the total volumetric concentration of major greenhouse gases (%). The reference temperatures T_e and T_{na} were calculated from Equation (3) and (4c), respectively.

Results

Function (5) was fitted to each one of the 12 sets of logarithmic π_i pairs generated by Equations (1) and (2) and shown in Table 4. Figures 1 and 2 display the resulting curves of individual regression models with planetary data plotted in the background for reference. Table 5 lists the statistical scores of each non-linear regression. Model 12 depicted in Figure 2f had the highest R^2 = 0.9999 and the lowest standard error σ_t = 0.0078 among all regressions. Model 1 (Figure 1a) provided the second best fit with R^2 = 0.9844 and σ_{est} = 0.1529. Notably, Model 1 shows almost a 20-time larger standard error on the logarithmic scale than Model 12. Figure 3 illustrates the difference in predictive skills between the two top-performing Models 1 and 12 upon conversion of vertical axes to a linear scale. Taking an antilogarithm weakens the relationship of Model 1 to the point of becoming immaterial and highlights the superiority of Model 12. The statistical results shown in Table 5 indicate that the explanatory power and descriptive accuracy of Model 12 surpass those of all other models by a wide margin.

Since Titan and Earth nearly overlap on the logarithmic scale of Figure 2f, we decided to experiment with an alternative regression for Model 12,

Intermediate Variable or Dimensionless Product	Venus	Earth	Moon	Mars	Titan	Triton
Average molar mass of greenhouse gases, M_{gh} (kg mol^{-1}) (Eq. 7)	0.0440	0.0216	0.0	0.0440	0.0160	0.0160
Near-surface partial pressure of greenhouse gases, P_{gh} (Pa) (Eq. 8)	8,974,500.0 ± 96,500	283.8 ± 0.02	0.0	667.7 ± 13.8	7,188.3 ± 4.9	$9.6 \times 10^{-4} \pm 2.9 \times 10^{-4}$
Near-surface density of greenhouse gases ρ_{gh} (kg m^{-3}) (Eq. 9)	64.441 ± 0.429	$2.57 \times 10^{-3} \pm 4.3 \times 10^{-6}$	0.0	$0.018 \pm 3.1 \times 10^{-4}$	$0.148 \pm 8.4 \times 10^{-4}$	$4.74 \times 10^{-8} \pm 1.3 \times 10^{-8}$
Radiating equilibrium temperature, T_e (K) (Eq. 3)	185.0	256.4	269.7	211.9	83.6	39.2
Average airless spherical temperature, T_{na} (K) (Eq. 4c)	231.7	197.0	197 0	159.6	63.6	35.9
T_s / T_e	3.985 ± 0.016	1.121 ± 0.002	0.732 ± 0.003	0.899 ± 0.003	1.120 ± 0.008	0.994 ± 0 026
T_s / T_{na}	3.181 ± 0.013	1.459 ± 0.002	1.002 ± 0.004	1.194 ± 0.004	1.473 ± 0.011	1.086 ± 0 028
$\ln(T_s / T_e)$	1.3825 ± 0.0041	0.1141 ± 0.0017	-0.3123 ± 0.0046	-0.1063 ± 0.0037	0.1136 ± 0.0075	$-5.2 \times 10^{-3} \pm 0.0256$
$\ln(T_s / T_{na})$	1.1573 ± 0.0041	0.3775 ± 0.0017	$1.59 \times 10^{-3} \pm 0.0046$	0.1772 ± 0.0037	0.3870 ± 0.0075	0.0828 ± 0 0256
$\ln[P_{gh}^3 / (\rho_{gh} S^2)]$	28.1364	8.4784	Undefine	10.7520	23.1644	-4.7981
$\ln[P^3 / (\rho_{gh} S^2)]$	28 2433	26.0283	+∞	10.8304	32.2122	20.2065
$\ln[P_{gh}^3 / (\rho S^2)]$	28.1145	2.3370	Undefine	10.7396	19.6102	-13.6926
$\ln[P_{gh} / P_r]$	9.5936	-0.7679	Undefine	0.0876	2.4639	-13.3649
$\ln[P^3 / (\rho S^2)]$	28 2214	19.8869	-46.7497	10.8180	28.6580	11.3120
$\ln(P / P_r)$	9.6292 ± 0.0108	$5.0820 \pm 6.6 \times 10^{-5}$	-28.3570 ± 0.3516	0.1137 ± 0.0207	$5.4799 \pm 6.8 \times 10^{-4}$	-5.0300 ± 0.3095

Table 4: Intermediate variables and dimensionless products required for the regression analyses and calculated from data in Table 2. Equations used to compute intermediate variables are shown in parentheses. The reference pressure is set to the barometric triple point of water, i e. P_r = 611.73 Pa.

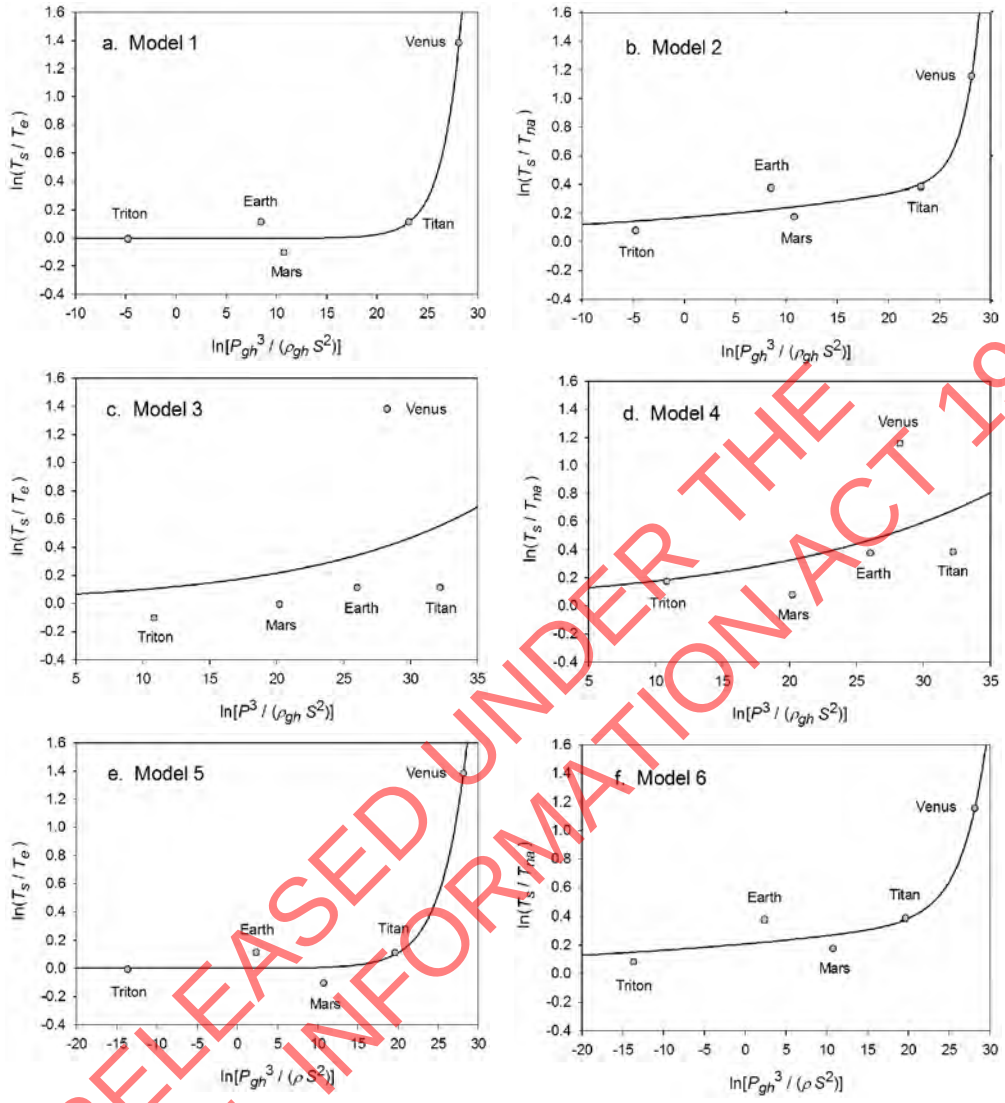

Figure 1: The rela ive atmospheric thermal enhancement (T_s/T_r) as a function of various dimensionless forcing variables generated by DA using data on solar irradiance, near-surface partial pressure/den ity of greenhouse gases, and total atmospheric pressure/density from Table 4. Panels *a* through *f* depict six regression models suggested by DA with the underlying celestial bodies plotted in the background for reference. Each pair of horizontal graphs represents different reference temperatures (T_r) defined as either $T_r = T_e$ (left) or $T_r = T_{na}$ (right).

which excludes Titan from the input dataset. This new curve had R^2 = 1.0 and σ_{est} = 0.0009. Although the two regression equations yield similar results over most of the relevant pressure range, we chose the one without Titan as final for Model 12 based on the assumption that Earth's GMAT is likely known with a much greater accuracy than Titan's mean annual temperature. Taking an antilogarithm of the final regression equation, which excludes Titan, yielded the following expression for Model 12:

$$\frac{T_s}{T_{na}} = \exp\left[0.174205\left(\frac{P}{P_r}\right)^{0.150263} + 1.83121 \times 10^{-5}\left(\frac{P}{P_r}\right)^{1.04193}\right] \quad (10a)$$

The regression coefficients in Eq. (10a) are intentionally shown in full precision to allow an accurate calculation of RATE (i.e. the T_s/T_{na} ratios) provided the strong non-linearity of the relationship and to facilitate a successful replication of our results by other researchers. Figure 4 depicts Eq. (10a) as a dependence of RATE on the average surface air pressure. Superimposed on this graph are the six planetary bodies from Table 4 along with their uncertainty ranges.

Equation (10a) implies that GMATs of rocky planets can be calculated as a product of two quantities: the planet's average surface temperature in the absence of an atmosphere (T_{na}, K) and a non-dimensional factor ($E_a \geq 1.0$) quantifying the relative thermal effect of the atmosphere, i.e.

$$T_s = T_{na}\, E_a \quad (10b)$$

where T_{na} is obtained from the SAT model (Eq. 4a) and E_a is a function of total pressure (P) given by:

$$E_a(P) = \exp\left[0.174205\left(\frac{P}{P_r}\right)^{0.150263}\right]\exp\left[1.83121\times10^{-5}\left(\frac{P}{P_r}\right)^{1.04193}\right] \quad (11)$$

Note that, as P approaches 0 in Eq. (11), E_a approaches the physically realistic limit of 1.0. Other physical aspects of this equation are discussed below.

For bodies with tangible atmospheres (such as Venus, Earth,

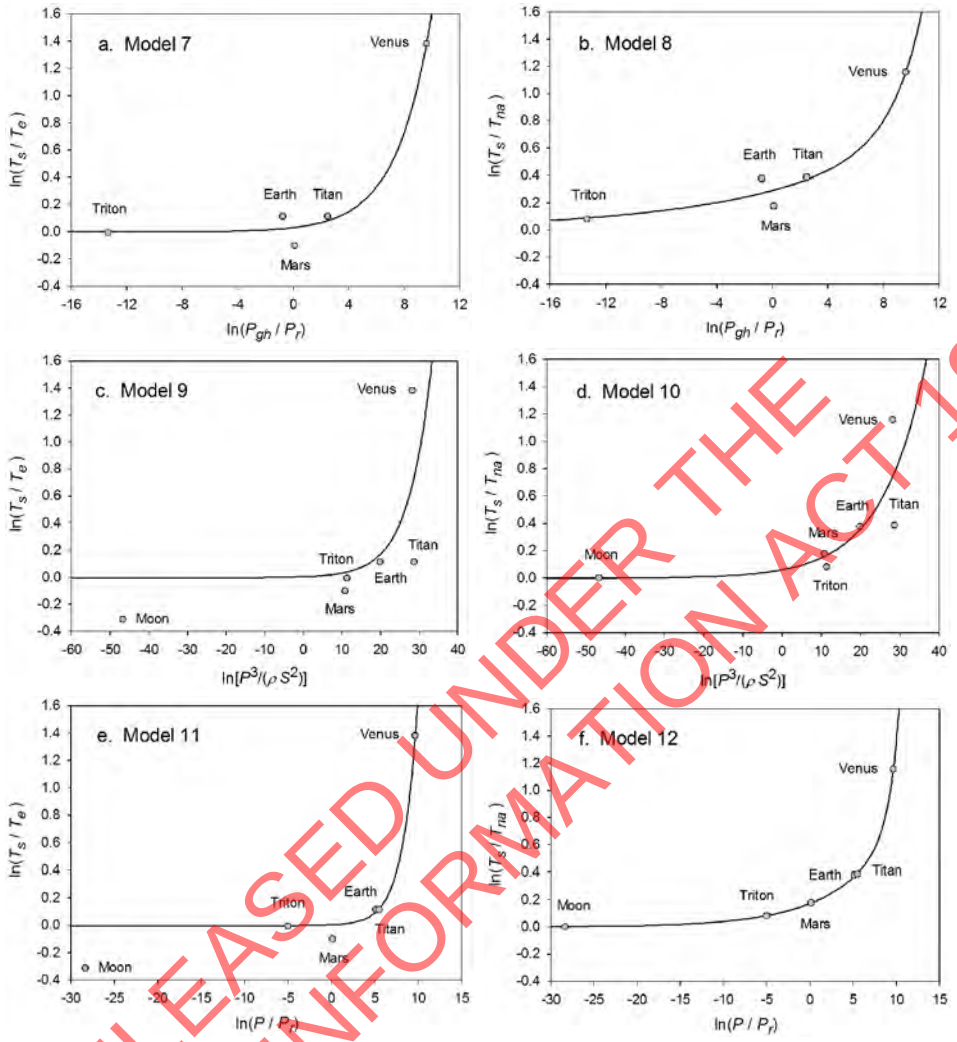

Figure 2: The same as in Figure 1 but for six additional regression models (panels *a* through *f*).

Mars, Titan and Triton), one must calculate T_{na} using α_e = 0.132 and η_e = 0.00971, which assumes a Moon-like airless reference surface in accordance with our pre-analysis premise. For bodies with tenuous atmospheres (such as Mercury, the Moon, Calisto and Europa), T_{na} should be calculated from Eq. (4a) (or Eq. 4b respectively if $S > 0.15$ W m^{-2} and/or Rg ≈ 0 W m^{-2}) using the body's observed values of Bond albedo α_e and ground heat storage fraction η_e. In the context of this model, a tangible atmosphere is defined as one that has significantly modified the optical and thermo-physical properties of a planet's surface compared to an airless environment and/or noticeably impacted the overall planetary albedo by enabling the formation of clouds and haze. A tenuous atmosphere, on the other hand, is one that has not had a measurable influence on the surface albedo and regolith thermo-physical properties and is completely transparent to shortwave radiation. The need for such delineation of atmospheric masses when calculating T_{na} arises from the fact that Eq. (10a) accurately describes RATEs of planetary bodies with tangible atmospheres over a wide range of conditions without explicitly accounting for the observed large differences in albedos (i.e. from 0.235 to 0.90) while assuming constant values of α_e and η_e for the airless equivalent of these bodies. One possible explanation for this counterintuitive empirical result is that atmospheric pressure alters the planetary albedo and heat storage properties of the surface in a way that transforms these parameters from independent controllers of the global temperature in airless bodies to intrinsic byproducts of the climate system itself in worlds with appreciable atmospheres. In other words, once atmospheric pressure rises above a certain level, the effects of albedo and ground heat storage on GMAT become implicitly accounted for by Eq. (11). Although this hypothesis requires a further investigation beyond the scope of the present study, one finds an initial support for it in the observation that, according to data in Table 2, GMATs of bodies with tangible atmospheres do not show a physically meaningful relationship with the amounts of absorbed shortwave radiation determined by albedos. Our discovery for the need to utilize different albedos and heat storage coefficients between airless worlds and worlds with tangible atmospheres is not unique as a methodological approach. In many areas of science and engineering, it is sometime necessary to use disparate model parameterizations to successfully describe different aspects of the same phenomenon. An example is the distinction made in fluid mechanics between laminar and turbulent flow, where the non-dimensional Reynold's number is employed to separate the two regimes that are subjected to different mathematical treatments.

No.	Functional Model	Coefficient of Determination (²)	Adjusted R²	Standard Error σ_{est}
1	$\frac{T_s}{T_e} = f\left(\frac{P_{gh}^{\ 3}}{\rho_{gh} S^2}\right)$	0.9844	0.9375	0.1529
2	$\frac{T_s}{T_{na}} = f\left(\frac{P_{gh}^{\ 3}}{\rho_{gh} S^2}\right)$	0.9562	0.8249	0.1773
3	$\frac{T_s}{T_e} = f\left(\frac{P^3}{\rho_{gh} S^2}\right)$	0.1372	-2.4511	1.1360
4	$\frac{T_s}{T_{na}} = f\left(\frac{P^3}{\rho_{gh} S^2}\right)$	0.2450	-2.0200	0.7365
5	$\frac{T_s}{T_e} = f\left(\frac{P_{gh}^{\ 3}}{\rho S^2}\right)$	0.9835	0.9339	0.1572
6	$\frac{T_s}{T_{na}} = f\left(\frac{P_{gh}^{\ 3}}{\rho S^2}\right)$	0.9467	0.7866	0.1957
7	$\frac{T_s}{T_e} = f\left(\frac{P_{gh}}{P_r}\right)$	0.9818	0.927	0.1648
8	$\frac{T_s}{T_{na}} = f\left(\frac{P_{gh}}{P_r}\right)$	0.9649	0.8598	0.1587
9	$\frac{T_s}{T_e} = f\left(\frac{P^3}{\rho S^2}\right)$	0.4488	-0.3780	0.7060
10	$\frac{T_s}{T_{na}} = f\left(\frac{P^3}{\rho S^2}\right)$	0.6256	0.0639	0.4049
11	$\frac{T_s}{T_e} = f\left(\frac{P}{P_r}\right)$	0.9396	0.8489	0.2338
12	$\frac{T_s}{T_{na}} = f\left(\frac{P}{P_r}\right)$	0.9999	0.9997	0.0078

Table 5: Performance statistics of the twelve regression models suggested by DA. Statistical scores refer to the model logarithmic forms shown in Figures 1 and 2.

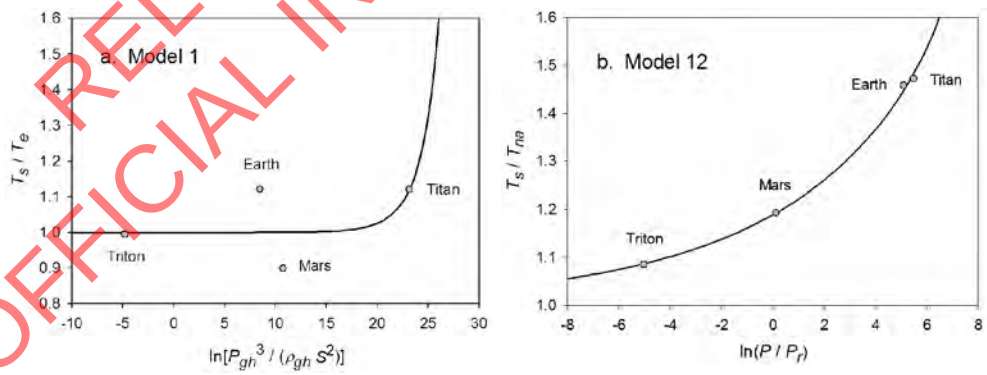

Figure 3: Comparison of the two best-performing regression models according to statistical scores listed in Table 5. Vertical axes use linear scales to better illustrate he difference in skills between the models.

We do not currently have sufficient data to precisely define the limit between *tangible* and *tenuous* atmospheres in terms of total pressure for the purpose of this model. However, considering that an atmospheric pressure of 1.0 Pa on Pluto causes the formation of layered haze [93], we surmise that this limit likely lies significantly below 1.0 Pa. In this study, we use 0.01 Pa as a tentative threshold value. Thus, in the context of Eq. (10b), we recommend computing T_{na} from Eq. (4c) if $P > 10^{-2}$ Pa, and from Eq. (4a) (or Eq. 4b, respectively) using observed values of α_e and η_e if $P \leq 10^{-2}$ Pa. Equation (4a) should also be employed in cases, where a significant geothermal flux exists such as on the Galilean moons of Jupiter due to tidal heating, and/or if $S \leq 0.15$ W m^{-2}. Hence, the 30-year mean global equilibrium surface temperature of rocky planets depends in general on five factors: TOA stellar irradiance (S), a reference airless surface albedo (α_e), a reference airless ground heat storage fraction

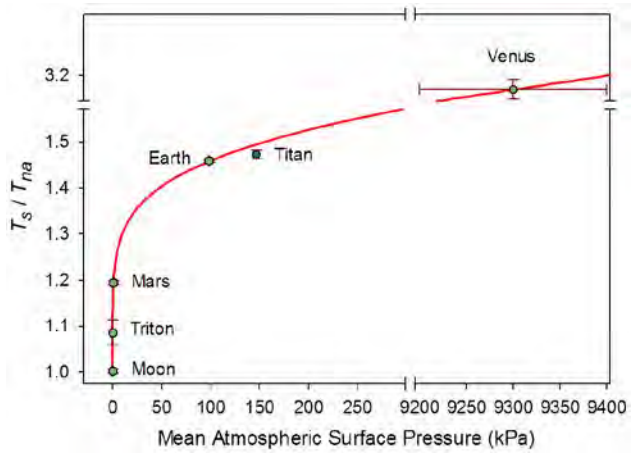

Figure 4: The relative atmospheric thermal enhancement (T_s/T_{na} ratio) as a function of the average surface air pressure according to Eq. (10a) derived from data representing a broad range of planetary environments in the solar system. Saturn's moon Titan has been excluded from the regression analysis leading to Eq. (10a). Error bars of some bodies are not clearly visible due to their small size relative to the scale of the axes. See Table 2 for the actual error estimates.

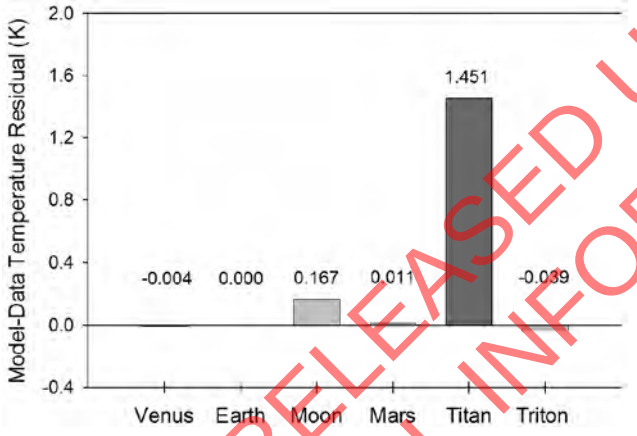

Figure 5: Absolute differences between modeled average global temperatures by Eq. (10b) and observed GMATs (Table 2) for the studied celestial bodies. Saturn's moon Titan represents an independent data point, since it was excluded from the regression analysis leading to Eq. (10a).

(η_e), the average geothermal flux reaching the surface (R_g), and the total surface atmospheric pressure (P). For planets with tangible atmospheres ($P > 10^{-2}$ Pa) and a negligible geothermal heating of the surface ($R_g \approx 0$), the equilibrium GMAT becomes only a function of two factors: S and P, i.e. $T_s = 32.44\ S^{0.25} E_a(P)$. The final model (Eq. 10b) can also be cast in terms of T_s as a function of a planet's distance to the Sun (r_{au}, AU) by replacing S in Equations (4a), (4b) or (4c) with $1360.9\ r_{au}^{-2}$.

Environmental scope and numerical accuracy of the new model

Figure 5 portrays the residuals between modeled and observed absolute planetary temperatures. For celestial bodies participating in the regression analysis (i.e. Venus, Earth, Moon, Mars and Triton), the maximum model error does not exceed 0.17 K and is well within the uncertainty of observations. The error for Titan, an independent data point, is 1.45 K or 1.5% of that moon's current best-known GMAT (93.7 K). Equation (10b) produces 95.18 K for Titan at Saturn's semi-major axis (9.582 AU) corresponding to a solar irradiance $S = 14.8$ W m^{-2}. This estimate is virtually identical to the 95 K average surface temperature reported for that moon by the NASA JPL Voyager Mission website [94]. The Voyager spacecraft 1 and 2 reached Saturn and its moons in November 1980 and August 1981, respectively, when the gas giant was at a distance between 9.52 AU and 9.60 AU from the Sun corresponding approximately to Saturn's semi-major axis [95].

Data acquired by Voyager 1 suggested an average surface temperature of 94 ± 0.7 K for Titan, while Voyager 2 indicated a temperature close to 95 K [41]. Measurements obtained between 2005 and 2010 by the Cassini-Huygens mission revealed $T_s \approx 93.4 \pm 0.6$ K [42,43]. Using Saturn's perihelion (9.023 AU) and aphelion (10.05 AU) one can compute Titan's TOA solar irradiance at the closest and furthest approach to the Sun, i.e 16.7 W m^{-2} and 13.47 W m^{-2}, respectively. Inserting these values into Eq. (10b) produces the expected upper and lower limit of Titan's mean global surface temperature according to our model, i.e. $92.9\ \text{K} \le T_s \le 98.1$ K. Notably this range encompasses all current observation-based estimates of Titan's GMAT. Since both Voyager and Cassini mission covered shorter periods than a single Titan season (Saturn's orbital period is 29.45 Earth years), the available measurements may not well represent that moon's annual thermal cycle. In addition, due to a thermal inertia, Titan's average surface temperature likely lags variations in the TOA solar irradiance caused by Saturn's orbital eccentricity. Thus, the observed 1.45 K discrepancy between our independent model prediction and Titan's current best-known GMAT seems to be within the range of plausible global temperature fluctuations on that moon. Hence, further observations are needed to more precisely constrain Titan's long-term GMAT.

Measurements conducted by the Voyager spacecraft in 1989 indicated a global mean temperature of 38 ± 1.0 K and an average atmospheric pressure of 1.4 Pa at the surface of Triton [73]. Even though Eq. (10a) is based on slightly different data for Triton (i.e. T_s = 39 ±1.0 K and P = 4.0 Pa) obtained by more recent stellar occultation measurements [73], employing the Voyager-reported pressure in Eq. (10b) produces T_s = 38.5 K for Triton's GMAT, a value well within the uncertainty of the 1989 temperature measurements.

The above comparisons indicate that Eq. (10b) rather accurately describes the observed variation of the mean surface temperature across a wide range of planetary environments in terms of solar irradiance (from 1.5 W m^{-2} to 2,602 W m^{-2}), total atmospheric pressure (from near vacuum to 9,300 kPa) and greenhouse-gas concentrations (from 0.0% to over 96% per volume). While true that Eq. (10a) is based on data from only 6 celestial objects, one should keep in mind that these constitute virtually all bodies in the Solar System meeting our criteria for availability and quality of measured data. Although function (5) has 4 free parameters estimated from just 5-6 data points, there are no signs of model overfitting in this case because (*a*) Eq. (5) represents a monotonic function of a rigid shape that can only describe well certain exponential pattern as evident from Figures 1 and 2 and the statistical scores in Table 5; (*b*) a simple scatter plot of $\ln(P/P_r)$ vs. $\ln(T_s/T_{na})$ visibly reveals the presence of an exponential relationship free of data noise; and (*c*) no polynomial can fit the data points in Figure 2f as accurately as Eq. (5) while also producing a physically meaningful response curve similar to known pressure-temperature relationships in other systems. These facts indicate that Eq. (5) is not too complicated to cause an over-fitting but just right for describing the data at hand.

The fact that only one of the investigated twelve non-linear regressions yielded a tight relationship suggests that Model 12 describes

a macro-level thermodynamic property of planetary atmospheres heretofore unbeknown to science. A function of such predictive power spanning the entire breadth of the Solar System cannot be just a result of chance. Indeed, complex natural systems consisting of myriad interacting agents have been known to sometime exhibit emergent responses at higher levels of hierarchical organization that are amenable to accurate modeling using top-down statistical approaches [96]. Equation (10a) also displays several other characteristics discussed below that lend further support to the above notion.

Model robustness

Model robustness defines the degree to which a statistical relationship would hold when recalculated using a different dataset. To test the robustness of Eq. (10a) we performed an alternative regression analysis, which excluded Earth and Titan from the input data and only utilized logarithmic pairs of T_s/T_{na} and P/P_r for Venus, the Moon, Mars and Triton from Table 4. The goal was to evaluate how well the resulting new regression equation would predict the observed mean surface temperatures of Earth and Titan. Since these two bodies occupy a highly non-linear region in Model 12 (Figure 2f), eliminating them from the regression analysis would leave a key portion of the curve poorly defined. As in all previous cases, function (5) was fitted to the incomplete dataset (omitting Earth and Titan), which yielded the following expression:

$$\frac{T_s}{T_{na}} = \exp\left[0.174222\left(\frac{P}{P_r}\right)^{0.150275} + 5.25043\times10^{-15}\left(\frac{P}{P_r}\right)^{3.32375}\right] \quad (12a)$$

Substituting the reference temperature T_{na} in Eq. (12a) with its equivalent from Eq. (4c) and solving for T_s produces

$$T_s = 32.44 S^{0.25} \exp\left[0.174222\left(\frac{P}{P_r}\right)^{0.150275}\right]\exp\left[5.25043\times10^{-15}\left(\frac{P}{P_r}\right)^{3.32375}\right] \quad (12b)$$

It is evident that the regression coefficients in the first exponent term of Eq. (12a) are nearly identical to those in Eq. (10a). This term dominates the T_s-P relationship over the pressure range 0-400 kPa accounting for more than 97.5% of the predicted temperature magnitudes. The regression coefficients of the second exponent differ somewhat between the two formulas causing a divergence of calculated RATE values over the pressure interval 400–9,100 kPa. The models converge again between 9,000 kPa and 9,300 kPa. Figure 6 illustrates the similarity of responses between Equations (10a) and (12a) over the pressure range 0–300 kPa with Earth and Titan plotted in the foreground for reference.

Equation (12b) reproduces the observed global surface temperature of Earth with an error of 0.4% (-1.0 K) and that of Titan with an error of 1.0% (+0.9 K). For Titan, the error of the new Eq. (12b) is even slightly smaller than that of the original model (Eq. 10b). The ability of Model 12 to predict Earth's GMAT with an accuracy of 99.6% using a relationship inferred from disparate environments such as those found on Venus, Moon, Mars and Triton indicates that (*a*) this model is statistically robust, and (*b*) Earth's temperature is a part of a cosmic thermodynamic continuum well described by Eq. (10b). The apparent smoothness of this continuum for bodies with tangible atmospheres (illustrated in Figure 4) suggests that planetary climates are well-buffered and have no 'tipping points' in reality, i.e. states enabling rapid and irreversible changes in the global equilibrium temperature as a result of destabilizing positive feedbacks assumed to operate within climate systems. This robustness test also serves as a cross-validation suggesting that the new model has a universal nature and it is not a product of overfitting.

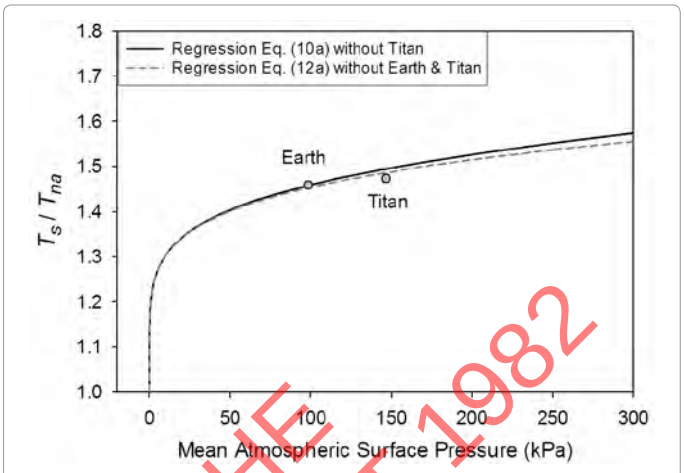

Figure 6: Demonstration of the robustness of Model 12. The solid black curve depicts Eq. (10a) based on data from 5 celestial bodies (i.e. Venus, Earth, Moon, Mars and Triton). The dashed grey curve portrays Eq. (12a) derived from data of only 4 bodies (i.e. Venus, Moon, Mars and Triton) while excluding Earth and Titan from the regression analysis. The alternative Eq. (12b) predicts the observed GMATs of Earth and Titan with accuracy greater than 99% indicating that Model 12 is statistically robust.

The above characteristics of Eq. (10a) including dimensional homogeneity, high predictive accuracy, broad environmental scope of validity and statistical robustness indicate that it represents an emergent macro-physical model of theoretical significance deserving further investigation. This conclusive result is also supported by the physical meaningfulness of the response curve described by Eq. (10a).

Discussion

Given the high statistical scores of the new model discussed above, it is important to address its physical significance, potential limitations, and broad implications for the current climate theory.

Similarity of the new model to Poisson's formula and the SB radiation law

The functional response of Eq. (10a) portrayed in Figure 4 closely resembles the shape of the dry adiabatic temperature curve in Figure 7a described by the Poisson formula and derived from the First Law of Thermodynamics and the Ideal Gas Law [4], i.e.

$$\frac{T}{T_o} = \left(\frac{p}{p_o}\right)^{R/c_p} \quad (13)$$

Here, T_o and p_o are reference values for temperature and pressure typically measured at the surface, while T and p are corresponding scalars in the free atmosphere, and c_p is the molar heat capacity of air (J mol^{-1} K^{-1}). For the Earth's atmosphere, $R/c_p = 0.286$. Equation (13) essentially describes the direct effect of pressure p on the gas temperature (T) in the absence of any heat exchange with the surrounding environment.

Equation (10a) is structurally similar to Eq. (13) in a sense that both expressions relate a temperature ratio to a pressure ratio, or more precisely, a relative thermal enhancement to a ratio of physical forces. However, while the Poisson formula typically produces $0 \le T/T_o \le 1.0$, Eq. (10a) always yields $T_s/T_{na} \ge 1.0$. The key difference between the two models stems from the fact that Eq. (13) describes vertical temperature changes in a free and dry atmosphere induced by a gravity-controlled pressure gradient, while Eq. (10a) predicts the equilibrium response of a planet's global surface air temperature to variations in total atmospheric

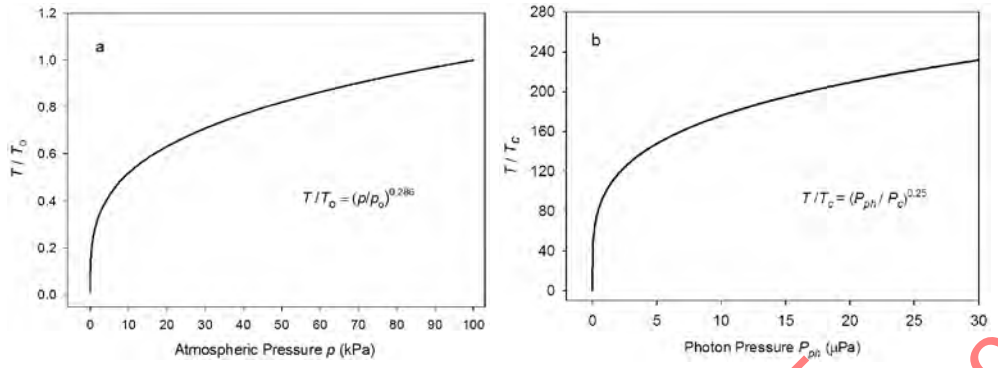

Figure 7: Known pressure-temperature kinetic relations: (*a*) Dry adiabatic response of the air/surface temperature ratio to pressure changes in a free dry atmosphere according to Poisson's formula (Eq. 13) with a reference pressure set to p_o = 100 kPa; (*b*) The SB radiation law expressed as a response of a blackbody temperature ratio to variations in photon pressure (Eq. 14). Note he qualitative striking similarity of shapes between these curves and the one portrayed in Figure 4 depicting the new planetary temperature model (Eq. 10a).

pressure. In essence, Eq. (10b) could be viewed as a predictor of the reference temperature T_o in the Poisson formula. Thus, while qualitatively similar, Equations (10a) and (13) are quantitatively rather different. Both functions describe effects of pressure on temperature but in the context of disparate physical systems. Therefore, estimates obtained from Eq. (10a) should not be confused with results inferred from the Poisson formula. For example, Eq. (10b) cannot be expected to predict the temperature lapse rate and/or vertical temperature profiles within a planetary atmosphere as could be using Eq. (13). Furthermore, Eq. (10a) represents a top-down empirical model that implicitly accounts for a plethora of thermodynamic and radiative processes and feedbacks operating in real climate systems, while the Poisson formula (derived from the Ideal Gas Law) only describes pressure-induced temperature changes in a simple mixture of dry gases without any implicit or explicit consideration of planetary-scale mechanisms such as latent heat transport and cloud radiative forcing.

Equation (10a) also shows a remarkable similarity o the SB law relating the equilibrium skin temp rature f an isotherma blackbody (T_b, K) to the electromagnetic radiati e flux (I, W m^{-2}) absorbed/emitted by the body's surface, i $T = (I / \sigma)^{0.25}$. Dividing each side of this fundamental relationship by the irreducible temperature of deep Space T_c = 2.725 K and its causative CMBR R_c = 3.13 × 10^{-6} W m^{-2} respectively, yields $T_b/T_c = (I/R_c)^{0.25}$. Further, expressing the radiative fluxes I and R_c on the right-hand side as products of photon pressure and the speed of light (c, m s^{-1}) in a vacuum, i.e. $I = cP_{ph}$ and $R_c = cP_c$, leads to the following alternative f rm of the SB law:

$$\frac{T_b}{T_c} = \left(\frac{P_{ph}}{P_c}\right)^{0.25} \quad (14)$$

where P_c = 1.043 × 10^{-14} Pa is the photon pressure of CMBR. Clearly, Eq. (10a) is analogous to Eq. (14), while the latter is structurally identical to the Poisson formula (13). Figure 7b depicts Eq. (14) as a dependence of the T_b/T_c ratio on photon pressure P_{ph}.

It is evident from Figures 4 and 7 that formulas (10a), (13) and (14) describe qualitatively very similar responses in quantitatively vastly different systems. The presence of such similar relations in otherwise disparate physical systems can fundamentally be explained by the fact that pressure as a force per unit area represents a key component of the internal kinetic energy (defined as a product of gas volume and pressure), while temperature is merely a physical manifestation of this energy. Adding a force such as gas pressure to a physical system inevitably boosts the int rnal kinetic energy and raises its temperature, a process known in thermodynamics as compression heating. The direct effect of pressure on a system's temperature is thermodynamically described by adi batic proce ses. The pressure-induced thermal enhancement at a planetary lev l portrayed in Figure 4 and accurately quantified by Eq (10a or 11) is analogous to a compression heating, but not fully i entical to an adiabatic process. The latter is usually characterized by a limited duration and oftentimes only applies to finite-size parcels of air moving vertically through the atmosphere. Equation (11), on the other hand, describes a surface thermal effect that is global in scope and permanent in nature as long as an atmospheric mass is present within the planet's gravitational field. Hence, the planetary RATE (T_s/T_{na} ratio) c uld be understood as a net result of countless simultaneous adiabatic processes continuously operating in the free atmosphere. Figures 4 and 7 also suggest that the pressure control of temperature is a universal thermodynamic principle applicable to systems ranging in complexity from a simple isothermal blackbody absorbing a homogeneous flux of electromagnetic radiation to diverse planetary atmospheres governed by complex non-linear process interactions and cloud-radiative feedbacks. To our knowledge, this cross-scale similarity among various pressure-temperature relationships has not previously been identified and could provide a valuable new perspective on the working of planetary climates.

Nevertheless, important differences exist between Eq. (10a) and these other simpler pressure-temperature relations. Thus, while the Poisson formula and the SB radiation law can mathematically be derived from 'first principles' and experimentally tested in a laboratory, Eq. (10a) could neither be analytically deduced from known physical laws nor accurately simulated in a small-scale experiment. This is because Eq. (10a) describes an emergent macro-level property of planetary atmospheres representing the net result of myriad process interactions within real climate systems that are not readily computable using mechanistic (bottom-up) approaches adopted in climate models or fully reproducible in a laboratory setting.

Potential limitations of the planetary temperature model

Equation (10b) describes long-term (30-year) equilibrium GMATs of planetary bodies and does not predict inter-annual global temperature variations caused by intrinsic fluctuations of cloud albedo and/or ocean heat uptake. Thus, the observed 0.82 K rise of Earth's global temperature since 1880 is not captured by our model, as this warming was likely

not the result of an increased atmospheric pressure. Recent analyses of observed dimming and brightening periods worldwide [97-99] suggest that the warming over the past 130 years might have been caused by a decrease in global cloud cover and a subsequent increased absorption of solar radiation by the surface. Similarly, the mega shift of Earth's climate from a 'hothouse' to an 'icehouse' evident in the sedimentary archives over the past 51 My cannot be explained by Eq. (10b) unless caused by a large loss of atmospheric mass and a corresponding significant drop in surface air pressure since the early Eocene. Pleistocene fluctuations of global temperature in the order of 3.0–8.0 K during the last 2 My revealed by multiple proxies [100] are also not predictable by Eq. (10b) if due to factors other than changes in total atmospheric pressure and/or TOA solar irradiance.

The current prevailing view mostly based on theoretical considerations and results from climate models is that the Pleistocene glacial-interglacial cycles have been caused by a combination of three forcing agents: Milankovitch orbital variations, changes in atmospheric concentrations of greenhouse gases, and a hypothesized positive ice-albedo feedback [101,102]. However, recent studies have shown that orbital forcing and the ice-albedo feedback cannot explain key features of the glacial-interglacial oscillations such as the observed magnitudes of global temperature changes, the skewness of temperature response (i.e. slow glaciations followed by rapid meltdowns), and the mid-Pleistocene transition from a 41 Ky to 100 Ky cycle length [103-105]. The only significant forcing remaining in the present paleo-climatological toolbox to explicate the Pleistocene cycles are variations in greenhouse-gas concentrations. Hence, it is difficult to explain, from a standpoint of the current climate theory, the high accuracy of Eq. (11) describing the relative thermal effect of diverse planetary atmospheres without any consideration of greenhouse gases. If presumed forcing agents such as greenhouse-gas concentrations and the planetary albedo were ind ed responsible for the observed past temperature dynamics on Earth, why did these agents not show up as predictors of contemporary planetary temperatures in our analysis as well? Could it be because the e agents have not really been driving Earth's climate on geological time scales? We address the potential role of greenhouse gases in more d tails below. Since the relationship portrayed in Figure 4 is undoubtedly real, our model results point toward the need to reexamine some fundamental climate processes thought to be well understood for decades. For example, we are currently testing a hypo hesi that Pleistocene glacial cycles might have been caused by variations in Earth's total atmospheric mass and surface air pressure. Preliminary results based on the ability of an extended version of our planetary model (simulating meridional temperature gradients) to predict the observed polar amplification during the Last Glacial Maximum indicate that such a hypothesis is not unreasonable. However conclusive findings from this research will be discussed elsewhere.

According to the present understanding, Earth's atmospheric pressure has remained nearly invariant during the Cenozoic era (last 65.5 My). However, this notion is primarily based on theoretical analyses [106], since there are currently no known geo-chemical proxies permitting a reliable reconstruction of past pressure changes in a manner similar to that provided by various temperature proxies such as isotopic oxygen 18, alkenones and TEX_{86} in sediments, and Ar-N isotope ratios and deuterium concentrations in ice. The lack of independent pressure proxies makes the assumption of a constant atmospheric mass throughout the Cenozoic *a priori* and thus questionable. Although this topic is beyond the scope of our present study, allowing for the possibility that atmospheric pressure on Earth might have varied significantly over the past 65.5 My could open exciting new research venues in Earth sciences in general and paleoclimatology in particular.

Role of greenhouse gasses from a perspective of the new model

Our analysis revealed a poor relationship between GMAT and the amount of greenhouse gases in planetary atmospheres across a broad range of environments in the Solar System (Figures 1-3 and Table 5). This is a surprising result from the standpoint of the current Greenhouse theory, which assumes that an atmosphere warms the surface of a planet (or moon) via trapping of radiant heat by certain gases controlling the atmospheric infrared optical depth [4,9,10]. The atmospheric opacity to LW radiation depends on air density and gas absorptivity, which in turn are functions of total pressure, temperature and greenhouse-gas concentrations [9]. Pressure also controls the broadening of infrared absorption lines in individual gases. Therefore, the higher the pressure, the larger the infrared optical depth of an atmosphere, and the stronger the expected greenhouse effect would be. According to the current climate theory, pressure only indirectly affects global surface temperature through the atmospheric infrared opacity and its presumed constraint on the planet's LW emission to Space [9,107].

There are four plausible explanations for the apparent lack of a close relationship between GMAT and atmospheric greenhouse gasses in ur results: 1) The amounts of greenhouse gases considered in our analysis only refer to near-surface atmospheric compositions and do not de cribe the infrared optical depth of the entire atmospheric column; 2) The analysis lumped all greenhouse gases together and did not take into account differences in the infrared spectral absorptivity of individual gasses; 3) The effect of atmospheric pressure on broadening the infrared gas absorption lines might be stronger in reality than simulated by current radiative-transfer models, so that total pressure overrides the effect of a varying atmospheric composition across a wide range of planetary environments; and 4) Pressure as a force per unit area directly impacts the internal kinetic energy and temperature of a system in accordance with thermodynamic principles inferred from the Gas Law; hence, air pressure might be the actual physical causative factor controlling a planet's surface temperature rather than the atmospheric infrared optical depth, which merely correlates with temperature due to its co-dependence on pressure.

Based on evidence discussed earlier, we argue that option #4 is the most likely reason for the poor predictive skill of greenhouse gases with respect to planetary GMATs revealed in our study (Figures 1-3). By definition, the infrared optical depth of an atmosphere is a dimensionless quantity that carries no units of force or energy [3,4,9]. Therefore, it is difficult to fathom from a fundamental physics standpoint of view, how this non-dimensional parameter could increase the kinetic energy (and temperature) of the lower troposphere in the presence of free convection provided that the latter dominates the heat transport in gaseous systems. Pressure, on the other hand, has a dimension of force per unit area and as such is intimately related to the internal kinetic energy of an atmosphere E (J) defined as the product of gas pressure (P, Pa) and gas volume (V, m^3), i.e. E (J) = PV. Hence, the direct effect of pressure on a system's internal energy and temperature follows straight from fundamental parameter definitions in classical thermodynamics. Generally speaking, kinetic energy cannot exist without a pressure force. Even electromagnetic radiation has pressure.

In climate models, the effect of infrared optical depth on surface temperature is simulated by mathematically decoupling radiative transfer from convective heat exchange. Specifically, the LW

radiative transfer is calculated in these models without simultaneous consideration of sensible- and latent heat fluxes in the solution matrix. Radiative transfer modules compute the so-called heating rates (K/day) strictly as a function of atmospheric infrared opacity, which under constant-pressure conditions solely depends on greenhouse-gas concentrations. These heating rates are subsequently added to the thermodynamic portion of climate models and distributed throughout the atmosphere. In this manner, the surface warming becomes a function of an increasing atmospheric infrared opacity. This approach to modeling of radiative-convective energy transport rests on the principle of superposition, which is only applicable to linear systems, where the overall solution can be obtained as a sum of the solutions to individual system components. However, the integral heat transport within a free atmosphere is inherently nonlinear with respect to temperature. This is because, in the energy balance equation, radiant heat transfer is contingent upon power gradients of absolute temperatures, while convective cooling/heating depends on linear temperature differences in the case of sensible heat flux and on simple vapor pressure gradients in the case of latent heat flux [4]. The latent heat transport is in turn a function of a solvent's saturation vapor pressure, which increases exponentially with temperature [3]. Thus, the superposition principle cannot be employed in energy budget calculations. The artificial decoupling between radiative and convective heat-transfer processes adopted in climate models leads to mathematically and physically incorrect solutions with respect to surface temperature. The LW radiative transfer in a real climate system is intimately intertwined with turbulent convection/advection as both transport mechanisms occur simultaneously. Since convection (and especially the moist one) is orders of magnitude more efficient in transferring energy than LW radiation [3,4], and because heat preferentially travels along the path of least resistance, a properly coupled radiative-convective algorithm of energy exchange will produce quantitatively and qualitatively different temperature solutions in response to a changing atmospheric composition than the ones obtained by current climate models. Specifically, a correctly coupled convective-radiative system will render the surface temperature insensitive to variations in the atmospheric infrared optical depth, a result indirectly supported by our analysis as well. This topic requires further investigation beyond the scope of the present study.

The direct effect of atmospheric pressure on the global surface temperature has received virtually no attention in climate science thus far. However, the results from our empirical data analysis suggest that it deserves a serious consideration in the future.

Theoretical implications of the new interplanetary relationship

The hereto discovered pressure-temperature relationship quantified by Eq. (10a) and depicted in Figure 4 has broad theoretical implications that can be summarized as follows:

Physical nature of the atmospheric 'greenhouse effect': According to Eq. (10b), the heating mechanism of planetary atmospheres is analogous to a gravity-controlled adiabatic compression acting upon the entire surface. This means that the atmosphere does not function as an insulator reducing the rate of planet's infrared cooling to space as presently assumed [9,10], but instead adiabatically boosts the kinetic energy of the lower troposphere beyond the level of solar input through gas compression. Hence, the physical nature of the atmospheric 'greenhouse effect' is a pressure-induced thermal enhancement (PTE) independent of atmospheric composition. This mechanism is fundamentally different from the hypothesized 'trapping' of LW radiation by atmospheric trace gases first proposed in the 19th century and presently forming the core of the Greenhouse climate theory. However, a radiant-heat trapping by freely convective gases has never been demonstrated experimentally. We should point out that the hereto deduced adiabatic (pressure-controlled) nature of the atmospheric thermal effect rests on an objective analysis of vetted planetary observations from across the Solar System and is backed by proven thermodynamic principles, while the 'trapping' of LW radiation by an unconstrained atmosphere surmised by Fourier, Tyndall and Arrhenius in the 1800s was based on a theoretical conjecture. The latter has later been coded into algorithms that describe the surface temperature as a function of atmospheric infrared optical depth (instead of pressure) by artificially decoupling radiative transfer from convective heat exchange. Note also that the Ideal Gas Law ($PV = nRT$) forming the basis of atmospheric physics is indifferent to the gas chemical composition.

Effect of pressure on temperature: Atmospheric pressure provides in and of itself only a relative thermal enhancement (RATE) to the surface quantified by Eq. (11). The absolute thermal effect of an atmosphere depends on both pressure and the TOA solar irradiance. For example, at a total air pressure of 98.55 kPa, Earth's RATE is 1.459, which keeps our planet 90.4 K warmer in its present orbit than it would be in the absence of an atmosphere. Hence, our model fully explains the new ~90 K estimate of Earth's atmospheric thermal effect derived by Volokin and ReLlez [1] using a different line of reasoning. If one moves Earth to the orbit of Titan (located at ~9.6 AU from the Sun) without changing the overall pressure, our planet's RATE will remain the same, but the absolute thermal effect of the atmosphere would drop to about 29.2 K due to a vastly reduced solar flux. In other words, the absolute effect of pressure on a system's temperature depends on the background energy level of the environment. This implies that the absolute temperature of a gas may not follow variations of pressure if the gas energy absorption changes in opposite direction to that of pressure. For instance, the temperature of Earth's stratosphere increases with altitude above the tropopause despite a falling air pressure, because the absorption of UV radiation by ozone steeply increases with height, thus offsetting the effect of a dropping pressure. If the UV absorption were constant throughout the stratosphere, the air temperature would decrease with altitude.

Atmospheric back radiation and surface temperature: Since (according to Eq. 10b) the equilibrium GMAT of a planet is mainly determined by the TOA solar irradiance and surface atmospheric pressure, the down-welling LW radiation appears to be globally a product of the air temperature rather than a driver of the surface warming. In other words, on a planetary scale, the so-called back radiation is a consequence of the atmospheric thermal effect rather than a cause for it. This explains the broad variation in the size of the observed down-welling LW flux among celestial bodies irrespective of the amount of absorbed solar radiation. Therefore, a change in this thermal flux brought about by a shift in atmospheric LW emissivity cannot be expected to impact the global surface temperature. Any variation in the global infrared back radiation caused by a change in atmospheric composition would be compensated for by a corresponding shift in the intensity of the vertical convective heat transport. Such a balance between changes in atmospheric infrared heating and the upward convective cooling at the surface is required by the First Law of Thermodynamics. However, current climate models do not simulate this compensatory effect of sensible and latent heat fluxes due to an improper decoupling between radiative transfer and turbulent convection in the computation of total energy exchange.

Role of planetary albedos: The fact that Eq. (10b) accurately describes planetary GMATs without explicitly accounting for the observed broad range of albedos, i.e. from 0.136 to 0.9 (Table 2), indicates that the shortwave reflectivity of planetary atmospheres is mostly an intrinsic property (a byproduct) of the climate system itself rather than an independent driver of climate as currently believed. In other words, it is the internal energy of the atmosphere maintained by solar irradiance and air pressure that controls the bulk of the albedo. An indirect support for this unorthodox conclusion is provided by the observation that the amounts of absorbed shortwave radiation determined by albedos show no physically meaningful relationship with planetary GMATs. For example, data in Table 2 indicate that Venus absorbs 3.7 times less solar energy per unit area than Earth, yet its surface is about 450 K hotter than that of Earth; the Moon receives on average 54 W m^{-2} more net solar radiation than Earth, but it is about 90 K cooler on average than our planet. The hereto proposed passive nature of planetary albedos does not imply that the global cloud cover could not be influenced by an external forcing such as solar wind, galactic cosmic rays, and/or gravitational fields of other celestial objects. Empirical evidence strongly suggests that it can [108-113], but the magnitude of such influences is expected to be small compared to the total albedo due to the presence of stabilizing negative feedbacks within the system. We also anticipate that the sensitivity of GMATs to an albedo change will greatly vary among planetary bodies. Viewing the atmospheric reflectivity as a byproduct of the available internal energy rather than a driver of climate can also help explain the observed remarkable stability of Earth's albedo [54,114].

Climate stability: Our semi-empirical model (Equations 4a, 10b and 11) suggests that, as long as the mean annual TOA solar flux and the total atmospheric mass of a planet are stationary, the equilibrium GMAT will remain stable. Inter-annual and decadal variations of global temperature forced by fluctuations of cloud cover, for example, are expected to be small compared to the magnitude of the background atmospheric warming because of strong negative feedbacks limiting the albedo changes. This implies a relatively stable climate for a planet such as Earth absent significant shifts in the total atmospheric mass and the planet's orbital distance to the Sun. Hence, planetary climates appear to be free of tipping points, i.e. functional states fostering rapid and irreversible changes in the global temperature as a result of hypothesized positive feedbacks thought to operate within the system. In other words, our results suggest that the Earth's climate is well buffered against sudden changes.

Effect of oceans and water vapor on global temperature: The new model shows that the Earth's global equilibrium temperature is a part of a cosmic thermodynamic continuum controlled by atmospheric pressure and total solar irradiance. Since our planet is the only one among studied celestial bodies harboring a large quantity of liquid water on the surface, Eq. (10b) implies that the oceans play virtually no role in determining Earth's GMAT. This finding may sound inexplicable from the standpoint of the radiative Greenhouse theory, but it follows logically from the new paradigm of a pressure-induced atmospheric warming. The presence of liquid water on the surface of a planet requires an air pressure greater than 612 Pa and an ambient temperature above 273.2 K. These conditions are provided by the planet's size and gravity, its distance to the Sun, and the mass of the atmosphere. Hence, the water oceans on Earth seem to be a thermodynamic consequence of particular physical conditions set by cosmic arrangements rather than an active controller of the global climate. Similarly, the hydrocarbon lakes on the surface of Titan [115,116] are the result of a high atmospheric pressure and an extremely cold environment found on that moon. Thus, our analysis did not reveal evidence for the existence of a feedback between planetary GMAT and a precipitable liquid solvent on the surface as predicted by the current climate theory. Consequently, the hypothesized *runaway greenhouse*, which requires a net positive feedback between global surface temperature and the atmospheric LW opacity controlled by water vapor [117], appears to be a model artifact rather than an actual physical possibility. Indeed, as illustrated in Figure 4, the hot temperature of Venus often cited as a product of a 'runaway greenhouse' scenario [117,118] fits perfectly within the pressure-dependent climate continuum described by Equations (10b) and (11).

Model Application and Validation

Encouraged by the high predictive skill and broad scope of validity of Model 12 (Figure 2f) we decided to apply Eq. (10b) to four celestial bodies spanning the breadth of the Solar System, i.e. Mercury, Europa, Callisto and Pluto which global surface temperatures are not currently known with certainty. Each body is the target of either ongoing or planned robotic exploration missions scheduled to provide surface thermal data among other observations, thus offering an opportunity to validate our planetary temperature model against independent measurements.

The MESSENGER spacecraft launched in 2004 completed the first comprehensive mapping of Mercury in March 2013 (http://messenger.jhuapl.edu/). Among other things, the spacecraft also took infrared measurements of the planet's surface using a special spectrometer [119] that should soon become available. The New Horizons spacecraft launched in January 2006 [120] reached Pluto in July of 2015 and performed a thermal scan of the dwarf planet during a flyby. The complete dataset from this flyby were received on Earth in October of 2016 and are currently being analyzed. A proposed joint Europa-Jupiter System Mission by NASA and the European Space Agency is planned to study the Jovian moons after year 2020. It envisions exploring Europa's physical and thermal environments both remotely via a NASA Orbiter and *in situ* by a Europa Lander [121].

All four celestial bodies have somewhat eccentric orbits around the Sun. However, while Mercury's orbital period is only 88 Earth days, Europa and Callisto circumnavigate the Sun once every 11.9 Earth years while Pluto takes 248 Earth years. The atmospheric pressure on Pluto is believed to vary between 1.0 and 4.0 Pa over the course of its orbital period as a function of insolation-driven sublimation of nitrogen and methane ices on the surface [122]. Each body's temperature was evaluated at three orbital distances from the Sun: aphelion, perihelion, and the semi-major axis. Since Mercury, Europa and Callisto harbor tenuous atmospheres ($P << 10^{-2}$ Pa), the reference temperature T_{na} in Eq. (10b) must be calculated from Eq. (4a), which requires knowledge of the actual values of α_e, η_e, and R_g. We assumed that Mercury had R_g = 0.0 W m^{-2}, α_e = 0.068 [123] and Moon-like thermo-physical properties of the regolith (η_e = 0.00971). Input data for Europa and Callisto were obtained from Spencer et al. [124] and Moore et al. [125], respectively. Specifically, in order to calculate η_e and R_g for these moons we utilized equatorial temperature data provided by Spencer et al. [124] in their Figure 1, and by Moore et al. [125] in their Fig. 17.7 along with a theoretical formula for computing the average nighttime surface temperature T at the equator based on the SB law, i.e.

$$T = \left[\frac{S(1-\alpha)\eta_e + R_g}{0.98\sigma}\right]^{0.25} \quad (15)$$

where $S(1-\alpha)\eta_e$ is the absorbed solar flux (W m^{-2}) stored as heat into the subsurface. The geothermal heat flux on Europa is poorly known. However, based on thermal observations of Io reported by Veeder et al. [126], we assumed R_g = 2.0 W m^{-2} for Europa. Using S = 50.3 W m^{-2}, an observed nighttime equatorial temperature T = 90.9 K and an observed average night-side albedo α = 0.58 [124], we solved Eq. (15) for the surface heat storage fraction to obtain η_e = 0.085 for Europa. A similar computational procedure was employed for Callisto using α = 0.11 and equatorial surface temperature data from Fig. 17.7 in Moore et al. [125]. This produced R_g = 0.5 W m^{-2} and η_e = 0.057. Using these values in Eq. (15) correctly reproduced Callisto's nighttime equatorial surface temperature of ≈ 86.0 K. The much higher η_e estimates for Europa and Callisto compared to η_e = 0.00971 for the Moon can be explained with the large water-ice content on the surface of these Galilean moons. Europa is almost completely covered by a thick layer of water ice, which has a much higher thermal conductivity than the dry regolith. Also, sunlight penetrates deeper into ice than it does into powdered regolith. All this enables a much larger fraction of the absorbed solar radiation to be stored into the subsurface as heat and later released at night boosting the nighttime surface temperatures of these moons. Volokin and ReLlez [1] showed that GMAT of airless bodies is highly sensitive to η_e.

Table 6 lists the average global surface temperatures of the four celestial bodies predicted by Eq. (10b) along with the employed input data. According to our model, Mercury is about 117 K cooler on average than NASA's current estimate of 440 K [32], which is based on Eq. (3) and does not represent a spherically averaged surface temperature [1]. Our prediction of Europa's GMAT, 99.4 K, agrees well with the ≈ 100 K estimate reported for this moon by Sotin et al. [127]. Our estimate of Pluto's average surface temperature at perihelion (38.6 K) is similar to the mean temperature computed for that dwarf planet by Olkin et al. [124] using a mechanistic model of nitrogen ice volatilization at the surface. Stern et al. [128] and Gladstone et al. [93] reported initial results from flyby observations of Pluto taken by the Radio Experiment (REX) instrument aboard the New Horizons spacecraft in July 2015, when the dwarf planet was approximately at 32.9 AU from the Sun. Using the observed surface pressure of 1.05 ± 0.1 Pa (10.5 ± 1 μbar) [93] our model predicts an average global temperature of 36.7 K for Pluto. Stern et al. [128] reported a near-surface temperature of ≈ 38 K. However, this value was calculated from pre-flyby global brightness measurements rather than derived via spherical integration of spatially resolved surface temperatures (Stern, personal communication). Since global brightness temperatures tend to be higher than spherically averaged kinetic surface temperatures [1], our model prediction may well be within the uncertainty of Pluto's true global temperature. We will know more about this in 2017 when spatially resolved thermal measurements obtained by New Horizons become available.

One should use caution when comparing results from Eq. (10b) to remotely sensed 'average temperatures' commonly quoted for celestial bodies with tenuous atmospheres such as the moons of Jupiter and Neptune. Studies oftentimes report the so-called 'brightness temperatures' retrieved at specific wavelengths that have not been subjected to a proper spherical integration. As pointed out by Volokin and ReLlez [1], due to Hölder's inequality between integrals, calculated brightness temperatures of spherical objects can be significantly higher than actual mean kinetic temperatures of the surface. Since Eq. (10b) yields spherically averaged temperatures, its predictions for airless bodies are expected to be lower than the disk integrated brightness temperatures typically quoted in the literature.

Conclusion

For 190 years the atmosphere has been thought to warm Earth by absorbing a portion of the outgoing LW infrared radiation and reemitting it back toward the surface, thus augmenting the incident solar flux. This conceptualized continuous absorption and downward reemission of thermal radiation enabled by certain trace gases known to be transparent to solar rays while opaque to electromagnetic long wavelengths has been likened to the trapping of heat by glass greenhouses, hence the term 'atmospheric greenhouse effect'. Of course, we now know that real greenhouses preserve warmth not by trapping infrared radiation but by physically obstructing the convective heat exchange between a greenhouse interior and the exterior environment. Nevertheless, the term 'greenhouse effect' stuck in science.

The hypothesis that a freely convective atmosphere could retain (trap) radiant heat due its opacity has remained undisputed since its introduction in the early 1800s even though it was based on a theoretical conjecture that has never been proven experimentally. It is important to note in this regard that the well-documented enhanced absorption of thermal radiation by certain gases does not imply an ability of such gases to trap heat in an open atmospheric environment. This is because, in gaseous systems, heat is primarily transferred (dissipated) by convection (i.e. through fluid motion) rather than radiative exchange. If gases of high LW absorptivity/emissivity such as CO_2, methane and water vapor were indeed capable of trapping radiant heat, they could be used as insulators. However, practical experience has taught us that thermal radiation losses can only be reduced by using materials of very low LW

	Surface Atmospheric Pressure (Pa)	α_e (fraction) η_e (fraction) R_g (W m^2)	Predicted Average Global Surface Temperature at Specific Orbital Distances from the Su		
			Aphelion	Semi-major Axis	Perihelion
Mercury	5 × 10^{-10}	α_e = 0.068 η_e = 0.00971 R_g = 0.0	296.8 K (0.459 AU)	323.3 K (0.387 AU)	359.5 K (0.313 AU)
Europa	10^{-7}	α_e = 0.62 η_e = 0.085 R_g = 2.0	98.1 K (5.455 AU)	99.4 K (5.203 AU)	100.7 K (4.951 AU)
Callisto	7.5 × 10^{-7}	α_e = 0.11 η_e = 0.057 R_g = 0.5	101.2 K (5.455 AU)	103.2 K (5.203 AU)	105.4 K (4.951 AU)
Pluto	1.05	α_e = 0.132 η_e = 0.00971 R_g = 0.0	30.0 K (49.310 AU)	33.5 K (39.482 AU)	38.6 K (29.667 AU)

Table 6: Average global surface temperatures predicted by Eq. (10b) for Mercury, Europa, Calisto and Pluto. Input data on orbital distances (AU) and total atmospheric pressure (Pa) were obtained from the NASA Solar System Exploration [48] website, the NASA Planetary Factsheet [32] and Gladstone et al. [93]. Solar irradiances required by Eq. (10b) were calculated from reported orbital distances as explained in the text. Values of α_e, η_e and R_g for Europa and Callisto were estimated from observed data by Spencer et al. [124] and Moore et al. [125] respectively (see text for details).

absorptivity/emissivity and correspondingly high thermal reflectivity such as aluminum foil. These materials are known among engineers at NASA and in the construction industry as *radiant barriers* [129]. It is also known that high-emissivity materials promote radiative cooling. Yet, all climate models proposed since 1800s are built on the premise that the atmosphere warms Earth by limiting radiant heat losses of the surface through the action of infrared absorbing gases aloft.

If a trapping of radiant heat occurred in Earth's atmosphere, the same mechanism should also be expected to operate in the atmospheres of other planetary bodies. Thus, the Greenhouse concept should be able to mathematically describe the observed variation of average planetary surface temperatures across the Solar System as a continuous function of the atmospheric infrared optical depth and solar insolation. However, to our knowledge, such a continuous description (model) does not exist. Furthermore, measured magnitudes of the global down-welling LW flux on planets with thick atmospheres such as Earth and Venus indicate that the lower troposphere of these bodies contains internal kinetic energy far exceeding the solar input [6,12,14]. This fact cannot be explained via re-radiation of absorbed outgoing thermal emissions by gases known to supply no additional energy to the system. The desire to explicate the sizable energy surplus evident in the tropospheres of some terrestrial planets provided the main impetus for this research.

We combined high-quality planetary data from the last three decades with the classical method of dimensional analysis to search for an empirical model that might accurately and meaningfully describe the observed variation of global surface temperatures throughout the Solar System while also providing a new perspective on the nature of he atmospheric thermal effect. Our analysis revealed that the equilibrium global surface temperatures of rocky planets with tangible a mospheres and a negligible geothermal surface heating can reli bly be estimated across a wide range of atmospheric compositions and radiative regimes using only two forcing variables: TOA solar irradiance and total surf ce atmospheric pressure (Eq. 10b with T_{na} computed from Eq. 4c). Furthermore, the relative atmospheric thermal enhancement (RATE) defined as a ratio of the planet's actual global surface temperature to the temperature it would have had in the ab ence of a mosphere is fully explicable by the surface air pressure lone (Eq. 10a and Figure 4). At the same time, greenhouse-gas oncentrations and/or partial pressures did not show any meaningful relationship to surface temperatures across a broad span of plan tary environments considered in our study (see Figures 1 and 2 and Table 5).

Based on statistical criter a including numerical accuracy, robustness, dimensional homogeneity and a broad environmental scope of validity, the new relationship (Figure 4) quantified by Eq. (10a) appears to describe an emergent macro-level thermodynamic property of planetary atmospheres heretofore unbeknown to science. The physical significance of this empirical model is further supported by its striking qualitative resemblance to the dry adiabatic temperature curve described by the Poisson formula (Eq. 13) and to the photon-pressure form of the SB radiation law (Eq. 14). Similar to these well-known kinetic relations, Eq. (10a) also predicts the direct effect of pressure on temperature albeit in the context of a different macro-physical system. To our knowledge, this is the first model accurately describing the average surface temperatures of planetary bodies throughout the Solar System in the context of a thermodynamic continuum using a common set of drivers.

The planetary temperature model consisting of Equations (4a), (10b), and (11) has several fundamental theoretical implications, i.e.

- The 'greenhouse effect' is not a radiative phenomenon driven by the atmospheric infrared optical depth as presently believed, but a pressure-induced thermal enhancement analogous to adiabatic heating and independent of atmospheric composition;
- The down-welling LW radiation is not a global driver of surface warming as hypothesized for over 100 years but a product of the near-surface air temperature controlled by solar heating and atmospheric pressure;
- The albedo of planetary bodies with tangible atmospheres is not an independent driver of climate but an intrinsic property (a byproduct) of the climate system itself. This does not mean that the cloud albedo cannot be influenced by external forcing such as solar wind or galactic cosmic rays. However, the magnitude of such influences s expected to be small due to the stabilizing effect of negative feedbacks operating within the system. This understanding explains the observed remarkable stability of planetary albedos;
- The equilibrium surface temperature of a planet is bound to remain stable (i.e. within ± 1 K) as long as the atmospheric mass and the TOA mean solar irradiance are stationary. Hence, Earth's climate system is well buffered against sudden changes and has n tipping points;

  The proposed net positive feedback between surface temperature and the atmospheric infrared opacity controlled by water vapor appears to be a model artifact resulting from a mathematical decoupling of the radiative-convective heat transfer rather than a physical reality.

The hereto reported findings point toward the need for a paradigm shift in our understanding of key macro-scale atmospheric properties and processes. The implications of the discovered planetary thermodynamic relationship (Figure 4, Eq. 10a) are fundamental in nature and require careful consideration by future research. We ask the scientific community to keep an open mind and to view the results presented herein as a possible foundation of a new theoretical framework for future exploration of climates on Earth and other worlds.

Appendices

Appendix A. Construction of the Dimensionless π Variables

Table 1 lists 6 generic variables (T_s, T_r, S, P_x, P_r and ρ_x) composed of 4 fundamental dimensions: mass [M], length [L], time [T], and absolute temperature [Θ]. According to the Buckingham Pi theorem [27], this implies the existence of two dimensionless π_i products per set. To derive the π_i variables we employed the following objective approach. First, we hypothesized that a planet's GMAT (T_s) is a function of all 5 independent variables listed in Table 1, i.e.

$$T_s = f\left(T_r, S, P_x, P_r, \rho_x\right) \tag{A.1}$$

This unknown function is described to a first approximation as a simple product of the driving variables raised to various powers, i.e.

$$T_s \approx T_r^a S^b P_x^c P_r^d \rho_x^e \tag{A.2}$$

where a, b, c, d and e are rational numbers. In order to determine the power coefficients, Eq. (A.2) is cast in terms of physical dimensions of the participating variables, i.e.

$$[\Theta] \approx [\Theta]^a \left[\mathrm{M\,T^{-3}}\right]^b \left[\mathrm{M\,L^{-1}\,T^{-2}}\right]^c \left[\mathrm{M\,L^{-1}\,T^{-2}}\right]^d \left[\mathrm{M\,L^{-3}}\right]^e \tag{A.3}$$

Satisfying the requirement for dimensional homogeneity of Eq.

(A.2) implies that the sum of powers of each fundamental dimension must be equal on both sides of Eq. (A.3). This allows us to write four simultaneous equations (one per fundamental dimension) containing five unknowns, i.e.

$$\begin{cases} a = 1 & :[\Theta] \\ b + c + d + e = 0 & :[M] \\ -c - d - 3e = 0 & :[L] \\ -3b - 2c - 2d = 0 & :[T] \end{cases} \quad \text{(A.4)}$$

System (A.4) is underdetermined and has the following solution: $a = 1$, $b = 2e$, and $c = -(3e + d)$. Note that, in the DA methodology, one oftentimes arrives at underdetermined systems of equations, simply because the number of independent variables usually exceeds the number of fundamental physical dimensions comprising such variables. However, this has no adverse effect on the derivation of the sought dimensionless π_i products.

Substituting the above roots in Eq. (A.2) reduces the original five unknowns to two: d and e, i.e.

$$T_s \approx T_r^1 \; S^{2e} \; P_x^{-(3e+d)} \; P_r^d \; \rho_x^e \quad \text{(A.5a)}$$

These solution powers may now be assigned arbitrary values, although integers such as 0, 1 and -1 are preferable, for they offer the simplest solution leading to the construction of proper π_i variables. Setting $d = 0$ and $e = -1$ reduces Eq. (A.5a) to

$$T_s \approx T_r^1 \, S^{-2} \, P_x^3 \, \rho_x^{-1} \quad \text{(A.5b)}$$

providing the first pair of dimensionless products:

$$\pi_1 = \frac{T_s}{T_r}; \qquad \pi_2 = \frac{P_x^3}{\rho_x S^2} \quad \text{(A.6)}$$

The second pair of π_i variables emerges upon setting $d = -1$ and $e = 0$ in Eq. (A.5a), i.e.

$$\pi_1 = \frac{T_s}{T_r}; \qquad \pi_2 = \frac{P_x}{P_r} \quad \text{(A.7)}$$

Thus, the original function (A.1) consisting of six dimensioned variables has been reduced to a relationship between two dimensionless quantities, i.e. $\pi_1 = f(\pi_2)$. This relationship must further be investigated through regression analysis

Appendix B. Estimation of Mars' GMAT and Surface Atmospheric Pressure

Although Mars is the third most studied planetary body in the Solar System after Earth and the Moon, there is currently no consensus among researchers regarding its mean global surface temperature (T_M). T_M values reported over the past 15 years span a range of 40 K. Examples of disparate GMATs quoted for the Red Planet include 200 K [79], 202 K [82,130], 210 K [32], 214 K [80], 215 K [6,81], 218 K [77], 220 K [76], 227 K [131] and 240 K [78]. The most frequently cited temperatures fall between 210 K and 220 K. However, a close examination of the available thermal observations reveals a high improbability for any of the above estimates to represent Mars' true GMAT.

Figure B.1 depicts hourly temperature series measured at 1.5 m aboveground by Viking Landers 1 and 2 (VL1 and VL2 respectively) in the late 1970s [60]. The VL1 record covers about half of a Martian year, while the VL2 series extends to nearly 1.6 years. The VL1 temperature series captures a summer-fall season on a site located at about 1,500 m below Datum elevation in the subtropics of Mars' Northern Hemisphere (22.5° N). The arithmetic average of the series is 207.3 K (Fig. B.1a). Since the record lacks data from the cooler winter-spring season, this value is likely higher than the actual mean annual temperature at that location. Furthermore, observations by the Hubble telescope from the mid-1990s indicated that the Red Planet may have cooled somewhat since the time of the Viking mission [132,133]. Because of a thin atmosphere and the absence of significant cloud cover and perceptible water, temperature fluctuations near the surface of Mars are tightly coupled to diurnal, seasonal and latitudinal variations in incident solar radiation. This causes sites located at the same latitude and equivalent altitudes to have similar annual temperature means irrespective of their longitudes [134]. Hence, one could reliably estimate a latitudinal temperature average on Mars using point observations from any elevation by applying an appropriate lapse-rate correction for the average terrain elevation of said latitude.

At 22.5° absolute latitude, the average elevation between Northern and Southern Hemisphere on Mars is close to Datum level, i.e. about 1,500 m above the VL1 site. Adjusting the observed 207.3 K temperature average at VL1 to Datum elevation using a typical near-surface Martian lapse rate of -4.3 K km^{-1} [78] produces ~201 K for the average summer-fall temperature at that latitude. Since the mean surface temperature

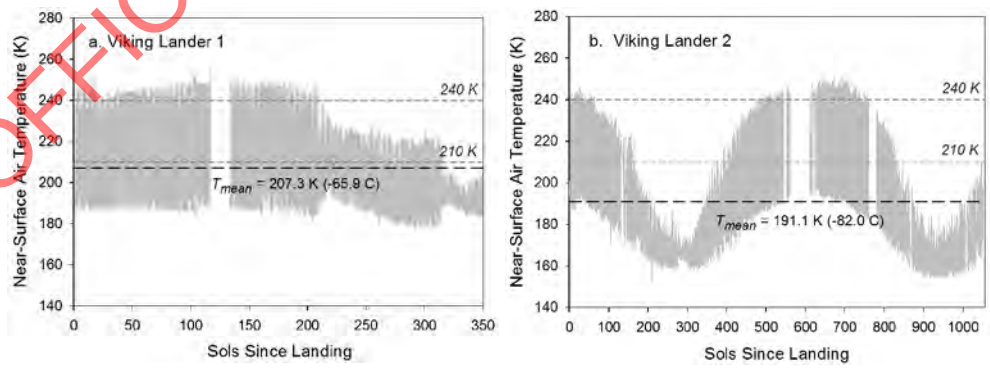

Figure B.1: Near-surface hourly temperatures measured on Mars by (*a*) Viking Lander 1 at Chryse Planitia (22.48° N, 49.97° W, Elevation: -1,500 m); and (*b*) Viking Lander 2 at Utopia Planitia (47.97° N, 225.74° W, Elevation: -3,000 m) (Kemppinen et al. [60]; data downloaded from: http://www-k12.atmos.washington.edu/k12/resources/mars_data-information/data.html). Black dashed lines mark the arithmetic average (T_{mean}) of each series. Grey dashed lines highlight the range of most frequently reported GMAT values for Mars, i.e. 210–240 K. The average diurnal temperature can only exceed 210 K during the summer; hence, all Martian latitudes outside the Equator must have mean annual temperatures significantl lower than 210 K.

of a sphere is typically lower than its subtropical temperature average, we can safely conclude based on Figure B.1a that Mars' GMAT is likely below 201 K. The mean temperature at the VL2 site located at ~48° N latitude and 3,000 m below Datum elevation is 191.1 K (Fig. B.1b). The average terrain elevation between Northern and Southern Hemisphere at 48° absolute latitude is about -1,500 m. Upon adjusting the VL2 annual temperature mean to -1,500 m altitude using a lapse rate of -4.3 K km^{-1} we obtain 184.6 K. Since a planet's GMAT numerically falls between the mean temperature of the Equator and that of 42° absolute latitude, the above calculations suggest that Mars' GMAT is likely between 184 K and 201 K.

A close examination of the Viking record also reveals that average diurnal temperatures above 210 K only occur on Mars during the summer season and, therefore, cannot possibly represent an annual mean for any Martian latitude outside the Equator. On the other hand, frequently reported values of Mars' GMAT in excess of 210 K appear to be based on the theoretical expectation that a planet's average surface temperature should exceed the corresponding effective radiating temperature produced by Eq. (3) [6,78], which is $T_e \approx 212$ K for Mars. This presumption is rooted in the a priori assumption that T_e represents a planet's average surface temperature in the absence of atmospheric greenhouse effect. However, Volokin and ReLlez [1] have shown that, due to Hölder's inequality between integrals, the mean physical temperature of a spherical body with a tenuous atmosphere is always lower than its effective radiating temperature computed from the globally integrated absorbed solar flux. In other words, Eq. (3) yield non-physical temperatures for spheres. Indeed, based on results from a 3-D climate model Haberle [130] concluded that Mars' mean global surface temperature is at least 8 K cooler than the planet's effective radiating temperature. Therefore, Mars' GMAT must be inferred from actual measurements rather than from theoretical calculations.

In order to obtain a reliable estimate of Mars' GMAT, we calculated the mean annual temperatures at several Martian latitudes employing near-surface time series measured *in-situ* by Viking Landers and the Curiosity Rover, and remotely by the Mars Global Surveyor (MGS) spacecraft. The Radio Science Team (RST) at Stanford University utilized radio occultation of MGS refra tion data to retrieve seasonal time-series of near-surface atmosph ric temperature and pressure on Mars [61,62,135]. We utilized MGS-RST data obtained between 1999 and 2005. Calculated mean temperatures from *in-situ* measurements were adjusted to corresponding average errain elevations of target latitudes using a lapse rate of -4.3 K km^{-1} [78]. Figure B.2 portrays the estimated Mean Annual n ar surface Temperatures (MAT) at five absolute Martian latitudes (gray dots) along with their standard errors (vertical bars). The equatorial MAT was calculated from Curiosity Rover observations; tempera ures at absolute latitudes 0.392 rad (22.48°) and 0.837 rad (47.97°) were derived from VL measurements, while these at latitudes 1.117 rad (64°) and 1.396 rad (80°) were estimated from MGS-RST data. The black curve represents a third-order polynomial fitted through the latitudinal temperature averages and described by the polynomial:

$$T(L) = 202.888 - 0.781801L - 22.3673L^2 - 3.16594L^3 \qquad (B.1)$$

with L being the absolute latitude (rad). MAT values predicted by Eq. (B.1) for Mars' Equatorial and Polar Regions agree well with independent near-surface temperatures remotely measured by the Mars Climate Sounder (MCS), a platform deployed after MGS in 2006 [136]. Shirley et al. [136] showed that, although separated in time by 2-5 years, MCS temperature profiles match quite well those retrieved by MGS-RST especially in the lower portion of the Martian atmosphere. Figures 2 and 3 of Shirley et al. [136] depict nighttime winter temperature profiles over the Mars' northern and southern Polar Regions, respectively at about 75° absolute latitude. The average winter surface temperature between the two Hemispheres for this latitude is about 148.5 K. This compares favorably with 156.4 K produced by Eq. (B.1) for 75° (1.309 rad) latitude considering that MAT values are expected to be higher than winter temperature averages. Figures 4 and 5 of Shirley et al. [136] portray average temperature profiles retrieved by MGS-RST and MCS over lowlands (165° – 180° E) and highlands (240° - 270° E) of the Mars' equatorial region (8° N - 8° S), respectively. For highlands (≈5 km above Datum), the near-surface temperature appears to be around 200 K, while for lowlands (≈2.5 km below Datum) it is ≈211 K. Since most of Mars' equatorial region lies above Datum, it is likely that Mars' equatorial MAT would be lower than 205.5 K and close to our independent estimate of ≈203 K based on Curiosity Rover measurements.

Mars' GMAT (T_M) was calculated via integration of polynomial (B.1) using the formula:

$$T_M = \int_0^{\pi/2} T(L)\cos L\, dL \qquad (B.2)$$

where $0 \le \cos L \le 1$ is a polar-coordinate area-weighting factor. The result is $T_M = 190.56 \pm 0.7$ K (Figure B.2). This estimate, while significantly lower than GMAT values quoted in recent publications, agrees quite well with spherically integrated brightness temperatures of Mars retrieved from remote microwave observations during the late 1960s and early 1970s [85-87]. Thus, according to Hobbs et al. [85] and Klein [86], the Martian mean global temperature (inferred from measurements at wavelengths between 1 and 21 cm) is 190 – 193 K. Our T_M estimate is also consistent with the new mean surface temperature of the Moon (197.35 K) derived by Volokin and ReLlez [1] using output from a validated NASA thermo-physical model [29]. Since Mars receives 57% less solar ittadiance than the Moon and has a thin atmosphere that only delivers a weak greenhouse effect [9], it makes a physical sense that the Red Planet would be on average cooler than our Moon (i.e. $T_M < 197.3$K). Moreover, if the average temperature

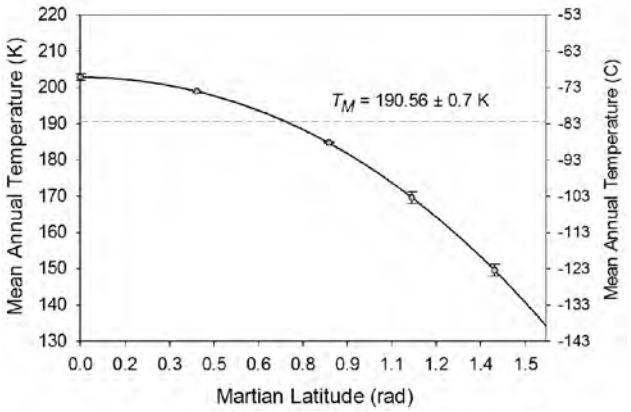

Figure B.2: Mean annual surface air temperatures at five Martian absolute latitudes (gray dots) es imated from data provided by Viking Landers, Curiosity Rover, and the Mars Global Surveyor Radio Science Team. Each dot represents a mean annual temperature corresponding to the average terrain elevation between Northern and Southern Hemisphere for particular latitude. The black curve depicts a third-order polynomial (Eq. B.1) fitted through the latitudinal temperature means using a non-linear regression. Mars' GMAT, T_M = 190.56 K (marked by a horizontal gray dashed line) was calculated via integration of polynomial (B.1) using formula (B.2).

of the lunar equator (Moon's warmest latitude) is 213 K as revealed by NASA Diviner observations [1,29], it is unlikely that Mars' mean global temperature would be equal to or higher than 213 K as assumed by many studies [6,76-78,80,131]

Published values of Mars' average surface atmospheric pressures range from 600 Pa to 700 Pa [6,32,78,80,83,84]. Since this interval was too broad for the target precision of our study, we employed MGS-RST data retrieved from multiple latitudes and seasons between 1999 and 2005 to calculate a new mean surface air pressure for the Red Planet. Our analysis produced $P = 685.4 \pm 14.2$ Pa, an estimate within the range of previously reported values.

Funding Sources

This research did not receive any specific grant from funding agencies in the public, commercial, or not-for-profit sectors

References

1. Volokin D, ReLlez L (2014) On the average temperature of airless spherical bodies and the magnitude of Earth's atmospheric thermal effect. Springer Plus 3: 723.
2. Hansen J, Johnson D, Lacis A, Lebedeff S, Lee P, et al. (1981) Climate impact of increasing atmospheric carbon dioxide. Science 213: 957-966.
3. Peixoto JP, Oort AH (1992) Physics of climate. Springer-Verlag, New York.
4. Wallace JM, Hobbs PV (2006) Atmospheric science: An Introductory survey, Academic Press, California.
5. Lacis AA, Schmidt GA, Rind D, Ruedy RA (2010) Atmospheric CO_2: Principal control knob governing Ear h's temperature. Science 330.
6. Lacis AA, Hansen JE, Russell GL, Oinas V, Jonas J (2013) The role of long lived greenhouse gases as principal LW control knob that governs the global surface temperature for past and future climate change. Tellus B 65: 19734.
7. Schmidt GA, Ruedy R, Miller RL, Lacis AA et al. (2010) The attribution of he present-day total greenhouse effect. J Geophys Res 115: D20106.
8. RamanathanV, Inamdar A (2006) The radiative forcing due to clouds and water vapor. Frontiers of Climate Modeling. Cambridge University Press, Cambridg , pp. 119-151.
9. Pierrehumbert R (2010) Principles of planeta y climate. Cambridge University Press, New York.
10. Pierrehumbert R (2011) Infrared radiat on and planetary temperature. Phys Today 64: 33-38.
11. Trenberth KE, Fasullo JT, Kiehl J (2009) Earth's global energy budget. B Am Meteorol Soc March: 311-323.
12. Stephens GL, Li1 J, Wild M, Clayson CA, Loeb N, et al. (2012) An update on Earth's energy balance in light of the latest global observations. Nat Geosci 5: 691–696.
13. Wild M, Folini D, Schär C, Loeb N, Dutton EG, et al. (2013) The global energy balance from a surface perspective. Clim Dyn 40: 3107–3134.
14. Wild M, Folini D, Hakuba MZ, Schar C, Seneviratne SI, et al. (2015) The energy balance over land and oceans: An assessment based on direct observations and CMIP5 climate models. Clim Dyn 44: 3393.
15. Bengtsson L, Bonnet R-M, Grinspoon D, Koumoutsaris D, Lebonnois S, et al. (2013) Towards understanding the climate of Venus: Applications of terrestrial models to our sister planet, ISSI scientifi report series, Springer.
16. Rashevsky N (1960) Mathematical biophysics: Physico-mathematical foundations of biology. Dover Publications, New York.
17. Albertson ML, Barton JR, Simons DB (1961) Fluid mechanics for engineers. Prentice Hall, New Jersey.
18. Yalin MS (1971) Theory of hydraulic models. MacMillan.
19. Taylor ES (1974) Dimensional analysis for engineers. Clarendon Press, Oxford.
20. Bender EA, (1978) An introduction to mathematical modeling. John Wiley and Sons, NY.
21. Vignaux GA, Jain S (1988) An approximate inventory model based on dimensional analysis. Asia-Pacifi Journal of Operational Research 5: 117-123.
22. Huntley HE (1967) Dimensional analysis. Dover Publications, New York.
23. Vignaux GA (1991) Dimensional analysis in data modeling. In: Smith CR, Erickson G, Neudorfer PO (eds) Maximum entropy and Bayesian methods. Kluwer Academic Publishers, Seattle, pp 121-126
24. Vignaux GA, Scott JL (1999) Theory and methods: Simplifying regression models using dimensional analysis. Aust N Z J Stat 41: 31–42.
25. Van Der Ha JC, Lappas VJ (2007) Long-term attitude drift of spinning spacecraft under solar radiation torques. Journal of Guidance, Control and Dynamics 30: 1470-1479.
26. McMahon J, Scheeres D (2010) A new navigation force model for solar radiation pressure. Journal of Guidance, Control and Dynamics 33: 1418-1428.
27. Buckingham E (1914) On physically similar systems: Illustrations of the use of dimensional equations. Phys Rev 4: 345-376.
28. Taylor FW (2010a) Planeta y a mospheres. Oxford University Press, USA.
29. Vasavada AR, Bandfiel JL, Greenhagen BT, Hayne PO, Siegler MA, et al. (2012) Lunar equa orial surface temperatures and regolith properties from the diviner lunar radiometer experiment. J Geophy Res 117: E00H18.
30. Blanco VM, McCuskey SW (961) Basic physics of the solar system. Addison-Wesley, R ading MA.
31. Mölle F (1964) Optics of he lower atmosphere. Appl Optics 3: 157-166.
32. Will ams DR (2015) NASA Planetary Factsheet. NASA online.
33. Beckenbach EF, Bellman R (1983) Inequalities. Springer Verlag, Berlin.
34. Rubincam DP (2004) Black body temperature, orbital elements, the Milankovitch precession index and the Sever smith psychroterms. Theor Appl Climatol 79: 111–131.
35. Fix en DJ (2009) The temperature of the cosmic microwave background. Ap J 707: 916.
36. Paige DA, Foote MC, Greenhagen BT, Schofiel JT, Calcutt S, et al. (2010) The lunar reconnaissance orbiter diviner lunar radiometer experiment. Space Sci Rev 150: 125–160.
37. Leconte J, Forget F, Charnay B, Wordsworth R, Selsis F, et al. (2013) 3D climate modeling of close-in land planets: circulation patterns, climate moist bistability and habitability. Astron Astrophys 554, A69.
38. Cengel YA, Turner RH (2004) Fundamentals of thermal-flui sciences. McGraw-Hill, Boston.
39. Steel RGD, Torrie J H (1960) Principles and procedures of statistics with special reference to the biological sciences. McGraw Hill.
40. Zwillinger D (2003) Standard mathematical tables and formulae. Chapman & Hall/CRC, p: 912.
41. Atreya SK, Lorenz RD, Waite JH (2009) Volatile origin and cycles: Nitrogen and methane. In: Brown RH, Lebreton JP, Waite JH (eds) Titan from Cassini-Huygens. Springer, New York, pp: 177–200
42. Jennings DE, Flasar FM, Kunde VG, Samuelson RE, Pearl JC, et al. (2009) Titan's surface brightness temperatures. Astrophys J 691: L103–L105.
43. Cottini V, Nixona CA, Jennings DE, et al. (2012) Spatial and temporal variations in Titan's surface temperatures from Cassini CIRS observations. Planetary Space Sci 60: 62–71.
44. Fegley B, Zolotov MY, Lodders K (1997) The oxidation state of the lower atmosphere and surface of Venus. Icarus 125: 416-439.
45. Basilevsky AT, Head JW (2003) The surface of Venus. Rep Prog Phys 66: 1699–1734.
46. Mallama A, Wang D, Howard RA (2006) Venus phase function and forward scattering from H_2SO_4. Icarus 182: 10–22.
47. Basilevsky AT, McGill GE (2007) Surface evolution of Venus: Esposito LW Exploring Venus as a Terrestrial Planet (Geophysical Monograph Series), Wiley 176: 23-43.
48. NASA Solar System Exploration (2014) Planets.

49. Kopp G, Lean JL (2011) A new, lower value of total solar irradiance: Evidence and climate significanc . Geophys Res Lett 38: L01706.

50. Jones PD, New M, Parker DE, Martin S, Rigor IG (1999) Surface air temperature and its changes over the past 150 years, Rev Geophys 37: 173–199.

51. NOAA National Climatic Data Center (2014) Global surface temperature anomalies. Online publication by NOAA.

52. Smith TM, Reynolds RW, Peterson TC, Lawrimore J, et al. (2008) Improvements to NOAA's Historical Merged Land-Ocean Surface Temperature Analysis (1880-2006). J Climate 21: 2283-2296.

53. Trenberth KE, Smith L (2005) The mass of the atmosphere: A constraint on global analyses. J Climate 18: 864-875.

54. Stephens GL, O'Brien D, Webster PJ, Pilewski P, Kato S, et al. (2015) The albedo of Earth. Rev Geophys 53.

55. Loeb NG, Wielicki BA, Doelling DR, Smith GL, Keyes DF, et al. (2009) Toward optimal closure of the Earth's top-of-atmosphere radiation budget. J Climate 22:748–766.

56. Lucey, P Korotev RL, Gillis JJ, Taylor LA, Lawrence D, et al. (2006) Understanding the lunar surface and space-Moon interactions. Reviews in Mineralogy and Geochemistry 60: 83–219.

57. Keihm SJ (1984) Interpretation of the lunar microwave brightness temperature spectrum: feasibility of orbital heat flo mapping. Icarus 60: 568–589.

58. Vasavada AR, Paige DA, Wood SE (1999) Near-surface temperatures on Mercury and the Moon and the stability of polar ice deposits. Icarus 141: 179–193.

59. Mat hews G (2008) Celestial body irradiance determination from an underfille satellite radiometer: Application to albedo and thermal emission measurements of the Moon using CERES. Applied Optics 47: 4981-4993.

60. Kemppinen O, Tillman JE, Schmidt W, Harri AM (2013) New analysis software for Viking Lander meteorological data. Geosci Instrum Me hod Data Syst 2: 61–69.

61. Hinson DP, Smith MD, Conrath BJ (2004) Comparison of atmospheric temperatures obtained through infrared sounding and radio occultation by Ma s Global Surveyor. J Geophys Res 109: E12002.

62. Hinson DP (2006) Radio occultation measurements of tran ient eddies in he northern hemisphere of Mars. J Geophys Res 11 : E05002.

63. Bandfiel JL, Wolff MJ, Smith MD, Daniel JM (2013) Radiome ric comparison of Mars Climate Sounder and Thermal Emis ion spectrometer measurements. Icarus 225: 28-39.

64. Younkin RL (1974) The albedo of Titan. Ic rus 21: 219–229.

65. Hanel RA, Pearl JC, Samuelson RE (1985) The bolometric bond albedo of Titan. Bulletin of the Astronomical Society 17: 739.

66. Neff JS, Ellis TA, Apt J, Bergstralh JT (1985) Bolometric albedos of Titan, Uranus, and Neptune. Icarus 62: 425–432.

67. Fulchignoni M, Ferri F, Angrilli F, Ball A , Nub-Bar A, et al. (2005) *In situ* measurements of the physical characte istics of Titan's environment. Nature 438: 785-791.

68. Niemann HB, Atreya SK, Bauer SJ, Carignan GR, Demick JE, et al. (2005) The abundances of constituents of Titan's atmosphere from the GCMS instrument on the Huygens probe. Nature 438: 779–784.

69. Griffit CA (2007) Titan's lower atmosphere. AIP Conf Proc 930: 3-36.

70. Mitri G, Showmana AP, Lunine JI, Lorenz RD (2007) Hydrocarbon lakes on Titan. Icarus 186: 385–394.

71. Li L, Nixon CA, Achterberg RK, Smith MA, Gorius NJP, et al. (2011) The global energy balance of Titan. Geophys Res Lett 38: L23201.

72. Schinder PJ, Flasar FM, Marouf EA, French RG, Mcghee-French C, et al. (2012) The structure of Titan's atmosphere from Cassini radio occultation: Occultation from the Prime and Equinox missions. Icarus 221: 1020–1031.

73. Lellouch E, de Bergh C, Sicardy B, Ferron S, Kaufl HU (2010) Detection of CO in Triton's atmosphere and the nature of surface-atmosphere interac ions. Astron Astrophys 512: L8.

74. Nelson RM, Burattl BJ, Wallis BD, Smythe WD, Horn LJ, et al. (1990) Spectral geometric albedo and bolometric Bond albedo of Neptune's satellite Triton from Voyager observations. Geophys Res Lett 17: 1761–1764.

75. Elliot JL, Hammel HB, Wasserman LH, Franz OG, McDonald SW, et al. (1998) Global warming on Triton. Nature 393: 765-767.

76. Smil V (2003) The Earth's biosphere: Evolution, dynamics and change. MIT Press.

77. Vázquez M. Hanslmeier A (2006) Ultraviolet radiation in the solar system. Springer, The Netherlands.

78. Barlow N (2008) Mars: An introduction to its interior, surface and atmosphere. Cambridge University Press, Cambridge.

79. Rapp D (2008) Human missions to Mars: Enabling technologie for exploring the red planet. Springer, Germany.

80. Taylor FW (2010b) The scientifi exploration of Mars Cambridge University Press, Cambridge NY

81. Lissauer JJ, Pater I (2013) Fundamental planetary science: Physics, chemistry and habitability. Cambridge University Press, New York NY.

82. Fenton LK, Geis ler PE, Haberle RM (2007) Global warming and climate forcing by recent a bedo changes on Mars. Nature 446: 647-649.

83. Jakosky BM, Phillips RJ (2001) Mars' vo atile and climate history. Nature 412: 237-244

84. Catling DC, Leovy C (2007) Ma s atmosphere: History and surface interactions. In: Encyclopedia of the Solar System. Academic Press, pp: 301-314.

85. Hobbs RW, McCullough TP, Waak JA (1968) Measurements of Mars at 1.55 cm and 0.95 cm wavelengths. Icarus 9: 360–363.

86. Klein MJ (1971) Mars: measurements of its brightness temperature at 1.85 and 3.75 cm wave ength. Icarus 14: 210-213.

87. Briggs FH, Drake FD (1972) Interferometric observations of Mars at 21 cm wavel ngth. Icarus 17: 543-547.

88. Van man D, Reedy R, Heiken G, Haskin L, Greive R, et al. (1991) The lunar environment. In: Lunar Sourcebook: A User's Guide to he Moon. Cambridge University Press, Cambridge, pp 27-60

89. Morice CP, Kennedy JJ, Rayner NA, Jones PD (2012) Quantifying uncertainties in global and regional temperature change using an ensemble of observational estimates: The HadCRUT4 data set. J Geophys Res 117: D08101.

90. Peterson TC, Vose RS (1997) An overview of the global historical climatology network temperature database. Bull Am Meteorol Soc 78: 2837-2849

91. Smith TM, Reynolds RW (2005) A global merged land air and sea surface temperature reconstruction based on historical observations (1880-1997). J Climate 18: 2021-2036.

92. Hansen J, Sato M, Russell G, Kharecha P (2013) Climate sensitivity, sea level and atmospheric carbon dioxide. Phil Trans R Soc A 371: 20120294.

93. Gladstone GR, Stern SA, Ennico K, Olkin CB, Weaver HA, et al. (2016) The atmosphere of Pluto as observed by New Horizons. Science 351.

94. NASA JPL Voyager Mission (2013) Titan. Online publica ion by the California Institute of Technology.

95. NASA JPL Ephemeris (2014) Horizons web interface: California Institute of Technology.

96. Stolk H, Gates K, Hanan J (2003) Discovery of emergent natural laws by hierarchical multi-agent systems. In: Proceedings of the International Conference on Intelligent Agent Technology. IEEE/WIC International Conference on Intelligent Agent Technology, Halifax, Canada, pp: 75-82.

97. Wild M (2009) Global dimming and brightening: A review. J Geophys Res 114: D00D16.

98. Herman J, DeLand MT, Huang L-K, Labow G, Larko D, et al (2013) A net decrease in the Earth's cloud, aerosol, and surface 340 nm reflectivit during the past 33 years (1979–2011). Atmos Chem Phys 13: 8505–8524.

99. Stanhill GO, Rosa AR, Cohen S, Achiman O (2014) The cause of solar dimming and brightening at the Earth's surface during he last half century: Evidence from measurements of sunshine dura ion J Geophys Res Atmos 119: 10902–10911.

100. Snyder CW (2016) Evolution of global temperature over the past two million years. Nature 538: 226–228.

101. Heinemann M, Timmermann A, Timm OE, Saito F, Abe-Ouchi A (2014) Deglacial ice sheet meltdown: orbital pace making and CO_2 effects. Clim Past 10: 1567–1579.

102. Stap LB, van de Wal RSW, de Boer B, Bintanja R, Lourens LJ (2014) Interaction of ice sheets and climate during the past 800 000 years. Clim Past 10: 2135–2152.

103. McGehee R, Lehman C (2012) A paleoclimate model of ice-albedo feedback forced by variations in Earth's orbit. Siam J App Dyn Sys 11: 684–707.

104. Doughty AM, Schaefer JM, Putnam AE, Denton GH, Kaplan MR, et al. (2015) Mismatch of glacier extent and summer insolation in Southern Hemisphere mid-latitudes. Geology G36477.1.

105. Maslin MA, Brierley CM (2015) The role of orbital forcing in the early middle Pleistocene transition. Quat Int 389: 47–55

106. Berner RA (2006) Geological nitrogen cycle and atmospheric N_2 over Phanerozoic ime. Geology 34: 413-415.

107. Vladilo G, Murante G, Silva L, Provenzale A, Ferri G, et al. (2013) The habitable zone of Earth-like planets with different levels of atmospheric pressure. Astrophys J 767: 65.

108. Svensmark H, Bondo T, Svensmark J (2009) Cosmic ray decreases affect atmospheric aerosols and clouds. Geophys Res Lett 36: L15101.

109. Svensmark J, Enghoff MB, Svensmark H (2012) Effects of cosmic ray decreases on cloud microphysics. Atmos Chem Phys Discuss 12: 3595–3617.

110. Svensmark J, Enghoff MB, Shaviv N, Svensmark H (2016) The response of clouds and aerosols to cosmic ray decreases. J Geophys Res Space Physics 121: 8152-8181.

111. Voiculescu M, Usoskin I, Condurache-Bota S (2013) Clouds blown by the solar wind. Environ Res Lett 8: 045032.

112. Scafetta N (2016) High resolu ion coherence analysis between planetary and climate oscillations. Adv Space Res 57: 2121–2135.

113. Kirkby J, Duplissy J, Sengupta K, Frege C, Gordon H, et al. (2016) Ion induced nucleation of pure biogenic particles. Nature 533: 521–526.

114. Palle E, Goode PR, Montañés-Rodríguez P, Shumko A, Gonzalez-Merino B, et al. (2016) Earth's albedo variations 1998–2014 as measured from ground-based earthshine observations. Geophys Res Lett 43: 4531–4538.

115. Raulin F (2008) Planetary science: Organic lakes on Titan. Nature 454: 587-589.

116. Sharma P, Byrne S (2011) Comparison of Titan's north polar lakes with terrestrial analogs. Geophys Res Lett 38: L24203.

117. Goldblatt C, Watson AJ (20 2) The runaway greenhouse: Implications for future climate change, geoengineering and planetary atmospheres. Phil Trans R Soc A 370: 4197–4216.

118. Kasting JF (1988) Runaway and moist greenhouse atmospheres and the evolution of Earth and Venus. Icarus 74: 72-494.

119. McClintock WE, Lankton MR (2007) The Mercury atmospheric and surface composition spectrometer for the MESSENGER mission. Space Sci Rev 131: 481-521.

120. Stern SA (2008) The New Horizons Pluto Kuiper belt mission: An overview with historical context. Sp Sci Rev 140: 3-21.

121. Pappalardo RT, Vance S, Bagenal F, Bills BG, Blaney DL, et al. (2013) Science potential from a Europa lander. Astrobiology 13: 740-773.

122. Olkin CB, Young LA, Borncamp D, Pickles A, Sicardy B, et al. (2013) Pluto's atmosphere does not collapse. Cornell University Library, USA.

123. Mallama A, Wang D, Howard RA (2002) Photometry of Mercury from SOHO/LASCO and Earth. Icarus 155: 253–264.

124. Spencer JR, Tamppari LK, Martin TZ, Travis LD (1999) Temperatures on Europa from Galileo photopolarimeter-radiometer: Nighttime thermal anomalies. Science 284: 1514-1516.

125. Moore JM, Chapman CR, Bierhaus EB, Greeley R, Chuang FC, et al. (2004) Callisto. In: Jupiter: The planet, satellites and magnetosphere. Cambridge University Press, pp 397-426.

126. Veeder GJ, Matson DL, J hnson TV, Blaney DL, Goguen JD (1994) Io's heat flo from infrared radiometry: 1983–1993. J Geophys Res 99: 17095–17162.

127. Sotin C, Head II JW, Tobie G (2002) Europa: Tidal heating of upwelling thermal plumes and the origin of lenticulae and chaos melting. Geophys Res Lett 29: 74-1–74-4.

128. Stern SA, Bagenal F, Ennico K, Gladstone GR, Grundy WM, et al. (2015) The Pluto system: initial results from its exploration by New Horizons. Science 350.

129. Asadi A, Hassan MM (2014) E aluation of the thermal performance of a roof-mo nted radiant b rrier in residential buildings: Experimental study. J Building Phys 38: 66–80.

130. Haberle RM (2013) Estimating the power of Mars' greenhouse effect. Icarus 223: 619-620.

131. Schulze Makuch D, Méndez A, Fairén AG, von Paris P, Turse C, et al. (2011) A two-tiered approach to assessing the habitability of exoplanets. Astrobiology 11: 1041–1052.

132. Savage D, Jones T, Villard R (1995) Hubble monitors weather on neighboring planets. Hubble News Release Archive.

133. Clancy RT, Grossman AW, Wolff MJ, James PB, Rudy DJ, et al. (1996) Water vapor saturation at low altitudes around Mars aphelion: A key to Mars climate? Icarus 122: 36–62.

134. Wilson RJ, Richardson MI (2000) The Martian atmosphere during the Viking mission: I Infrared measurements of atmospheric temperatures revisited. Icarus 145: 555–579.

135. Mars Global Surveyor Radio Science Team (2007) The Daily Martian Weather Report. Online publication by Stanford University, USA.

136. Shirley JH, Schofiel J, Kleinböhl A, Abbatt JPD, Lollar BS, et al. (2011) Comparison of MGS Radio Science Mean temperature profile with Mars Climate Sounder (MCS) results. In: Forget CF et al. (eds), 'The Fourth International Workshop on the Mars Atmosphere: Modelling and observation', Paris, France.

Citation: Nikolov N, Zeller K (2017) New Insights on the Physical Nature of the Atmospheric Greenhouse Effect Deduced from an Empirical Planetary Temperature Model. Environ Pollut Climate Change 1: 112.

Local Government New Zealand leads on global warming

Bryan
Leyland

Posted on July 1, 2018 By Bryan Leyland

Local Government New Zealand have embarked on a "Climate Change Project" focused on adapting and mitigating "climate change" – properly described as man-made global warming.

When faced with a potential risk, the rational approach is to make sure that the risk is real, assess its magnitude, decide if anything needs to be done, and if so, what is the cheapest and most effective solution.

In spite of the fact that no one has any convincing evidence based on observations that man-made global warming real and dangerous LGNZ have jumped to the conclusion that the risk is real, urgent action is needed and lots of our money and resources must be spent on "fighting climate change". Taking an objective look at all the evidence never even crossed their minds.

If they had looked at the evidence, they would have got a big surprise.

They would have discovered that world temperatures have increased by about half the predicted amount over the last 20 years and New Zealand has hardly warmed it all. This would – or should – tell them that the computer models which the climate scientists rely upon for predicting future climate are worthless. There is nothing abnormal about the modest amount of warming that has occurred as we recover from the Little Ice Age.

They would also discover that sea level rise in New Zealand – and the rest of the world – has been steady at between 1.5 and 2 mm per year for the last hundred years and shows no sign of the claimed recent rapid increase. They would also discover that there is no reason – other than the failed climate models – to assume that it will rise more rapidly in the future.

If they studied storms, floods and droughts in New Zealand and the rest of the world they would find that recent weather is rather better than it was in the past. The IPCC agrees.

If they looked at the history of atoll formation they would realise that coral atolls were able to keep up with a sea level rise of 3000 mm per century at the end of the ice age. It follows that they cannot be in danger from the current tiny rate of sea level rise. Pacific islands do have real problems, but they are not caused by sea level rise.

If they looked further they would discover that there are many very credible papers based on observations and experiments that indicate a very high probability that the world will soon enter a cooling cycle. Right now sunspot levels are lower than they have been since the Little Ice Age and the correlation between sunspot levels and temperatures is very strong.

A Danish professor has established a cause and effect relationship between sunspot cycles, cosmic rays, low clouds and global temperatures. When sunspot levels are low, the magnetic shield emitted by the sun is low and this allows more high energy cosmic rays to reach lower levels in the atmosphere. When they do, they cause condensation and this triggers cloud formation. Other scientists have analysed past climate cycles and concluded that there is a high risk of global cooling.

While they regard carbon dioxide as a dangerous pollutant, without it, life on earth could not exist. The reality is that it is essential to life and plant growth and the recent rise in concentration has increased agricultural productivity by about 15%. A big win for New Zealand's economy..

They might also be interested to discover that neither the United Nations Intergovernmental Panel on Climate Change, the Royal Society of New Zealand nor Prof Jim Renwick can provide convincing evidence based on observations of the real world that man-made greenhouse gases cause dangerous global warming. The evidence simply does not exist. Until this evidence is discovered – if it ever is – the only rational conclusion is that man-made global warming is, in all probability, the biggest hoax in the history of the world.

It is tragic that Local Government New Zealand have bought into the global warming hoax.

We should not be squandering our money and damaging our economy in a futile attempt to solve a problem that, according to the evidence, does not exist.